

1
2
3
4
5
6
7
8
9
10
11
12
13
14
15
16
17
18
19
20
21
22

Measurement report: Impact of domestic heating on dust
deposition sources in hyper-arid Qaidam Basin, northern
Qinghai-Xizang Plateau

Haixia Zhu^{abc}, Lufei Zhen^{abc}, Suping Zhao^{d*}, Xiying Zhang^{ab*}

^a Key Laboratory of Green and High-end Utilization of Salt Lake Resources, Qinghai Institute of Salt Lakes, Chinese Academy of Sciences, Xining, 810008, China.
^b Qinghai Provincial Key Laboratory of Geology and Environment of Salt Lakes, Qinghai Institute of Salt Lakes, Chinese Academy of Sciences, Xining, 810008, China.
^c University of the Chinese Academy of Sciences, Beijing, 100049, China
^d Key Laboratory of Cryospheric Science and Frozen Soil Engineering, Northwest Institute of Eco-Environment and Resources, Chinese Academy of Sciences, Lanzhou, 730000, China
** Corresponding author. E-mail address: xyzhchina@isl.ac.cn (Xiying Zhang) and zhaosp@lzb.ac.cn (Suping Zhao)*

23 **Highlights**

24 1. The spatiotemporal distribution of carbonaceous aerosols in the basin's atmospheric dust
25 deposition was analyzed using various carbon indicators.

26 2. Domestic heating significantly increased associated pollutants in rural atmospheric dust
27 deposition.

28 3. The basin's unique energy structure suggests its emissions and deposition could affect regional
29 glaciers on the Qinghai-Xizang Plateau.

30

31 **Abstract**

32 Given the unique energy structure of the Qaidam Basin (QDB), this study systematically reveals the
33 spatiotemporal variations in the chemical composition of atmospheric dust deposition and clarifies
34 the key contributions of coal and biomass burning to carbonaceous aerosols, as well as their potential
35 impacts on the Qinghai-Xizang Plateau (QXP) and global atmospheric systems. Monthly dust
36 deposition samples were collected at six sites in the southern QDB between 2020 and 2023. Results
37 indicated heightened carbon emissions and the higher char/soot ratio during the heating period (HP,
38 5.06 ± 4.08) than the non-heating period (NHP, 4.42 ± 3.09), indicating intensified seasonal solid
39 fuel consumption. Spatially, the organic carbon (OC) and elemental carbon (EC) ratio was
40 significantly lower in urban (3.97 ± 2.04) than that in rural areas (10.99 ± 10.00). Char-EC
41 dominated EC (80.44%), especially in urban areas (85.00%), while secondary organic carbon (SOC)
42 dominated OC (72.61%), particularly in rural areas (87.32%). The coal combustion (15.19%) and
43 biomass burning (33.55%) as major contributors in rural areas, strongly associated with domestic
44 heating, whereas urban dust predominantly originated from traffic (46.83%) and industrial
45 emissions (16.41%). Coal consumption in QDB was greater during the HP relative to other dust
46 sources on the QXP leads to increased atmospheric pollutant emissions, which may accelerate
47 regional glacier melting. Consequently, integrating QDB carbonaceous aerosols into future
48 environmental policies and climate models for the QXP is essential. This study provides a reference
49 for investigating carbonaceous aerosols in climatically similar hyper-arid basins with intensive
50 human activity and salt lake regions.

51 **Keywords:** Qinghai-Xizang Plateau; Qaidam Basin; Biomass burning; carbonaceous elements;
52 atmospheric dust deposition.

53

54 **Short summary**

55 This study collected dust samples from six sites in the Qaidam Basin over three years to investigate
56 the impact of domestic heating on atmospheric dust in hyper-arid region. Our results indicate that
57 rural dust is significantly influenced by heating, particularly from coal and biomass burning, which
58 accounts for over 70% of total sources. The unique energy structure here has resulted in distinct
59 environmental effects from the emitted carbonaceous aerosols and useful for similar dry areas.

60 **1. Introduction**

61 Atmospheric dust, a key component of particulate matter (PM), comprises solid particles,
62 typically ranging in size from below 1 μm to 100 μm , which may become airborne depending on
63 their origin, physical characteristics and ambient conditions (Xu, 2014). Within this size spectrum,
64 larger particles (10-100 μm) that settle under gravity are defined as atmospheric dust deposition.
65 Notably, during long-distance transport, these coarse particles can undergo fragmentation into fine
66 particles ($\text{PM}_{2.5}$) and subsequently actively participate in atmospheric chemical and climatic
67 processes (Noll and Fang, 1989). As the dominant natural component of PM, atmospheric dust
68 deposition serves not only a crucial indicator of regional air quality but also a key biogeochemical
69 process linking the atmosphere, cryosphere, hydrosphere, and biosphere, with global-scale
70 influences that significantly shape environmental and climate systems (Feng et al., 2019).

71 Arid and semi-arid regions are the primary global sources of atmospheric dust (Griffin et al.,
72 2002; Schepanski, 2018). Long-distance transport of this dust via wind currents exerts multi-faceted
73 impacts on the environment and human society. A particularly critical effect is the alteration of the
74 cryosphere: dust deposition on snow and ice lowers surface albedo and modifies ice crystal structure,
75 thereby accelerating glacier and snowpack melt (Tuzet et al., 2017). This process disrupts regional
76 snow energy balance, which is directly linked to glacier retreat and water resource security. Dust
77 deposition also influences the atmospheric energy budget by attenuating solar radiation reaching the
78 surface and participates in the global carbon cycle through biogeochemical pathways, such as
79 delivering nutrients to oceans and affecting marine primary productivity (Mahowald et al., 2009;
80 Parajuli et al., 2022). For human health, harmful components associated with dust can induce
81 respiratory and cardiovascular diseases and even damage cellular DNA (Shahram et al., 2016). For
82 terrestrial ecosystems, the shading effect of dust on leaves can inhibit plant photosynthesis and
83 reduce biological productivity.

84 Given the complexity and regional variability of atmospheric dust impacts, identifying dust
85 sources (source apportionment) is fundamental for understanding its environmental behavior and
86 effects. Recent advancements in understanding PM characteristics, particularly chemical
87 composition (e.g. water-soluble ions, carbonaceous components, and trace elements) and source
88 apportionment, have been driven by the integrated application of methodological tools. These

89 receptor models include principal component analysis (PCA), chemical mass balance (CMB), and
90 positive matrix factorization (PMF) models, are used to quantify source contributions. Specifically,
91 the PMF model mathematically deconstructs the chemical composition matrix of ambient samples
92 to achieve this. Additionally, multivariate statistical approaches like backward trajectory simulations
93 (e.g., the HYSPLIT model) trace air mass transport pathways to identify potential source regions
94 (Lai et al., 2016; Yao et al., 2016; Zhang et al., 2015a). This multi-method approach has greatly
95 enhanced the precision of dust deposition source analysis. For instance, PMF analysis of
96 atmospheric dust in urban areas such as Lanzhou, Taiyuan, and Jinan have identified diverse sources,
97 including coal combustion, industrial emissions, construction dust, windblown dust, vehicle
98 emissions, and resuspended road dust. Seasonal variations indicate that coal combustion during the
99 domestic heating period and regional meteorological conditions significantly influence dust
100 deposition (Hu and Liu, 2022; Chen et al., 2024; Yang et al., 2024; Zhang et al., 2022). These
101 findings underscore the urgency of region-specific pollution control strategies. When considering
102 the global scale, arid and semi-arid regions are unequivocally the dominant sources, contributing
103 over 60% of the global atmospheric dust flux (Zan et al., 2025). Therefore, a comprehensive
104 investigation of atmospheric dust processes in these key regions, encompassing emission intensity,
105 physicochemical properties, transport pathways, and environmental effects, is indispensable for
106 elucidating global dust cycle mechanisms and assessing their profound impacts on the cryosphere
107 (e.g., glacial melting) and regional climate.

108 The Qinghai-Xizang Plateau (QXP) often referred to as the “Roof of the World” due to its
109 immense elevation, plays a crucial role in regulating the regional and global climate by altering
110 large-scale atmospheric circulation. Its vast glaciers and snow cover influence regional energy
111 balance through the albedo effect, and as the source of many major Asian rivers, it is known as the
112 “Asian Water Tower” (Liu et al., 2019; Liu et al., 2020b). However, rapid glacier retreat on the
113 plateau poses risks to the Asian hydrological cycle and the monsoon system, with potential adverse
114 impacts if unchecked (Luo et al., 2020). Beyond climate warming and moistening, black carbon
115 (BC), a light-absorbing carbonaceous aerosol component emitted from incomplete combustion
116 processes of solid and liquid fuels during household cooking, heating, and coke production (Bond
117 et al., 2013), significantly accelerates glacial melt. By depositing on ice, BC reduces surface albedo,
118 enhances radiative absorption and thus raises its temperatures, promoting glacial melt (Bond and

119 Bergstrom, 2006; Chen et al., 2015). Notably, biomass burning in South and Central Asia during
120 winter serves as a major source of BC, further exacerbating glacier decline on the plateau (Zhang et
121 al., 2015b; Zheng et al., 2017; Xu et al., 2018b). In addition to these external sources, local dust
122 sources within the QXP itself remain significant. Among these, the Qaidam Basin (QDB) in the
123 northeastern plateau is a particularly important contributor, identified as a key dust source for the
124 plateau (Wei et al., 2017; Zheng et al., 2021) and a critical, unique arid dust source area.

125 The QDB, known as the “Treasure Basin” of the QXP, is rich in mineral resources (e.g., copper,
126 iron, and tin) as well as abundant oil and gas reserves. It serves as a key economic development
127 zone in northwest China, accounting for approximately 30% of the plateau's industrial and
128 agricultural output despite comprising only about 8% of its registered population (Fu, 2023).
129 Extensive resource extraction has rendered its ecosystem fragile (Li and Sha, 2022), exacerbating
130 the impact of atmospheric pollution. The region is also highly sensitive and vulnerable to climate
131 change, with severe and extreme vulnerability zones covering 45.98% of its area (Xu et al., 2024).
132 Unlike South Asia, Central Asia, and Xizang, where biomass fuels dominate, the QDB relies
133 primarily on distinct mix of coal (about 60%) and biomass fuels like yak dung, firewood (about
134 35%) for winter domestic heating, reflecting a unique energy structure (Liu et al., 2008; Xiao et al.,
135 2015; Behera et al., 2015; Kerimray et al., 2018; Jiang et al., 2020; Shen et al., 2021). The
136 combustion of coal releases significant pollutants, including light-absorbing aerosols like BC and
137 brown carbon (BrC) (Munawer, 2018; Ye et al., 2020; Zhou et al., 2025). Brown carbon refers to
138 organic compounds that can absorb light, particularly at shorter wavelengths, resulting in a reddish
139 orange or brown appearance (Donahue, 2018). Both BC and BrC can influence solar radiation
140 absorption and cloud properties, exerting a positive radiative forcing on climate (Ramanathan and
141 Carmichael, 2008; Bond et al., 2013). When deposited on snow and ice, they further accelerate
142 glacial melt (Qian et al., 2015; Kang et al., 2020a). Additionally, BC and BrC are significant
143 contributors to global warming and can exacerbate adverse health effects by carrying toxic
144 components (Ramanathan and Carmichael, 2008; Shrivastava et al., 2017). Notably, QDB's
145 widespread use of yak dung as a fuel, a practice less common in other coal-intensive heating regions
146 of northern China, releases pollutants like carbon monoxide (CO), volatile organic compounds
147 (VOCs), and polycyclic aromatic hydrocarbons (PAHs), further affecting local air quality and health
148 (Zhang et al., 2022). Consequently, we posit that seasonal carbon emissions in QDB, particularly

149 during winter domestic heating, could exert a unique influence on the climate and ecological
150 stability of the QXP.

151 The QDB, as a representative arid region with intensive human activity, exhibits climatic and
152 environmental conditions comparable to other hyper-arid basins (e.g., the Tarim and Junggar Basins
153 in Xinjiang, the Great Basin in the United States) and high-altitude salt lake regions (e.g., Uyuni in
154 Bolivia, Atacama in Chile). These regions are characterized by low precipitation, rich mineral
155 resources subject to significant anthropogenic impact, and abundant salt lakes. Research in the
156 Tarim and Junggar Basins has predominantly focused on dust events, their sources, and associated
157 gas emissions (Gao and Washington, 2010; Liu et al., 2016b; Filonchyk et al., 2018; Yu et al., 2019;
158 Zhou et al., 2023). In the Great Basin, studies largely address ozone and dust sources (Hahnenberger
159 and Nicoll, 2012; Vancuren and Gustin, 2015; Miller et al., 2015). Research on salt lake atmospheres
160 has predominantly focused on high-salinity dust emissions resulting from lakebed desiccation due
161 to resource extraction (Löw et al., 2013; Gholampour et al., 2015; Moravek et al., 2019; Christie et
162 al., 2025), with limited research on atmospheric carbon components, their sources, and
163 environmental impacts. Therefore, this research aims to investigate atmospheric carbonaceous
164 aerosols in arid basins with intensive human activity and climates comparable to the QDB, as well
165 as in salt lakes environments.

166 From January 2020 to March 2023, monthly dust deposition samples were collected at six
167 urban and rural monitoring sites in the southern QDB. Samples were categorized into two seasonal
168 periods: the domestic heating period (HP) and the non-domestic heating period (NHP). Measured
169 parameters included dust deposition flux, soluble ions, trace elements, and key carbonaceous
170 components. The objectives of this study were: (1) to clarify the variation trends of carbonaceous
171 components in atmospheric dust deposition under the unique energy structure of the QDB, and to
172 quantify the contribution of domestic heating; and (2) to identify the major sources of atmospheric
173 dust deposition in the basin and to evaluate their associated environmental impacts. To achieve these
174 aims, we applied OC/EC and char/soot ratios, the HYSPLIT trajectory, and PMF model for source
175 apportionment. Furthermore, these findings offer a scientific basis and reference for examining
176 atmospheric carbonaceous aerosols in arid basins with similar climates and human activities to the
177 QDB, as well as in salt lake regions.

178

179 **2. Materials and methods**

180 **2.1 Sampling**

181 The QDB, situated in the northeastern part of the QXP, is bordered by the Altyn-Tagh, Kunlun,
182 and Qilian mountains, making it one of China's largest intermontane basins (Zhang, 1987). With an
183 average elevation of 3,000 m, the basin features an extremely arid climate characterized by less than
184 20 mm of annual precipitation in the northwestern region, while evaporation rates exceed 2,000 mm
185 (Feng et al., 2022). The QDB is rich in salt lakes, non-ferrous metals, and hydrocarbon resources,
186 with significant coal deposits. As a major salt lake resource area, it hosts 33 lakes, including Qarhan,
187 Dachaidan, and Caka Salt Lake, and faces notable conflicts between resource extraction and
188 ecological preservation. Agriculturally, it cultivates crops like goji berries, quinoa, and forage grass,
189 and hosts China's largest resource-rich circular economy pilot zone. The permanent population of
190 the basin is approximately 400,000, primarily using coal, yak dung, and firewood for domestic
191 heating (Jiang et al., 2020). Additionally, annual tourism peaks from May to September, attracting
192 around 17 million visitors (Qinghai Statistical Yearbook, 2023), which likely amplifies atmospheric
193 pollutant emissions.

194 From January 2020 to March 2023, monthly dust deposition samples were collected from six
195 monitoring stations in the southern QDB. The stations included Xiao Zaohuo (XZH), Golmud
196 (GEM), Da Gele (LTC), Nuo Muhong (NMH), Balong (BLX), and Dulan station (DLX) (Figure 1).
197 Dry deposition collection employed the glass ball method using Marble dust collector (MDCO)
198 designed dust collection cylinders (Sow et al., 2006). The MDCO sampler operates on the principle
199 of gravitational settling. It uses a collection vessel with a known opening to capture particulate
200 matter that settles naturally from the air. In field measurements, surrogate surfaces or deposition
201 traps are commonly employed to better quantify atmospheric deposition. These surfaces mimic the
202 original ground surface, are easy to deploy, and can be integrated without significantly disturbing
203 airflow. Examples include glass beads (Ganor, 1975; Offer et al., 1992), moist filter paper (Goossens
204 and Offer, 1993), plastic surfaces (Gregory, 1961), and water or antifreeze solutions (Smith and
205 Twiss, 1965). The MDCO deposition vessel is based on the original concept of Ganor (1975), using
206 glass beads as a surrogate collection surface. Due to their very low microscopic roughness, the beads
207 help prevent the resuspension of particles once they have been captured (Goossens and Offer, 1993).

208 The stainless steel collection device (50×30×30 cm) contained a plastic sieve container of
209 identical dimensions, with the sieve base positioned 10 cm above the opening and perforated with
210 0.5 cm diameter holes (Figure S1). To minimize dust resuspension during high wind events (Qian
211 and Dong, 2004), two layers of 16 mm glass balls were placed within the sieve container. A high-
212 density polyethylene bag was attached to the base for sample collection. According to Sow et al
213 (2006), the collection efficiency of the MDCO decreases with increasing wind speed, dropping
214 below 20% when wind speed exceeds 3 m/s, and it preferentially collects the finer fraction of
215 atmospheric dust particles ranging from 10 to 31 μm in size (Chow, 1995). Furthermore, collection
216 efficiency decreases significantly as the size of dust-fall increases. Based on our findings, more than
217 50% of the collected dust particles are below 40 μm (Figure S2), whereas the mean particle size of
218 atmospheric dust deposition reported in other studies is approximately 80 μm (Lin et al., 2022a; Lin
219 et al., 2022b). This confirms that the MDCO sampler preferentially collects relatively finer particles.
220 Consequently, this study may place greater emphasis on analyzing the chemical activity of the finer
221 fraction of atmospheric dust, thereby enhancing the detection sensitivity for components such as
222 secondary ions and carbonaceous species in deposited dust. However, this particle-size selectivity
223 introduces a sampling bias that can amplify inter-site differences in deposition flux between sites,
224 complicate local source apportionment, strengthen signals from distant sources (e.g., combustion
225 and vehicle emissions), and weaken the contribution from local, coarse-particle-dominated sources
226 (e.g., resuspended dust and construction dust). These factors may affect the accuracy of both
227 deposition flux estimates and source apportionment. Future research should enhance data
228 comparability and the reliability of ecological assessments through efficiency correction and the
229 combined application of multiple methods. The collection efficiency at each site was calculated
230 based on local dust grain-size distribution and wind speed; details are provided in Supplementary
231 Text S1. This type of collector has been widely used in many studies to evaluate local dust conditions
232 (Abdollahi et al., 2021; Barjoe et al., 2021; Alzahrani et al., 2024).

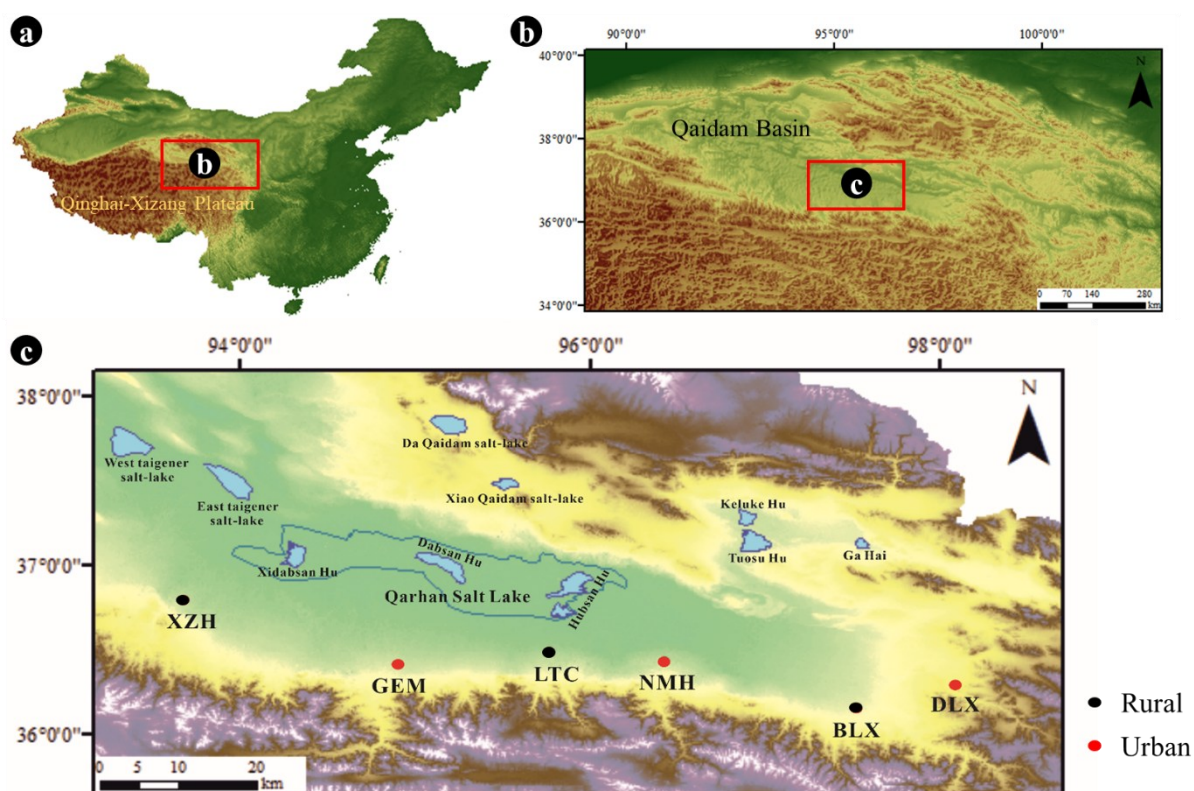
233 In this study, dust samples were collected monthly, with each sampling period lasting 30 or 31
234 days. The installation height and environment of the samplers are provided in Table S1. To ensure
235 only dry dust was collected, collection devices were manually-operated covered during rain or
236 snowfall. A total of 37, 39, 23, 30, 16, and 29 samples were obtained from XZH, GEM, LTC, NMH,
237 BLX, and DLX stations, respectively, and no duplicate samples were collected during the sampling

238 period. Laboratory protocols incorporated biannual analyses with negative controls and appropriate
 239 control samples. As continuous dust monitoring commenced in 2020, site blanks were evaluated
 240 during initial sampling. Stations were classified as Urban (GEM, NMH, DLX) and Rural (XZH,
 241 LTC, BLX) based on location characteristics. Consistent with the cold-arid climate in QDB, the HP
 242 was defined as October-April, while the NHP spanned May-September.

243 Materials such as plant remnants, microfauna, and bird droppings were removed from the
 244 sample bags with tweezers. The samples were then measured on a balance (0.0001 g) to determine
 245 the total dust deposition flux (DF) (Eq. 1) (Yu et al., 2016):

$$246 \quad M = \frac{m \times 30}{S \times K}, \quad (1)$$

247 where M is dust deposition [$\text{g}/(\text{m}^2 \cdot 30\text{d})$]; m is the sample mass (g); S is the area of the dust collection
 248 device (m^2); and K is the actual number of sampling days per month (d).



249
 250 **Figure 1.** Spatial distribution of monitoring stations in the southern Qaidam Basin. Urban stations
 251 (red) and rural stations (black) are labeled as follows: XZH (Xiao Zaohuo), GEM (Golmud), LTC
 252 (Da Gele), NMH (Nuo Muhong), BLX (Balong), DLX (Dulan).

253

254 2.2 Water-soluble inorganic ions

255 A 100 mg sample was weighed and transferred into a 250 mL bottle. The mixture underwent
256 ultrasonic extraction for 20 minutes to ensure complete solubilization. The resulting supernatant
257 was then filtered through a 0.45 μm filter for analysis. Based on preliminary experimental results,
258 the concentrations of major ions (K^+ , Na^+ , Mg^{2+} , and Ca^{2+}) were measured using Inductively
259 Coupled Plasma Optical Emission Spectrometer (ICP-OES, NexIon 2000). Anions (Cl^- , SO_4^{2-} , and
260 NO_3^-) were quantified using ion chromatography (IC). To ensure measurement accuracy, samples
261 were organized in sets of twenty, with one randomly selected sample from each group serving as a
262 replicate, achieving an error margin of less than 10%. The detection limits for the various
263 components were as follows: K^+ (0.0560 mg/L), Na^+ (0.0100 mg/L), Ca^{2+} (0.0037 mg/L), Mg^{2+}
264 (0.0390 mg/L), SO_4^{2-} (0.0090 mg/L), NO_3^- (0.0125 mg/L), Cl^- (0.0100 mg/L). All standard solutions
265 employed in the analysis were sourced from the National Standard Material Center.

266

267 **2.3 Trace element analysis**

268 According to the Chinese State Standard “Ambient air and waste gas from stationary sources
269 emission-determination of metal elements in ambient particles” (HJ 777-2015), the concentrations
270 of elements such as iron (Fe), aluminum (Al), silicon (Si), titanium (Ti), copper (Cu), cadmium (Cd),
271 chromium (Cr), manganese (Mn), nickel (Ni), zinc (Zn), lead (Pb), and vanadium (V) were
272 quantified using Inductively Coupled Plasma Mass Spectrometry (ICP-MS) and ICP-OES. A dust
273 sample weighing 0.100 g was placed in a Teflon cup, to which 20.0 mL of a nitric acid-hydrochloric
274 acid digestion solution was added. The sample was heated to reflux at $100 \pm 5^\circ\text{C}$ for 2 h under a
275 watch glass, then cooled. Following this, the inner walls of the cup were rinsed with water, and
276 approximately 10 mL of water was added, allowing the mixture to stand for 30 minutes for
277 extraction. The extract was then filtered into a 100 mL volumetric flask and diluted to volume with
278 distilled water for analysis. In cases where organic matter content was high, an appropriate amount
279 of hydrogen peroxide was introduced during digestion to decompose the organic materials. Prior to
280 sample analysis, the system was flushed with a rinse solution until the blank intensity value reached
281 a minimum, and samples were analyzed only after the signal stabilized. If the concentration of any
282 element exceeded the calibration range, the sample was diluted and reanalyzed.

283

284 **2.4 Carbon analysis**

285 This study utilized a combination of wet chemical treatment and thermal/optical reflection
286 (TOR) to analyze carbon elements in dust deposition (Han et al., 2007b; Han et al., 2007a; Han et
287 al., 2016). Dust samples were digested stepwise to remove inorganic materials: first samples were
288 treated with 10 mL of 2 N hydrochloric acid (HCl) for 24 h at room temperature to dissolve
289 carbonates and partial metals, followed by centrifugation (4500 rpm, 12 min) to separate the
290 residue; then with 15 mL of a 1:2 (v/v) mixture of 6 N HCl and 48% hydrofluoric acid (HF) for 24
291 h at room temperature to dissolve silicates and residual metals; and finally with 15 mL of 4 N HCl
292 for 24 h at 60 °C to remove minerals such as fluorite formed during demineralization. After each
293 step, the mixture was centrifuged, and the supernatant was collected. The solid residue was diluted
294 with 200 mL of deionized water and filtered through a pre-combusted quartz fiber filter (Whatman,
295 450°C for 4 h, diameter 47 mm) (Han et al., 2007a). This method has been widely applied to measure
296 OC and EC contents in lake sediments and urban soils (Han et al., 2009; Khan et al., 2009; Han et
297 al., 2011). Studies have shown that the EC collection efficiency of this method is approximately
298 99.6% (Zhan et al., 2013). However, because OC includes polar, basic, and mineral-bound
299 compounds that may dissolve in HCl/HF and be lost during filtration, the supernatant from all three
300 acid-digestion steps was collected and analyzed for water-soluble OC using a carbon-nitrogen
301 analyzer (Shimadzu, TOCN-4200, Japan). Total OC was obtained by summing the dissolved OC
302 and the particulate OC measured by TOR.

303 The filtered samples were air-dried and analyzed for carbon content using a DRI 2001
304 thermal/optical carbon analyzer (Atmoslytic Inc., Calabasas, CA) at the Institute of Earth
305 Environment, Chinese Academy of Sciences, adhering to the Interagency Monitoring of Protected
306 Visual Environments (IMPROVE) protocol. A 0.544 cm² disc was extracted from the filter and
307 placed in a quartz boat for analysis. During the carbon analysis, the samples were initially heated in
308 a 100% helium atmosphere, resulting in the production of four organic carbon (OC) fractions (OC1,
309 OC2, OC3, and OC4) at four different temperature levels (140, 280, 480, and 580°C). The
310 atmosphere was subsequently changed to 2% O₂/98% He, generating three elemental carbon (EC)
311 fractions (EC1, EC2, and EC3) at three temperatures (580, 740, and 840 °C). Volatile carbon
312 underwent carbonization in an anaerobic environment, indicated by a decrease in laser reflectance,

313 and is referred to as pyrolyzed organic carbon (OPC). In the oxidative atmosphere, OPC was emitted
314 along with the original EC from the filter. The amount of OPC is defined as the carbon evolved until
315 the laser reflectance returned to its baseline value (Han et al., 2007b). According to the IMPROVE
316 protocol, EC is calculated as the total of the three EC subfractions minus OPC (i.e., EC is defined
317 as the sum of EC1, EC2, and EC3, with OPC subtracted). The method enables differentiation
318 between soot and char, as determined by the gradual oxidation of these black carbon subtypes in
319 standard reference materials during the EC1 and the EC2 plus EC3 steps, where char is defined as
320 EC1 minus OPC and soot as the sum of EC2 and EC3 (Han et al., 2007a; Han et al., 2016).

321 Please note that in this manuscript, we interchangeably use the terms “EC” and “BC”. While
322 these terms do not strictly refer to the same component, they serve as an adequate approximation
323 within the scope of this study (Seinfeld et al., 1998; Bond et al., 2004). We use “EC” when
324 discussing emissions and modeling components, reserving “BC” for climate-related discussions.
325 Throughout this manuscript, the term “OC” refers to the total organic carbon (sum of the dissolved
326 OC and the particulate OC).

327

328 **2.5 The particle size analysis**

329 The grain size of dust-fall samples was measured using a laser particle analyzer (Malvern
330 Mastersizer 2000, UK). The particle size distribution was calculated for 100 grain size classes within
331 a range of 0.02-2000 μm . Sample preparation for grain size analysis included wet oxidation of
332 organic matter by adding 10 mL of 30% hydrogen peroxide (H_2O_2) per 1.5 g dry sample. Carbonates
333 were dissolved by boiling with 10 mL (10% HCl) over 10 min. The glass beakers were filled with
334 150 mL distilled water and suspended particles were left to deposit. After siphoning the supernatant
335 water, 10 mL of 0.05 N sodium hexametaphosphat [$(\text{NaPO}_3)_6$] were added, and the residue was
336 dispersed for 5 min in an ultrasonic bath before measurement (Lu and An, 1997), the results are
337 expressed as volume percentages.

338

339 **2.6 Collection of Meteorological Factors**

340 Meteorological data used in this study were obtained from the Qinghai Meteorological Bureau
341 during the sampling period. Monthly meteorological parameters, including wind speed (WS), wind

342 direction (WD), temperature (Temp), relative humidity (RH), Precipitation (RF), sunshine duration
343 (SUN), and the frequency of visibility ≤ 10 km (VIS), were collected from four national-level
344 meteorological stations: XZH, GEM, DLX, and NMH. All of these stations are standard
345 meteorological observatories established by the state, equipped with standardized monitoring
346 capabilities, and provided continuous and reliable data for this study (<https://data.cma.cn>). In
347 addition, two atmospheric dust deposition sampling sites (LTC and BLX) were established
348 specifically for collecting dust samples. Due to field-monitoring constraints and research-budget
349 limitations, no meteorological instruments were deployed at these two sites.

350

351 **2.7 Statistical analysis**

352 2.7.1 Estimation of Secondary Organic Carbon

353 Organic carbon consists of primary organic carbon (POC) and secondary organic carbon (SOC).
354 Due to the intricate physical and chemical processes involved, SOC in urban atmospheres cannot
355 be directly measured. Therefore, an indirect estimation method, known as the EC tracer method, has
356 been developed (Turpin and Huntzicker, 1991). If the concentrations of OC and EC are available
357 and primary OC from non-combustion sources ($OC_{\text{non-comb}}$) can be disregarded, EC can be utilized
358 as a tracer for POC from combustion sources, facilitating the estimation of SOC (Turpin and
359 Huntzicker, 1995):

$$360 \quad \text{POC} = \text{EC} \times (\text{OC}/\text{EC})_{\text{pri}}, \quad (2)$$

$$361 \quad \text{SOC} = \text{OC}_{\text{total}} - \text{POC}, \quad (3)$$

362 where OC_{total} represents total organic carbon.

363 Traditional methods for determining $(\text{OC}/\text{EC})_{\text{pri}}$ involve regressing OC and EC within a fixed
364 percentile range of the lowest (OC/EC) ratio data (typically 5-20%) or relying on sampling days
365 characterized by low photochemical activity and local emissions (Castro et al., 1999; Lim and
366 Turpin, 2002). However, these approaches are limited by their empirical nature, lacking clear
367 quantitative criteria for selecting the data subsets used to establish $(\text{OC}/\text{EC})_{\text{pri}}$, defined as the
368 hypothetical primary OC/EC ratio. In this study, we employed the minimum R squared (MRS)
369 method (Millet et al., 2005; Wu and Yu, 2016; Wu et al., 2018a) to determine $(\text{OC}/\text{EC})_{\text{pri}}$. This
370 method calculates a set of hypothetical $(\text{OC}/\text{EC})_{\text{pri}}$ and SOC values to identify the minimum

371 correlation coefficient (R^2) between SOC and EC, allowing for the accurate derivation of $(OC/EC)_{pri}$.
 372 The computational procedure followed the algorithm developed by Wu and Yu (2016) (available at:
 373 <https://sites.google.com/site/wuchengust>), implemented within the Igor Pro environment
 374 (WaveMetrics, Inc., Lake Oswego, OR, USA). Due to the limited dataset size and low temporal
 375 resolution, the MRS analysis was performed collectively across all sampling sites. In this approach,
 376 the R^2 between SOC and EC was calculated iteratively for a range of $(OC/EC)_{pri}$ values spanning 0
 377 to 10. The minimum R^2 value of 1.33 (Figure S3) identified the optimal $(OC/EC)_{pri}$ representative
 378 of the true primary ratio.

379

380 2.7.2 Quantifying the contributions of playa salt (ps) and non-playa salt (nps) sources

381 To differentiate the contributions of salt lake sources to water-soluble ions in atmospheric
 382 deposition, we adopted a methodology similar to that used for marine aerosols. This approach relies
 383 on the ratio of water-soluble ions (SO_4^{2-} , Ca^{2+} , K^+ , Mg^{2+} , Cl^-) to Na^+ in the salt lakes of the QDB,
 384 enabling us to assess the contribution of ps- Na^+ components to nps (Zhang, 1987); details in Zhu
 385 (2025).

$$386 \quad nps-SO_4^{2-} = [SO_4^{2-}] - 0.333 \times ps-Na^+, \quad (4)$$

$$387 \quad nps-Ca^{2+} = [Ca^{2+}] - 0.062 \times ps-Na^+, \quad (5)$$

$$388 \quad nps-K^+ = [K^+] - 0.087 \times ps-Na^+, \quad (6)$$

$$389 \quad nps-Mg^{2+} = [Mg^{2+}] - 0.051 \times ps-Na^+, \quad (7)$$

$$390 \quad nps-Cl^- = [Cl^-] - 2.287 \times ps-Na^+, \quad (8)$$

391 This was accomplished using equations that incorporate total Na^+ , total Ca^{2+} , the average
 392 crustal ratio $(Na^+/Ca^{2+})_{crust} = 0.56$ w/w (Bowen, 1979), and the average (Ca^{2+}/Na^+) ratio for Qaidam
 393 salt lakes, $(Ca^{2+}/Na^+)_{salt\ lake} = 0.06$ w/w (Zhang, 1987). Among these, the mass concentration of
 394 $[SO_4^{2-}]$, $[Ca^{2+}]$, $[K^+]$, $[Mg^{2+}]$, $[Na^+]$ and $[Cl^-]$ were identified as constituents of dust-fall.

$$395 \quad ps-Na^+ = [Na^+] - nps-Na^+, \quad (9)$$

$$396 \quad nps-Na^+ = nps-Ca^{2+} \times (Na^+/Ca^{2+})_{crust}, \quad (10)$$

$$397 \quad nps-Ca^{2+} = [Ca^{2+}] - ps-Ca^{2+}, \quad (11)$$

$$398 \quad ps-Ca^{2+} = ps-Na^+ \times (Ca^{2+}/Na^+)_{salt\ lake}, \quad (12)$$

399

400 2.7.3 HYSPLIT backward trajectory model

401 Backward trajectory clustering analysis was conducted on sampling points using the TrajStat
402 plugin within Meteoinfo software. Daily backward trajectories for 48 hours were calculated from
403 January 2020 to March 2023 and classified monthly based on differences in the horizontal
404 movement direction and velocity of air masses. The trajectories were initiated at Universal Time
405 (UTC) 00:00, with a 6-hour increment, originating from 500 m above sea level (Yang et al., 2014).
406 Meteorological data utilized in this research were obtained from the Global Data Assimilation
407 System (GDAS) provided by the U.S. National Centers for Environmental Prediction (NCEP),
408 covering the period from December 2019 to February 2023 (Meteoinfo software website:
409 <http://meteothink.org>).

410

411 2.7.4 PMF model

412 The PMF is a multivariate factor analysis tool that decomposes a matrix of speciated sample
413 data into two matrices: factor contributions (G) and factor profiles (F). The goal of the PMF model
414 is to solve the chemical mass balance between measured species concentrations and the respective
415 source profiles, with the purpose of minimizing the objective function Q (Eq. 13) based upon the
416 uncertainties (u_{ij}) of measured species (Paatero and Tapper, 1994).

$$417 \quad e_{ij} = x_{ij} - \sum_{h=1}^p g_{ih} f_{hj}; \quad Q = \sum_{i=1}^m \sum_{j=1}^n (e_{ij}/h_{ij} s_{ij})^2, \quad (13)$$

418 where x_{ij} is the measured concentration of the j_{th} species in the i_{th} sample at receptor sites. f_{kj} is the
419 source profile of the j_{th} species in the k_{th} factor and g_{ik} is the mass contribution of the k_{th} factor in
420 the i_{th} sample. e_{ij} is the difference between modeled concentrations and measured concentrations.

421 The uncertainty for individual species (u_{ij}) was defined as the sum of two components: the x_{ij}
422 multiplied by an error fraction, and one-third of the method detection limit (MDL). For data below
423 the MDL, concentrations were replaced by 1/2 MDL and the corresponding uncertainty was set to
424 5/6 MDL (Reff et al., 2007). An extended description of the PMF parameters used in this study and
425 error estimate based on the model's Q value, displacement (DISP), and bootstrapping (BS) tests
426 (DISP-BS) are provided in the Supplementary Information. The error assessment and uncertainty
427 data for the PMF source apportionment can be found in Tables S2 and S3, respectively.

428

429 2.7.5 Statistical Analysis

430 A one-way analysis of variance (One-Way ANOVA) was performed to examine the differences
431 in dust deposition flux, soluble ions, carbonaceous components, and trace elements among various
432 monitoring sites and periods. All statistical analyses were conducted in SPSS (IBM SPSS Statistics
433 26.0.0), with the significance level (P) set at 0.05. Prior to ANOVA, the normality and homogeneity
434 of variance were tested for each dataset. The Shapiro-Wilk test was used to assess normality. If the
435 data met the normality assumption ($P > 0.05$), parametric ANOVA was applied directly. If not, the
436 data were log-transformed and retested; if the transformed data still violated this assumption, the
437 non-parametric Kruskal-Wallis H test was used instead. In this study, all datasets were confirmed to
438 follow a normal distribution. Homogeneity of variance was verified using Levene's test; meeting
439 this assumption ($P < 0.05$) is a prerequisite for conducting ANOVA. When the overall ANOVA
440 result was significant ($P < 0.05$), indicating that at least two group means differed statistically, a
441 post-hoc test was performed. Given the potentially unequal sample sizes among groups, Tukey's
442 Honestly Significant Difference test was used for pairwise comparisons to identify specific inter-
443 group differences. Data in this study are presented as mean \pm 1 standard deviation (Mean \pm 1 SD).

444 Furthermore, to investigate the influence of meteorological conditions on the chemical
445 composition of atmospheric dust, Pearson correlation analysis was applied to quantitatively assess
446 the linear relationships between meteorological factors (e.g., wind speed and direction, relative
447 humidity) and chemical components in dust (e.g., OC, EC, water-soluble ions). The underlying
448 assumptions of the Pearson correlation (continuous variables, bivariate normal distribution, and
449 linearity) were verified. All variables were tested for normality using the Shapiro-Wilk test and
450 screened for outliers. For data that did not meet the normality assumption, log transformation was
451 applied. The significance of correlation coefficients was tested using the t-test, with $P < 0.05$
452 considered statistically significant.

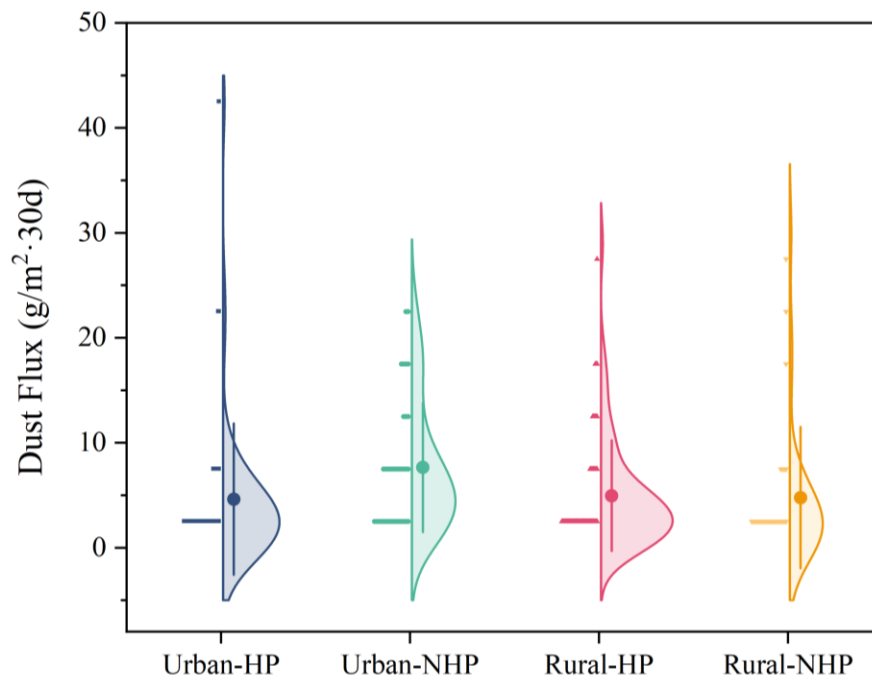
453

454 **3. Results and discussion**

455 **3.1 Atmospheric dust deposition flux and water soluble ions concentration**

456 The DF in the southern QDB is $5.41 \pm 5.33 \text{ g/m}^2 \cdot 30\text{d}$, slightly lower than that of the Lake Aibi
457 Basin ($10.77 \text{ g/m}^2 \cdot 30\text{d}$) (Li et al., 2022), but higher than the surrounding areas of Akatama Salt Lake
458 ($2.93 \text{ g/m}^2 \cdot 30\text{d}$) (Wang et al., 2014). Specifically, DF was $4.67 \pm 4.96 \text{ g/m}^2 \cdot 30\text{d}$ in rural and $5.97 \pm$

459 5.73 g/m²·30d in urban areas. During the HP, DF in rural and urban areas were 4.62 ± 4.15 g/m²·30d
460 and 4.95 ± 5.25 g/m²·30d, respectively. In contrast, NHP showed increased DF values of 4.77 ± 4.42
461 g/m²·30d (rural) and 7.66 ± 6.09 g/m²·30d (urban) (Figure 2). Notably, Urban DF during NHP
462 demonstrated a 54.6% increase relative to HP, while rural DF rose by 7.1% (not statistically
463 significant), contrasting previous findings that associated elevated DF with HP coal combustion
464 (Cheng et al., 2009; Gao et al., 2013; Guo et al., 2010; Qi et al., 2018). We hypothesize that the
465 increase in DF during the NHP is attributed to seasonal meteorological variations such as wind speed
466 (Yang et al., 2024), and heightened anthropogenic emissions associated with tourism (Zhang et al.,
467 2011). The NHP coincides with the peak tourist season (May-September) in the QDB, which
468 receives about 17 million visitors annually, a number that continues to rise (Qinghai Statistical
469 Yearbook, 2023). This elevated human activity likely enhances local emissions, contributing to
470 increased dust deposition during this period. The influence of meteorological factors on dust
471 deposition will be further examined in Section 3.5.



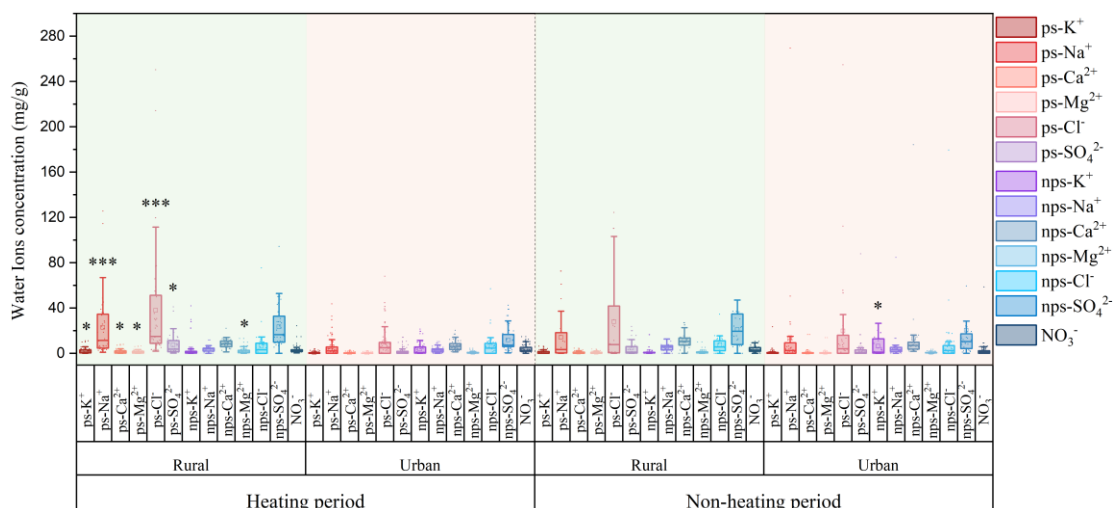
472 **Figure 2** Dust flux distribution in urban and rural. The distribution of dust flux in four contexts:
473 Urban with domestic heating period (Urban-HP), Urban with non-HP (Urban-NHP), Rural with
474 domestic heating period (Rural-HP), and Rural with non-HP (Rural-NHP). Each violin plot
475 illustrates the density distribution of dust flux values, with the central dot representing the mean,
476 and the vertical lines indicating the interquartile range.

478

479 Water-soluble ion concentrations differed between rural (115.31 mg/g) and urban (72.81 mg/g)
480 areas (not statistically significant). In rural, water-soluble ion content was greater during the HP
481 than in the NHP, while the opposite trend was observed in urban areas (not statistically significant)
482 (Figure 3 and S5). We categorized the water-soluble ions in dust deposits into ps and nps based on
483 their sources, following the model of marine aerosols (Zhu et al., 2025). Playa salt content
484 consistently surpassed nps in rural areas across both periods, while urban areas showed the opposite
485 trend (not statistically significant). Notably, during the NHP, ps content in urban and rural increased
486 by 54.46 and 36.86% respectively (not statistically significant). Backward trajectory analysis
487 indicated that airflow in both rural and urban areas primarily originated from the northwest QDB
488 and the eastern Tarim Basin during the HP, while during the NHP, it was influenced more broadly
489 by the salt lake of the QDB (Figure S6 and S7), aligning with the observed variations in ps content.
490 A similar increase in summer sea salt and non-sea salt ions has been reported in Rajkot, India,
491 attributed to ocean wind direction (Gupta and Dhir, 2022).

492 The ratio of $\text{nps-SO}_4^{2-}/\text{NO}_3^-$ in soluble ions is used to differentiate between coal combustion
493 (fixed sources) and vehicular emissions (mobile sources) (Arimoto et al., 1996; Shen et al., 2008).
494 The higher $\text{nps-SO}_4^{2-}/\text{NO}_3^-$ ratio in urban areas compared to rural areas (Figure S8) indicates that
495 during the study period, stationary sources (e.g., industrial emissions, coal, and biomass combustion)
496 contributed more significantly to the ionic composition of urban dust-fall (Pipal et al., 2019). In
497 contrast, the ratio was considerably lower during the NHP than during HP, suggesting that mobile
498 sources likely played a more important role in the dust ionic composition during the NHP. Generally,
499 emissions from coal combustion and biomass burning was intensified in northern China during the
500 HP (Liu et al., 2016), while vehicle emissions dominate during the NHP (Xu et al., 2012), supporting
501 the reliability of this analysis. Nevertheless, further investigation integrating atmospheric emission
502 inventories, source tracers, aerosol physicochemical processes, and meteorological conditions is
503 warranted.

504



505

506 **Figure 3** Concentrations of water ions in rural and urban across different seasonal periods (domestic
 507 heating and non-domestic heating periods). Asterisks indicate statistically significant differences
 508 between sites, with *, $P < 0.05$; **, $P < 0.01$; ***, $P < 0.001$.

509

510 3.2 Carbonaceous element compositions

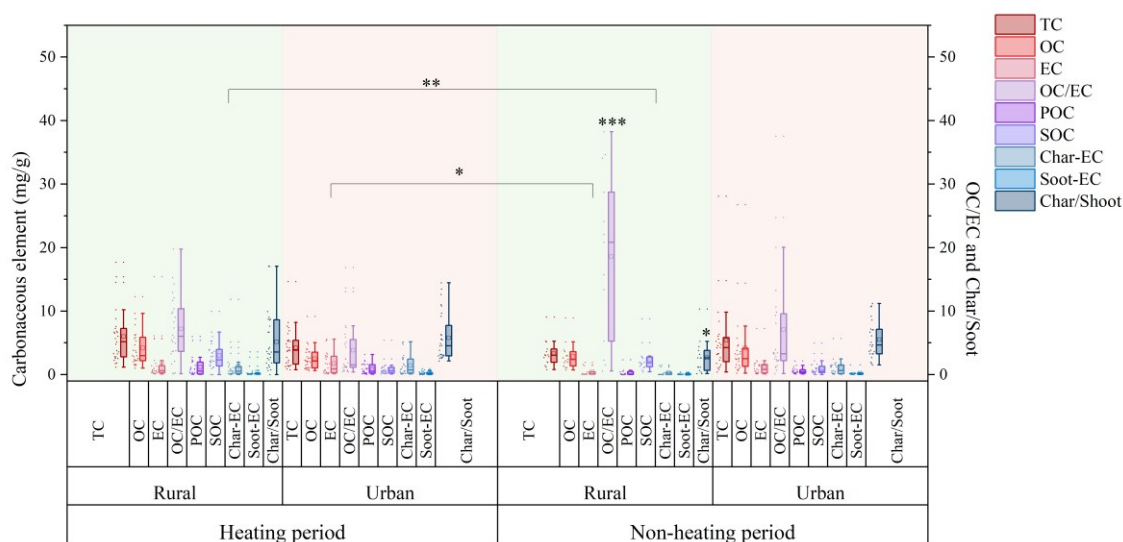
511 3.2.1 Organic carbon and elemental carbon

512 The average total carbon (TC) concentration in the southern QDB was 4.87 ± 4.18 mg/g,
 513 significantly lower than that of Huangshi, Hubei province (25.15 ± 11.79 mg/g) and Washington
 514 (157 ± 3.2 mg/g), Kumasi in West Africa (28 mg/g) and Xi'an (14.6 ± 5.8 mg/g) (Han et al., 2007a;
 515 Han et al., 2009b; Zhan et al., 2016; Bandowe et al., 2019), suggesting relatively low carbon
 516 emissions in the southern QDB. Average OC and EC levels in QDB (3.48 and 1.41 mg/g,
 517 respectively) are markedly lower than those in Xi'an (7.4 and 7.2 mg/g, respectively), Wuhu (33.26
 518 and 22.49 mg/g, respectively), and Nanchang (25.15 and 11.46 mg/g, respectively) (Han et al., 2009a;
 519 Deng et al., 2014; Zhang, 2014), but significantly higher, particularly for EC, than in Nam Co (0.35
 520 mg/g) (Chen et al., 2015).

521 In urban, TC content (4.75 ± 4.47 mg/g) was marginally lower than the rural level (5.02 ± 3.79
 522 mg/g), although this difference was not statistically significant. Contrasting spatial patterns emerged
 523 for carbon components: EC dominated urban areas (1.46 ± 1.60 mg/g), while OC prevailed in rural
 524 (2.25 ± 1.92 mg/g) (not statistically significant) (Figure 4 and S9). This disparity may be attributed
 525 to the long-term combustion of biomass, coal, and wood in rural settings (Na et al., 2004). It may
 526 also be associated with meteorological conditions, particularly heightened solar radiation resulting

527 from reduced primary emissions in rural areas, which facilitates the formation of SOC (Xu et al.,
 528 2018a; Wang et al., 2019). Overall, the contents of OC and EC showed small difference between
 529 rural (3.73 and 1.33 mg/g, respectively) and urban areas (3.28 and 1.47 mg/g, respectively).

530



531

532 **Figure 4** Concentrations of organic carbon (OC), elemental carbon (EC), secondary organic carbon
 533 (SOC), primary organic carbon (POC), char-EC, soot-EC and OC/EC, char/soot ratios in different
 534 sites (Rural, Urban) and seasonal variations (domestic heating and non-domestic heating period).
 535 Significant differences are indicated by asterisks (* $p < 0.05$; ** $p < 0.01$; *** $p < 0.001$).

536

537 Seasonal analysis revealed elevated carbonaceous compound concentrations, specifically OC
 538 and EC, during the HP (not statistically significant). This increase is primarily due to local domestic
 539 heating activities coupled with adverse meteorological conditions, such as low temperature, weak
 540 winds (Oliveira et al., 2007; Gong et al., 2017), weak atmospheric turbulence, and frequent
 541 atmospheric inversions (Guo et al., 2016). Rural emissions primarily stem from coal and biomass
 542 burning for heating and cooking (Zhang et al., 2000; He et al., 2004), contributing to reduced OC
 543 and EC content in the NHP, whereas elevated EC levels in urban areas are primarily linked to
 544 vehicular and industrial sources. Spatiotemporal transport dynamics show EC depletion during rural
 545 ward pollutant migration due to atmospheric dispersion, particularly affecting coarse particulate
 546 fractions.

547 Notably, rural carbon emissions exceed urban levels in the southern basin, potentially

548 attributable to extended HP duration (7 months) compelling low-grade fuel (crop residues, wood,
549 raw coal and yak dung) utilization (Na et al., 2004). In contrast, urban areas benefit from solar/wind
550 energy infrastructure and government-led clean heating initiatives (suitable electricity for electricity
551 policy), achieving 66.63% clean heating penetration (Statistical Yearbook of Haixi Xizang
552 Autonomous Prefecture of Qinghai Province, 2023), leading to a comparatively lower TC content.

553 The OC/EC ratio is a valuable indicator of carbonaceous aerosol sources. In this study, Urban
554 areas exhibited stable OC/EC ratios ranging from 0.15 to 16.89 (mean = 3.97), whereas rural areas
555 showed significantly higher ratios during NHP (18.58 ± 12.80) compared to HP (7.20 ± 4.99) ($P <$
556 0.001) (Figure 4 and S11). Typically, the OC/EC ratio for vehicle emissions ranges from 0.7 to 2.4,
557 for coal combustion emissions from 0.3 to 7.6, and for biomass burning from 3.8 to 14.5 (Schmidl
558 et al., 2008; Gonçalves et al., 2010; Pio et al., 2011; Popovicheva et al., 2016).

559 These findings suggest that urban OC/EC ratios (0.15-16.89) are primarily associated with
560 vehicle and coal combustion, while rural ratios (0.14-38.25) are predominantly linked to coal and
561 biomass burning. The rural OC/EC ratios are significantly higher than those in urban areas ($P <$
562 0.001), which is consistent with the general distribution pattern of carbonaceous aerosols and
563 reflects a greater contribution of SOC (Zhang et al., 2008; Sandrini et al., 2014). The higher OC/EC
564 ratio typically indicates a greater contribution from biomass combustion; in this study, the OC/EC
565 ratio of rural was 10.99 ± 10.00 , which is significantly lower than values recorded in Nam Co in
566 Xizang (16.3 ± 4.4) (Chen et al., 2015), yet higher than those observed in India (8.47) and Shanxi
567 (0.7-1.6), Beijing (1.9-2.7), and Tianjin rural (2.66) (Zhang et al., 2007; Saud et al., 2013; Cheng et
568 al., 2015; Wang et al., 2021). This finding indicates that carbonaceous aerosols in rural QDB derive
569 from both fossil fuel combustion and biomass burning, with a pronounced influence from the
570 burning of wood, yak dung, and similar biomass fuels, suggesting source specificity.

571

572 3.2.2 Char-EC and Soot-EC

573 Elemental carbon is classified into soot and char (Han et al., 2009b), with char-EC and soot-
574 EC defined as EC1 minus OPC and the sum of EC2 and EC3, respectively (Han et al., 2007). Char-
575 EC is typically produced from biomass burning at relatively low temperatures, whereas soot-EC
576 originates from high-temperature coal combustion and automotive emissions (Zhu et al., 2010; Cao
577 et al., 2013). The char-EC/soot-EC ratio, like the OC/EC ratio, serves as an indicator of carbon

578 aerosol sources. Since char and soot are mainly generated through combustion processes, their ratio
579 is typically influenced by two key factors: the primary emission source and the deposition removal
580 efficiency. For localized PM, such as in urban areas, the removal rate is generally negligible (Han
581 et al., 2009a).

582 Char-EC constitutes 75.88% of rural EC (74.71% HP; 78.84% NHP) and 85.00% of urban EC
583 (85.58% HP; 84.11% NHP) (Figure 4 and S10), demonstrating its dominance across spatial and
584 temporal scales (not statistically significant). Research suggests that char-EC constitutes a larger
585 proportion of coarse PM, while soot-EC is more predominant in fine particles, resulting in extended
586 atmospheric residence times for soot-EC due to reduced deposition velocities (Han et al., 2009b).
587 The increased levels of char-EC during the urban HP are linked to complex sources, including
588 biomass fuel usage and transportation emissions, resulting in elevated char concentrations in urban
589 areas and along busy roadways (Kim et al., 2011).

590 The char/soot ratios for automobile emissions, coal combustion, and biomass burning are 0.60,
591 1.9, and 11.6, respectively (Chow et al., 2004; Chuang et al., 2014). Generally, high-temperature
592 combustion (e.g., vehicle and industrial processes) yields lower char and soot concentrations, while
593 low-temperature combustion (e.g., household cooking and biomass burning) results in higher ratios
594 (Han et al., 2016; Han et al., 2012; Han et al., 2010; Han et al., 2009a). Differences in char/soot
595 ratios between urban and rural areas across seasons may be linked to wheat straw burning,
596 contrasting with minimal vegetation combustion impacts in cities like Xi'an (Cao et al., 2005). The
597 char/soot ratio for dust-fall observed in this study (4.97; Figure 4 and S11) is slightly higher than
598 those recorded in Jinchang (3.84) (Han et al., 2009a) and Daheihe, Inner Mongolia (3.2) (Han et al.,
599 2008). The relatively stable concentration of soot-EC in this study, along with the elevated char/soot
600 ratio, suggests a correlation with higher coal consumption among local residents and industries. This
601 indicates that, in comparison to other regions, carbon emissions in the remote QDB are
602 predominantly sourced from coal and biomass burning, supporting OC/EC ratio findings.
603 Furthermore, the char/soot ratio is elevated during HP (not statistically significant), highlighting the
604 predominant influence of coal and biomass burning in rural areas during HP, while fossil fuel
605 impacts are more pronounced in NHP.

606

607 3.2.3 Primary and secondary organic carbon

608 Aerosol samples with low OC/EC ratios typically exhibit low concentrations of POC, which
609 mainly comprises primary carbonaceous compounds. The MRS method enables discrimination of
610 OC into POC and SOC (Method 2.7.1) (Yoo et al., 2022; Liu et al., 2023). Secondary organic carbon
611 constitutes a dominant fraction of OC in atmospheric aerosols. Research on carbonaceous aerosols
612 in various Chinese cities indicates that SOC contributes 67% (53-83%) and 57% (48-62%) to rural
613 and urban OC, respectively (Zhang et al., 2008), marginally lower than the 72.61% observed in this
614 study (Figure 4 and S12). This is likely because SOC formation relies on solar radiation, the QDB
615 experiences high levels of solar energy (Liu et al., 2017), which may facilitate photochemical
616 oxidation of VOCs into SOC (Hama et al., 2022).

617 During the NHP, rural areas exhibit the highest SOC/OC ratio of 87.32% (Figure S13), while
618 urban areas record the lowest ratio of 52.94% during the HP. This trend reflects elevated potential
619 for photochemical activity and reduced contributions from POC, likely due to local emission sources,
620 such as traffic and coal combustion (Mbengue et al., 2018). The high SOC/OC ratio suggests that
621 SOC largely displaces OC. Our findings indicate that SOC levels are greater in rural areas (78.44%)
622 compared to urban regions (67.78%) (not statistically significant), which consistent with the
623 observation of higher OC/EC ratios in rural areas likely attributable to significant coal consumption
624 for domestic heating, which enhances emissions of semi-volatile organic compounds and organic
625 gases (Dan, 2004). As for seasonal variations, studies in California show an increase in SOC levels
626 during warmer months, which is consistent with our results (Na et al., 2004). This contrasts with the
627 broader observation that higher temperatures typically lead to lower SOC concentrations (Strader et
628 al., 1999; Sheehan and Bowman, 2001). This discrepancy may stem from varying sources of SOC
629 emissions throughout the seasons, necessitating further investigation in conjunction with other
630 carbonaceous indicators.

631 This study conducted a comparative analysis of carbonaceous element concentrations in
632 atmospheric dust-fall and road dust between the QDB and other global regions (Table S4). To ensure
633 data comparability, the selected road dust samples consisted of directly collected in-situ dust without
634 resuspension treatment. The results revealed that the concentrations of TC, OC, and EC in QDB
635 (4.87, 3.48, and 1.41 mg/g, respectively) were significantly lower than those in industrial or urban
636 areas such as Bolu, Turkey; New Delhi, India; and Ezhou, China, and were even lower than many
637 other Chinese cities (Table S4). The low concentrations of OC and EC in QDB indicate minimal

638 anthropogenic pollution influence in this region, and the data can represent the regional background
639 values of carbonaceous components in atmospheric dust-fall in the arid inland areas of East Asia
640 (Chen et al., 2019a). This is crucial for global models assessing the emission fluxes of carbonaceous
641 aerosols from dust source regions. In contrast, extremely high values of carbonaceous elements were
642 found primarily in urban road dust from locations like Bolu, Turkey (TC: 605.2 mg/g), Gwangju,
643 South Korea (TC: 31.97 mg/g), and Xi'an, China (TC: 36.53 mg/g), indicating strong influences
644 from traffic emissions (mainly non-exhaust emissions) (Wei et al., 2015; Lee et al., 2018; Demir et
645 al., 2022). For atmospheric dust-fall in major cities like New Delhi, India, and Wuhan, China, the
646 carbonaceous components are affected by the combination of traffic emissions (diesel vehicle
647 emissions being a major source of EC), industrial activities, and emissions from dense populations
648 (Deng et al., 2014; Zhang, 2014; Zhan et al., 2016; Mishra and Kulshrestha, 2017).

649 The OC/EC ratio in QDB (7.09) is an intermediate level. It is much lower than that in regions
650 dominated by biomass burning, such as Kumasi, West Africa (17.07) and Huainan, China (21.4),
651 but is higher to ratios found in cities like Gwangju, South Korea (5.63) and Ulaanbaatar, Mongolia
652 (5.69)(Lee et al., 2018; Bandowe et al., 2019; Liu et al., 2020). We primarily analyzed the OC/EC
653 ratios in cities across different regions of China to reveal the influence of varying economic
654 development levels.

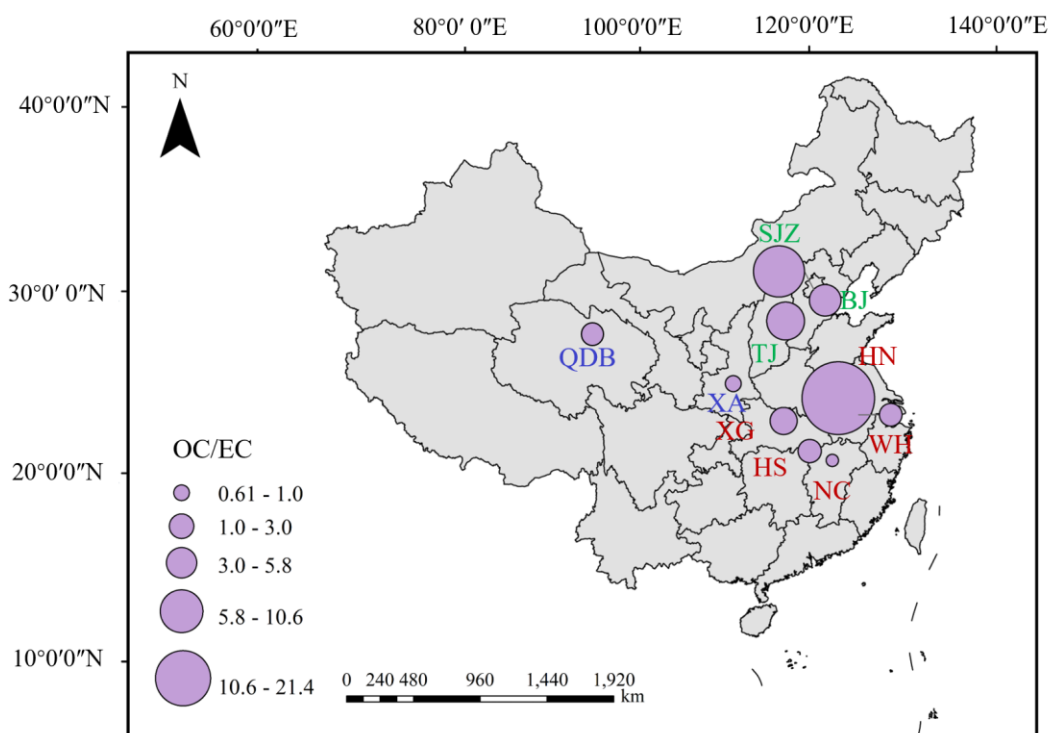
655 Figure 5 presents spatial variations in urban OC/EC ratios across China. The findings reveal
656 that the Northwest region, represented by QDB urban and Xi'an (XA) (Han et al., 2009b), exhibits
657 a significantly lower ratio (2.50 ± 1.47) compared to central regions, including Nanchang (NC)
658 (Zhang, 2014), Huangshi (HS) (Zhan et al., 2016), Wuhu (WH) (Deng et al. 2014), Xiaogan (XG)
659 (Zhan et al., 2022), and Huainan (HN) (Liu et al., 2020), where the ratio is 5.86 ± 7.81 . This ratio is
660 also lower than that observed in eastern cities such as Beijing (BJ) (Tang et al., 2013), Tianjin (TJ)
661 (Ma et al., 2019), and Shijiazhuang (SJZ) (Guo et al., 2018), which have a ratio of 6.83 ± 2.77 . This
662 pattern is consistent with the trends in atmospheric PM OC/EC ratios (Xie et al., 2023), suggesting
663 that the carbon in the dust of the QDB urban primarily results from coal combustion and industrial
664 emissions, leading to elevated EC concentrations and lower OC/EC ratios (Liu et al., 2022).
665 Conversely, cities with higher economic development, such as Beijing and Tianjin, characterized by
666 greater population density and income levels, typically experience secondary pollution, resulting in
667 higher OC/EC ratios.

668 While the MDCO sampler effectively captures dry deposition flux, the reported OC and EC
669 values must be interpreted with specific limitations in mind. First, passive sampling is governed by
670 aerodynamic drag and gravitational settling; therefore, the collected OC is likely skewed toward the
671 coarse fraction (e.g., re-suspended soil, biological debris) while potentially under-representing fine-
672 mode anthropogenic combustion aerosols which have negligible settling velocities. This implies
673 that the OC fluxes reported here should be interpreted as fluxes of deposited particulate OC, not as
674 a direct surrogate for total atmospheric OC. Second, the extended exposure period inherent to
675 passive sampling may lead to negative artifacts due to volatilization. Semi-volatile organic
676 compounds may partition from the particulate to the gas phase, a process accelerated in
677 environments with high solar radiation and ambient temperatures (Turpin et al., 1994).
678 Consequently, the OC fluxes reported here likely represent a conservative lower limit. Finally,
679 environmental factors such as wind speed and humidity affect collection efficiency. High wind
680 speeds can induce turbulence leading to the resuspension of lighter organic particles from the
681 collector, while high humidity may facilitate chemical or biological degradation of the organic
682 fraction prior to laboratory analysis (Chow et al., 2011). Taken together, these processes imply that
683 the OC collection efficiency of the MDCO sampler is not a fixed quantity but varies with
684 temperature, relative humidity, precipitation, wind direction and other environmental factors. The
685 role of these meteorological factors in atmospheric dust deposition is examined in detail in Section
686 3.5.

687 The char/soot ratio in QDB is notably high at 5.04, significantly exceeding that of other regions
688 such as Xi'an (0.99) and Wuhan (0.09) (Wei et al., 2015; Liu et al., 2021). Char-EC primarily
689 originates from incomplete combustion processes like biomass burning and coal combustion. Soot-
690 EC mainly derives from high-temperature combustion sources such as fuel oil and diesel vehicle
691 exhaust (Han et al., 2009). The exceptionally high char/soot ratio in QDB strongly indicates that its
692 limited carbonaceous components predominantly originated from relatively inefficient combustion
693 sources. These potentially included coal or small-scale biomass burning for local
694 residential/expedition activities (e.g., heating, cooking) and possibly long-range transported
695 biomass burning products (e.g., from forest/agricultural fires in South or Southeast Asia) (Han et al.,
696 2009; Han et al., 2006; Han et al., 2016). In contrast, the very low char/soot ratios observed in cities
697 like Wuhan and Xi'an clearly point to traffic source emissions as their primary contributor, a finding

698 likely influenced by the specific focus of those studies on road dust.

699



700

701 **Figure 5** Distribution of OC/EC ratios across various regions of China. Blue designations represent
702 the Northwest region, red indicates the Central region, and green denotes the Eastern region. The
703 circle size reflects the magnitude of the OC/EC ratios.

704

705 However, we fully recognize the fundamental differences in sources and composition between
706 road dust and atmospheric dust-fall. Road dust is primarily secondary dust formed from traffic
707 activities, construction dust, soil particles, and resuspended deposited atmospheric particles, with
708 its carbonaceous composition strongly reflecting intense local anthropogenic emissions (Casotti
709 Rienda and Alves, 2021). In contrast, atmospheric dust-fall integrates contributions from local
710 sources, regional transport, and even long-range transport. Therefore, direct comparison between
711 these two may introduce bias when interpreting regional pollution characteristics and the degree of
712 anthropogenic influence, which cannot be overlooked. Building on this analysis, the next phase of
713 this research will focus on the sampling and analysis of fine atmospheric particulate matter (PM_{2.5}
714 and PM₁) to more accurately elucidate the emission levels and environmental and climatic impacts
715 of carbonaceous aerosols in the QDB.

716

717 **3.3 Trace elements concentration**

718 The total concentration of major (Fe, Si, Al) and trace elements (Ti, Cr, Cd, Cu, Mn, Ni, Pb, V,
719 Zn) was determined to be 8.74 ± 5.82 mg/g, while arsenic (As) remained below the detection limit
720 in all analyzed samples. Crustally derived elements—Fe, Al, Si, and Ti—dominated the elemental
721 profile, aligning with dust composition patterns reported in Ira, Singapore, and Beijing-Hebei
722 regions, China (Joshi et al., 2009; Qiao et al., 2013; Eivazzadeh et al., 2021). In comparison to cities
723 such as Beijing, Shanghai, Xi'an, and Lanzhou, and Junggar Basin the levels of heavy metals in dust
724 from the QDB are relatively low (Jiang et al., 2018) (Supplementary Table S5).

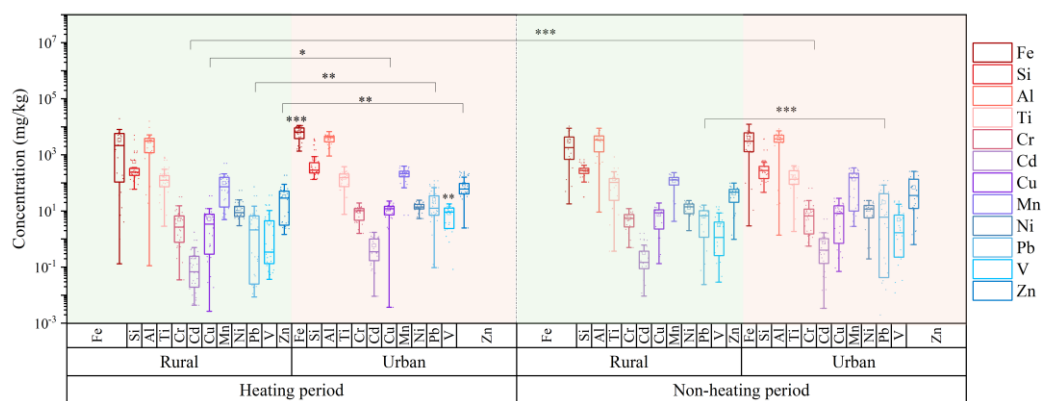
725 The low heavy metal content in dust deposition within the QDB can be attributed to the
726 following factors. The region has sparse human activity, lacks heavy industrial zones and dense
727 urban clusters, resulting in low total anthropogenic emissions of heavy metals. Furthermore, the
728 surface soil in the QDB itself has a low background level of heavy metals, primarily derived from
729 natural sources with relatively weak influence from human activities (Nuralykyzy et al., 2021; Chen
730 et al., 2021). From the meteorological perspectives, the basin's high altitude, strong winds, and arid
731 conditions with minimal precipitation favor the dispersion of atmospheric pollutants. This makes
732 the formation of prolonged stagnant weather conditions unlikely, thereby preventing the
733 accumulation of pollutants and the occurrence of high concentrations near the ground. A particularly
734 unique aspect of the QDB is its role as a significant source of salt dust. The recent study indicates
735 that salt dust emitted from the playa lakes within the basin contributes substantially to atmospheric
736 dust deposition (Zhu et al., 2025). These salt dust particles, composed mainly of soluble salts like
737 NaCl and gypsum, may dilute the relative concentration of non-salt components, such as heavy
738 metals, when released into the atmosphere in large quantities. The combined effect of these factors
739 leads to the observed low heavy metal content in dust deposition in this region.

740 Throughout both the HP and NHP, trace elements concentrations in urban areas were
741 consistently higher than in rural areas (not statistically significant), with the exception of Ti (Figure
742 6 and S14). During the HP, urban levels of Zn, Pb, and Cu were significantly elevated compared to
743 rural areas ($P < 0.05$), and Pb also demonstrated a significant increase in urban during the NHP (P
744 < 0.01). In rural, the differences in metal concentrations between HP and NHP were minimal. In

745 contrast, urban areas exhibited higher concentrations of all elements except for Ti, Cd, and Cr during
 746 the HP, with Fe and V showing notably elevated levels compared to other regions (not statistically
 747 significant). These variations in average concentrations indicate that coal combustion for domestic
 748 heating in urban areas contributes to increased atmospheric heavy metal levels (Duan and Tan, 2013;
 749 Meng et al., 2017). In contrast, Cd and Cr exhibited mixed anthropogenic sources with limited coal
 750 combustion contributions, while Ti concentrations remained stable across seasons, reflecting
 751 minimal anthropogenic influence.

752 Analysis of the carbonaceous components in QDB dust deposition reveals more intensive coal
 753 combustion in rural areas, yet the heavy metal concentrations in atmospheric deposition are lower
 754 than in urban area (not statistically significant). This observation can be explained by the following
 755 factors. First, pollution sources in rural areas are relatively singular, whereas urban areas are
 756 influenced by more complex heavy metal sources. During the heating period, heavy metals in the
 757 rural atmosphere of the QDB mainly originate from coal and biomass combustion. In contrast, urban
 758 areas are affected by a wider range of sources, including industrial activities, traffic emissions, and
 759 others (Liu et al., 2021; Huang et al., 2021a). Additionally, the dense building layout in urban areas
 760 hinders pollutant dispersion, leading to accumulation, while the open terrain in rural areas facilitates
 761 dilution and diffusion. This pattern, where rural heavy metal concentrations (particularly Pb, Cr, Cd,
 762 As, and other elements associated with coal combustion) are lower than those in urban areas during
 763 the heating season, has also been observed in studies conducted in Northeast China, Shanghai,
 764 Taiyuan, the Yangtze River Delta, and Southern Nigeria (Shi et al., 2012; Liu et al., 2021; Huang et
 765 al., 2021a; Liu et al., 2023b; Hilary et al., 2025).

766



767

768 **Figure 6** Concentration of heavy metals by rural and urban settings during domestic heating and

769 non-domestic heating periods. Significant differences are indicated by asterisks (* $p < 0.05$; ** $p <$
770 0.01 ; *** $p < 0.001$).

771

772 **3.4 Source apportionment**

773 We conducted a PMF source apportionment analysis on soluble ions, trace and carbonaceous
774 elements present in dust, specifically focusing on ps-SO₄²⁻, ps-Ca²⁺, ps-K⁺, ps-Mg²⁺, ps-Cl⁻, ps-Na⁺,
775 nps-SO₄²⁻, nps-Ca²⁺, nps-K⁺, nps-Mg²⁺, nps-Cl⁻, nps-Na⁺, Fe, Si, Al, Ti, Cr, Cd, Cu, Mn, Ni, Pb, V,
776 Zn, SOC, POC and char-EC, soot-EC. Seven source factors were identified based on prior research
777 and an understanding of potential local sources: salt lakes, soil, traffic emissions, secondary
778 inorganics, biomass and coal burning, and industrial activities (Figure 7 and S15. A plot of the time
779 series is provided in Figure S16. The generation of Figure 7a involved extracting factors identified
780 as the same source from the PMF factor profiles of each site (Urban and Rural) and each heating
781 season (HP and NHP) shown in Figure S15. The arithmetic mean of the contributions from
782 characteristic species (elements and ions) corresponding to each factor was calculated. Species with
783 average contributions exceeding 20% were defined as characteristic species of that source in
784 atmospheric dust over the QDB.

785 The factor profiles for each element in these source categories represent the arithmetic mean
786 of profiles from six stations, with detailed operational methods provided in Supplementary Text S1.
787 The uncertainty of the source contributions was calculated directly from the standard error of the
788 multiple regression coefficients between the deposition flux (independent variable) and the source
789 contribution (dependent variable) at different monitoring sites (Belis et al., 2015; Manousakas et al.,
790 2017). The regression method assumes that all factors explaining the mass have been identified;
791 however, if a significant portion of the mass not directly related to the species in the PMF analysis
792 is omitted, the source contributions may be overestimated, which could be an important additional
793 source of uncertainty. The results are shown in Table S6. It must be noted that this method captures
794 only a portion of the total uncertainty, as it does not include errors from profile uncertainty or
795 rotational ambiguity. The low errors calculated by this method indicate a good model fit. In this
796 study, the sample numbers used for PMF source apportionment were 690, 780, 480, and 750 for the
797 Urban-NHP, Urban-HP, Rural-NHP, and Rural-HP groups, respectively. Limited sample number can

798 increase the risk of model overfitting, reduce the representativeness of source profiles, and
799 potentially lead to the merging of multiple sources into a mixed factor (Norris et al., 2014). Future
800 research will extend the observation period and increase the sample number to further enhance the
801 reliability of the source apportionment results.

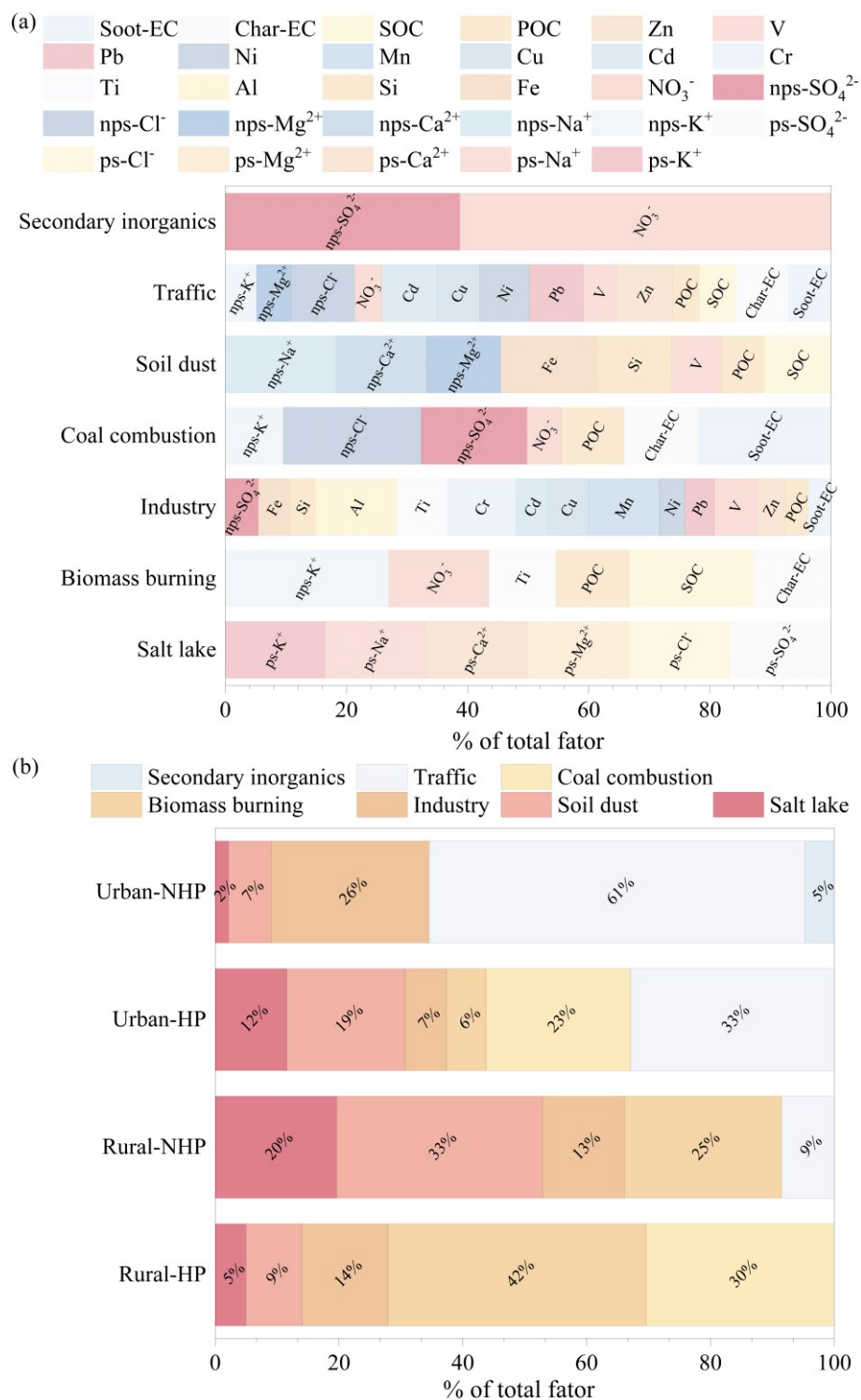
802 The ions $ss\text{-Na}^+$, $ss\text{-Cl}^-$, $ss\text{-SO}_4^{2-}$, $ss\text{-Ca}^{2+}$, $ss\text{-K}^+$, and $ss\text{-Mg}^{2+}$ are widely acknowledged as
803 indicators of sea salt (Ambade et al., 2022; Aswini et al., 2022; Gluscic et al., 2023). In this study,
804 we identified $ps\text{-Cl}^-$ (83.96%), $ps\text{-Ca}^{2+}$ (83.71%), and $ps\text{-SO}_4^{2-}$ (83.71%), $ps\text{-Na}^+$ (83.70%), $ps\text{-Mg}^{2+}$
805 (83.66%), $ps\text{-K}^+$ (82.35%) as key markers of salt lake sources. The contribution of salt lake sources
806 in rural (12.29%) was higher than in urban (6.87%). During the HP, the proportion of salt lake
807 sources in rural areas was 4.97%, compared to 19.61% in the NHP; urban showed contributions of
808 2.16% during the HP and 11.58% in the NHP, showing opposite seasonal trends. Backward
809 trajectory simulations indicated that during the HP, air mass in both urban and rural areas mainly
810 originated from the northwestern part of the basin and the eastern Tarim Basin, whereas during the
811 NHP, they were broadly influenced by the salt lake regions within the basin (Figure S6). The minor
812 wind direction differences and the inter-distributed sampling points (Figure 1), suggests no
813 substantial geographical disparity between urban and rural sites. Additionally, the ion content
814 derived from playa salts in dust deposits increased during the NHP in both areas. Therefore, we
815 propose that the anomalous increase in salt lake contribution during the urban HP may be closely
816 related to human activities. The enhanced Urban Heat Island (UHI) effect and temperature inversion
817 structures during the HP can alter boundary layer height, turbulence, and deposition conditions,
818 thereby increasing the residence time of externally transported particles within the urban boundary
819 layer and elevating their measured contribution (Cichowicz and Bochenek, 2024). Urban heat
820 sources and heating emissions may also modify local transport pathways, leading to more
821 concentrated deposition of dust originating from playa regions over urban areas. Furthermore, dry
822 road surfaces, increased traffic, and construction activities during the HP can promote the
823 resuspension of previously deposited playa dust. The use and subsequent resuspension of road de-
824 icing salts (e.g., NaCl , CaCl_2) may further amplify the contribution of tracer ions indicative of playa
825 salts (Gertler et al., 2006; Casotti Rienda and Alves, 2021).

826 The second factor pertains to soil dust, characterized by trace element such as Fe (47.03%) and
827 Si (36.22%), along with ions such as $nps\text{-Na}^+$ (54.21%), $nps\text{-Ca}^{2+}$ (44.05%), $nps\text{-Mg}^{2+}$ (32.30%),

828 (Pervez et al., 2018; Tian et al., 2021). Additionally, the proportions of elements such as SOC
829 (32.58%) and POC (20.84%) suggest that the dust is likely mixed with fossil fuel emissions.
830 Furthermore, V (24.62%) was detected at multiple sampling sites, indicating contributions from
831 both soil dust and traffic emissions. Mg, Ca²⁺, Al, Si, and Fe are typical tracers for soil dust (Liu et
832 al., 2003; Heo et al., 2009). Notably, the contribution of soil dust in rural areas (21.14%) exceeded
833 that in urban areas (12.97%), indicating that soil dust is a major source of atmospheric deposition.
834 In urban areas, the contribution during the NHP was relatively low (6.84%), likely due to higher
835 wind speeds and the effectiveness of frequent summer precipitation (Zhang et al., 2015a).

836 The third factor is traffic emissions, which are particularly pronounced in urban areas. Key
837 characteristic elements and ions include nps-Cl⁻(56.71%), Zn (50.13%), Cd (49.41%), Pb (47.84%),
838 Ni(44.22%), Cu(37.61%), nps-Mg²⁺ (30.54%), V (29.63%), nps-K⁺ (27.74%), NO₃⁻ (24.35%) and
839 char-EC (46.71%), soot-EC (38.12%), SOC (32.25%), POC (23.72%) (Adeniran et al., 2017). In
840 rural areas, traffic emissions contributed 8.52% to atmospheric deposition during the NHP, whereas
841 in urban areas, the contribution was significantly higher at 46.83%, with 32.91% during the HP and
842 60.75% in the NHP. These findings correlate with previous studies on OC/EC and char/soot ratios,
843 suggesting that carbonaceous elements in the NHP primarily derive from traffic emissions. The
844 traffic emission factor in the QDB represents a mixture of vehicle exhaust and non-exhaust sources
845 (e.g., tire and brake wear, and resuspended road dust). Elements and ions including V, NO₃⁻, Ni, and
846 carbonaceous components primarily associated with vehicle exhaust (Cong et al., 2011; Zhang et
847 al., 2012). For instance, Ni can be emitted from fuel combustion and vehicle exhaust (Pacyna and
848 Pacyna, 2001). In contrast, elements such as Cu, Zn, nps-Mg²⁺, and nps-K⁺ originate from non-
849 exhaust vehicle emissions, including brake and tire wear, as well as the resuspension of road dust
850 (Amato et al., 2014). For example, Zn may derive from the wear of rubber tires on roads (Rogge et
851 al., 1993), Pb emissions may be related to wear (tires/brakes) (Smichowski et al., 2007), and Cu is
852 associated with brake wear (Lin et al., 2015). Furthermore, the presence of crustal elements and ions
853 such as Fe, Si, and nps-Mg²⁺ in the traffic emission factor for Urban-NHP, Urban-HP, and Rural-
854 NHP suggests an additional contribution from resuspended road dust (Chen et al., 2019).

855



856

857 **Figure 7** Factor profile and contributions in urban and rural area. (a) presents the factor profiles,
 858 represented as the arithmetic mean of individual elements across various locations, highlighting
 859 only those elements that constitute more than 20% of each profile. (b) illustrates the contributions
 860 of different sources at each location. [HP, domestic heating period; NHP, non-domestic heating
 861 period].

862

863 The fourth factor is coal combustion, characterized by high concentrations of nps-Cl⁻ (75.40%),
864 nps-SO₄²⁻ (57.87%), nps-K⁺ (31.75%), NO₃⁻ (19.10%), and soot-EC (72.54%), char-EC (40.63%),
865 POC (34.10%) (Kundu and Stone, 2014; Contini et al., 2016). Zhang et al (2023) found that coal
866 combustion emits particles rich in Cl⁻. Coal combustion was more intense at site LTC in rural areas
867 and at site DLX in urban areas. Coal combustion occurs exclusively during the HP, contributing
868 30.38% in rural areas and 23.31% in urban areas. These results align with earlier studies on
869 carbonaceous aerosols, indicating that the carbon content from coal combustion emissions is higher
870 in rural than in urban areas. Consistent with northern China, air pollution in QDB urban has declined
871 due to the adoption of clean heating technologies (Zhang et al., 2021; Xue et al., 2023). However,
872 rural coal combustion remains a major source of carbonaceous aerosols during the HP.

873 The fifth factor, biomass burning, is characterized by significant concentrations of non-
874 precipitating species, including nps-K⁺ (56.99%), NO₃⁻(34.97%), Ti (23.26%) and SOC(43.68%),
875 char-EC (26.78%), POC (25.60%) (Simoneit, 2002; Sulong et al., 2019). K⁺ serves as an important
876 tracer for biomass burning (Cachier and Ducret, 1991). Biomass burning contributes 33.55% to rural
877 atmospheric dust deposition, with a higher proportion during the HP (41.67%) compared to NHP
878 (25.43%). In urban, biomass burning is primarily observed during the HP, contributing only 6.41%.
879 These findings underscore biomass burning as a major source of carbon emissions in rural settings,
880 aligning with the prevalent use of biomass fuels for cooking and domestic heating in Northern
881 China's rural areas (Meng et al., 2019), where 70% to 80% of energy demand are fulfilled by
882 materials such as dung cakes, firewood, charcoal, and crop residues (Tao et al., 2018; Shi et al.,
883 2019). Furthermore, increased biomass burning is also associated with the autumn harvest period
884 (Chen et al., 2017; Li et al., 2021).

885 The sixth factor pertains to industrial emissions, which are characterized by high
886 concentrations of Mn (61.98%), Cr (59.22%), Ti (44.90%), V (37.17%), Cu (34.95%), Cd (28.63%),
887 Fe (27.47%) Pb (25.75%) and Zn (24.03%) (Almeida et al., 2015; Yao et al., 2016). These elements
888 were consistently detected across all sampling sites, alongside Al (71.17%), nps-SO₄²⁻ (28.84%), Si
889 (22.24%) and POC (20.95%), soot-EC (19.97%), which indicate potential contributions from soil
890 dust. Zn, Cu, Fe, and Mn are major chemical components in industrial emission profiles; Cd is a
891 trace element found in metallurgical industries (Xu et al., 2022), while Zn and Mn emitte from oil

892 combustion, metallurgy, and steel manufacturing processes (You et al., 2017). Pb and Cd are
893 associated with metal smelting and processing (Fang et al., 2021). Industrial emissions showed
894 greater contributions during the HP at XZH and at DLX. In rural areas, industrial emissions
895 constitute 13.57% of carbon output, with contributions of 13.95% during the HP and 23.20% during
896 the NHP. In urban areas, industrial emissions account for 16.12% overall, with 6.69% during the HP
897 and 25.55% in the NHP. Due to the abundance of non-ferrous metal resources (e.g., lead-zinc ores),
898 oil, natural gas, and saline minerals (e.g., potassium, lithium) in the QDB, the primary industrial
899 activities are mining and associated chemical industries. Particularly around the GEM and DLX
900 sites, the presence of numerous Pb-Zn, Fe, and Cu mining enterprises leads to significant
901 contributions from industrial emissions to urban dust fallout, making it one of the major sources of
902 air pollution in the basin.

903 The seventh factor is secondary inorganic aerosols, primarily composed of NO_3^- (72.46%), nps-
904 SO_4^{2-} (45.79%), (Liu et al., 2015; Liu et al., 2016a). High mass loadings of NO_3^- and SO_4^{2-} are
905 characteristic of typical secondary inorganic aerosols (Huang et al., 2021). Research indicates that
906 NO_3^- and SO_4^{2-} primarily result from the conversion of gaseous precursors, such as SO_2 and NO_x ,
907 through photochemical reactions, predominantly sourced from local and regional emission (Liu et
908 al., 2015; Tao et al., 2013). Secondary inorganic aerosols are predominantly observed in urban areas
909 during the NHP, where they contribute 4.70% to total aerosol sources. This increase is likely due to
910 elevated temperatures and enhanced solar radiation during this period, which promote
911 photochemical activity (Pandolfi et al., 2010).

912 Dust deposition sources exhibit significant seasonal and spatial variations. In the QDB, coal
913 combustion (26.85%) and biomass burning (24.04%) dominate during HP, transitioning to traffic
914 emissions (34.64%), soil dust (20.04%) and industry emission (19.37%) as the primary contributor
915 in NHP. Rural areas predominantly contribute to dust through biomass burning and coal combustion,
916 as well as natural sources like windblown dust and salt lake emissions. This pattern aligns with
917 increased coal usage for winter domestic heating and heightened biomass burning for cooking and
918 heating in rural areas. In urban, dust deposition is briefly influenced by anthropogenic activities,
919 including traffic and industrial emissions, with minimal contributions from domestic heating. Such
920 differences can be attributed to varying economic development models, industrial and energy
921 structures, and levels of human activity (Kataki et al., 2016).

922 Time series analysis (Figure S16) indicates that atmospheric dust deposition in rural areas
923 primarily originates from natural processes and dispersed anthropogenic combustion due to sparse
924 human activities. During the NHP, the contribution of salt-lake emissions increases in May and June.
925 Strong winds in spring and summer in southern QDB transport saline soil particles, making them a
926 key source of dust deposition (Zhu et al., 2025). Soil-derived dust shows variations highly
927 synchronized with the salt-lake source, with elevated contributions also occurring in May and June,
928 reflecting the natural erosion of exposed surfaces under high wind conditions (Zhang, 2010). Traffic
929 contributions rise noticeably in July and August, likely linked to increased summer tourism and
930 transportation. During the HP, contributions from biomass and coal combustion increase, peaking
931 from November to January. This peak is attributed to the widespread use of biomass fuels such as
932 livestock dung for decentralized heating in rural areas, leading to increased particulate matter
933 emissions (Chen et al., 2023). In contrast, contributions from salt lakes and wind-blown dust
934 decrease significantly, likely due to lower wind speeds and reduced natural source emissions in
935 winter (Jiménez et al., 2018; Li et al., 2019a; Yang et al., 2024).

936 In urban areas, where human activities are more concentrated, pollution sources are dominated
937 by centralized anthropogenic emissions (industry, traffic, and centralized heating), with temporal
938 trends driven by both industrial activity and the heating cycle. During the NHP, industrial
939 contributions increase, especially in towns such as GEM and DLX, where surrounding mining
940 operations constitute a major anthropogenic source (Zhu et al., 2016). Traffic-related contributions
941 follow a trend similar to that in rural NHP, also peaking in July and August, reflecting the common
942 influence of increased vehicle flow during the tourism season. Meanwhile, precursors such as SO₂
943 and NO_x from industrial and traffic emissions undergo photochemical and gas-to-particle conversion
944 under summer sunlight, enhancing the formation of secondary inorganic aerosols (e.g., SO₄²⁻, NO₃⁻)
945 (Zhang et al., 2013; Ma et al., 2017). During the HP, trends in salt-lake emissions, soil dust, and
946 coal/biomass combustion are generally similar to those in rural areas. However, unlike in rural
947 regions, traffic contributions in urban areas continue to increase during the HP, highlighting the
948 higher intensity and less seasonally-variable nature of human activities in towns (Peng et al., 2021).

949 This study observed that the contribution of biomass burning to atmospheric dust deposition in
950 rural areas of the QDB during the HP was higher than that of soil dust. Given that the collected dust
951 samples had particle sizes >10 μm, while biomass burning typically emits aerosols in the submicron

952 range, we propose several potential explanations. Firstly, during the HP, factors such as increased
953 soil moisture and snow cover significantly suppress soil dust emission, resulting in a lower intensity
954 than in other seasons (An et al., 2018; Yang et al., 2019). Simultaneously, biomass and coal burning
955 for heating increases substantially, leading to intense, short-term emissions of fine particles.
956 Although it was fine initially, these high-concentration ultrafine particles can undergo coagulation
957 or coalescence, aggregating with each other or onto pre-existing coarse particles, thereby increasing
958 their size (Butler and Mulholland, 2004; Kulmala et al., 2004; Li et al., 2020). Furthermore, fine
959 particles from biomass burning (e.g., carbonaceous materials) may mix internally with coarse
960 particles like soil dust or salt dust from the QDB, forming internally mixed particles (Li et al., 2003;
961 Hand et al., 2010). During source apportionment, such coarse particles are more likely to be
962 attributed to the biomass burning source. Additionally, the QDB is a significant source of salt dust
963 (Zhu et al., 2025). Salt dust particles (e.g., halite, gypsum) provide excellent condensation nuclei
964 for soluble substances emitted from biomass burning, greatly promoting hygroscopic growth (Li et
965 al., 2003; Kumar, 2010; Wang, 2013). The basin's topography also favors stable inversion layers,
966 inhibiting pollutant dispersion and allowing particles more time to grow, mix, and age in the
967 atmosphere. Prevailing wintertime winds may also transport pollutants from surrounding regions
968 into the basin.

969 Moreover, the dust in this study was collected using a passive sampler. Over 90% of the
970 collected dust particles were smaller than 100 μm , with approximately 25% less than 10 μm (Figure
971 S2), indicating the presence of fine particles ($<10 \mu\text{m}$), albeit in a relatively small proportion. The
972 particle size distribution of atmospheric dust deposition is similar to that of TSP, with both primarily
973 consisting of particles smaller than 100 μm . Using PMF source apportionment, this study identified
974 a notably high contribution from biomass burning in rural areas, particularly during the heating
975 period. Similarly, studies on atmospheric TSP in Iran (Ashrafi et al., 2018), the Qinghai-Xizang
976 Plateau (Lulang) (Zhao et al., 2013), Northeast China (Jia et al., 2024), and Qingdao (Liu et al.,
977 2022) have also reported significant contributions from biomass and coal combustion. This suggests
978 that contributions from biomass and coal combustion can indeed be observed in particles larger than
979 10 μm . Finally, the PMF model may have uncertainties in resolving sources with similar chemical
980 profiles. If the chemical compositions of local soil dust and biomass burning particles overlap after
981 long-range transport and complex atmospheric reactions, the model might not fully separate them

982 (Cesari et al., 2016).

983

984 **3.5 Influence of meteorological factors**

985 Meteorological parameters critically influence the accumulation and dispersion of airborne
986 pollutants. To examine their impact on the chemical composition of dust deposition in this study,
987 monthly data for temperature, humidity, precipitation, wind speed and direction, sunshine duration,
988 frequency of visibility ≤ 10 km were obtained from four monitoring stations (XZH, GEM, NMH,
989 DLX) during the study period (Table 1 and Figure S17). Data from the LTC and BLX sites were
990 excluded from this analysis due to a lack of on-site meteorological instrumentation.

991 Based on ANOVA results, wind speed and temperature were significantly higher during the
992 NHP ($P < 0.05$), promoting dust emission and consequently increasing atmospheric dust flux
993 (Jiménez et al., 2018; Li et al., 2019b; Yang et al., 2024). However, at DLX, wind speed showed no
994 significant seasonal difference, while precipitation and relative humidity were significantly higher
995 in the NHP ($P < 0.05$). Since precipitation is a known suppressor of dust deposition (Li et al., 2019b),
996 meteorological factors were not the primary driver of the elevated dust flux at DLX during the NHP
997 (Figure S18); other factors, such as increased tourism, likely played a more important role.
998 Additionally, correlation analysis revealed that dust and salt dust flux were positively correlated
999 with the frequency of visibility ≤ 10 km and wind speed ($P < 0.05$) and negatively correlated with
1000 relative humidity ($P < 0.05$), consistent with previous findings (Wei et al., 2023).

1001 Pearson correlation analysis further elucidated the relationships between dust chemical
1002 components and meteorological parameters. Ions derived from salt lake (ps ions) and crustal
1003 elements (e.g., Al) showed significant correlations with wind direction and speed ($P < 0.05$, Figure
1004 S19), indicating the dominant control of wind on the emission and transport of both playa salt and
1005 soil dust. During the HP in both rural and urban areas, relative humidity was negatively correlated
1006 with ps ions and crustal elements ($P < 0.05$), suggesting that higher humidity promotes the removal
1007 of airborne particles (Deshmukh et al., 2011). Playa salt ions are hygroscopic, so higher relative
1008 humidity facilitates their deliquescence (Rörig-Dalgaard, 2021). The mean annual relative humidity
1009 in the QDB (about 34 %RH) is notably lower than Wuhan (75.4 %RH) (Zang et al., 2021), Handan
1010 (63.35 %RH) (Meng et al., 2016), Pearl River Delta region (67.05 %RH) (Yue et al., 2015), Jorhat,

1011 India (80.29 %RH) (Rabha et al., 2021) and other regions, providing favorable conditions for the
 1012 long-range transport of salt-lake-derived particles.

1013

1014 **Table 1** Meteorological conditions at the monitoring stations during the sampling periods.

Site	Period	Temperature (°C)	Relative humidity (%)	Precipitation (mm·d ⁻¹)	Wind speed (m·s ⁻¹)	Wind direction	Sunshine duration (h·m ⁻¹)	Frequency of visibility ≤10 km
Whole		4.27 ± 10.58	33.56 ± 5.74	2.63 ± 3.64	3.29 ± 0.63	WNW	237.73 ± 26.86	36.52 ± 15.27
XZH	HP	-3.16 ± 6.30	33.57 ± 6.36	1.47 ± 2.95	2.93 ± 0.49	WNW	240.58 ± 25.04	41.19 ± 16.61
	NHP	15.65 ± 2.86	33.54 ± 4.63	4.41 ± 3.97	3.83 ± 0.40	W	233.55 ± 28.82	29.36 ± 9.10
Whole		5.76 ± 9.80	31.22 ± 5.39	3.07 ± 4.03	1.94 ± 0.43	W	237.44 ± 30.10	65.89 ± 26.78
GEM	HP	-0.91 ± 5.94	30.38 ± 5.58	1.78 ± 1.69	1.75 ± 0.35	W	233.03 ± 30.95	83.54 ± 14.18
	NHP	16.45 ± 2.83	32.57 ± 4.38	6.1 ± 4.77	2.24 ± 0.36	W	244.21 ± 27.40	37.65 ± 15.71
Whole		5.42 ± 10.01	33.03 ± 6.99	2.93 ± 4.05	1.53 ± 0.39	WNW	221.93 ± 23.79	78.58 ± 16.21
NMH	HP	-1.57 ± 6.08	30.23 ± 6.09	0.54 ± 1.14	1.70 ± 0.37	W	218.58 ± 20.84	88.75 ± 8.04
	NHP	16.13 ± 2.77	37.32 ± 6.04	6.59 ± 4.17	1.29 ± 0.30	WNW	226.84 ± 26.79	62.99 ± 12.84
Whole		3.32 ± 9.07	38.24 ± 8.48	18.45 ± 23.90	2.40 ± 0.35	WNW	254.63 ± 56.83	33.69 ± 12.3
DLX	HP	-3.08 ± 5.39	34.04 ± 6.26	7.12 ± 8.89	2.42 ± 0.33	WNW	260.09 ± 49.28	34.5 ± 11.45
	NHP	13.12 ± 2.78	44.68 ± 5.95	35.83 ± 29.34	2.38 ± 0.35	W	230.33 ± 32.44	32.45 ± 11.98

1015 Note: HP = heating period; NHP = non-heating period.

1016

1017 For nps ions, nps-Cl⁻ (a tracer of coal combustion) during the HP was positively correlated
 1018 with wind direction ($P < 0.05$, Figure S19), indicating downwind transport. In contrast, nps-K⁺ (a
 1019 tracer of biomass burning) was negatively correlated with wind speed and solar radiation ($P < 0.05$),
 1020 consistent with the observed peak in combustion contributions during winter when solar radiation
 1021 is the lowest. Increased wind speed may suppress biomass-burning intensity (Zhang, 2024), while
 1022 higher solar radiation can reduce smoldering-phase nps-K⁺ emissions and enhance photochemical
 1023 removal of aerosols (Kuang et al., 2020; Huang and Gao, 2021).

1024 For carbonaceous components (Figure S20), in the rural NHP, soot-EC, OC, and the char/soot
 1025 ratio were positively correlated with precipitation and negatively with the frequency of visibility

1026 ≤ 10 km ($P < 0.05$). In the rural HP, the char/soot ratio was positively correlated with precipitation.
1027 In the urban NHP, char-EC, soot-EC, and their ratios showed positive correlations with humidity
1028 and precipitation ($P < 0.01$), while POC was positively correlated with the frequency of visibility
1029 ≤ 10 km ($P < 0.01$). Total carbon, OC, and SOC were negatively correlated with wind speed ($P <$
1030 0.05). In the urban HP, EC and char-EC were negatively correlated with the frequency of visibility
1031 ≤ 10 km; POC was positively correlated with wind speed and solar radiation but negatively with the
1032 frequency of visibility ≤ 10 km ($P < 0.05$); and the char/soot ratio was positively correlated with
1033 wind speed and negatively with the frequency of visibility ≤ 10 km ($P < 0.01$).

1034 Overall, wind speed was negatively correlated with TC, OC, SOC, POC, and the char/soot ratio
1035 ($P < 0.05$). This pattern aligns with findings from Xi'an (Cao et al., 2009), New Delhi (Tiwari et al.,
1036 2015), and Karachi (Bibi et al., 2017), although it was not observed in rural areas (Sharma et al.,
1037 2002). Increased wind speed enhances ventilation, promoting aerosol dispersion and reducing
1038 carbonaceous aerosol concentrations (Saha and Despiaiu, 2009). The low mean wind speed (about
1039 2.30 m/s) may also indicate that carbon emissions are predominantly local rather than distant sources
1040 (Shen et al., 2021). Positive correlations of precipitation and relative humidity with soot-EC,
1041 char-EC, OC, and the char/soot ratio likely reflect the hygroscopic nature of carbonaceous aerosols:
1042 under humid conditions, particles absorb water, increase in mass, and undergo accelerated dry
1043 deposition. For instance, PM_{2.5} deposition rates can increase 2-3 fold as relative humidity rises from
1044 30% to 70%, thereby shortening their atmospheric residence time (Wu et al., 2016). The negative
1045 correlations of EC, char-EC, and POC with the frequency of visibility ≤ 10 km align with findings
1046 in cities such as Suzhou (Zhang et al., 2010) and Beijing (Kong et al., 2021), attributable to the
1047 strong light-absorbing (EC) and light-scattering (OC) properties of these components, which jointly
1048 enhance atmospheric extinction and reduce visibility (Zhang et al., 2010; Kong et al., 2021). Weaker
1049 correlations in rural areas indicate that carbonaceous components are less influenced by local
1050 meteorological dilution and removal processes, pointing to more complex source influences.

1051 In summary, seasonal variations in atmospheric dust deposition result from the combined
1052 effects of meteorological conditions and anthropogenic emissions. In urban areas, meteorological
1053 factors, especially wind speed and relative humidity, play a dominant role in the dispersion and
1054 removal of local anthropogenic pollutants. In rural areas, dust composition is more strongly
1055 influenced by large-scale wind-driven dust transport and regional combustion activities.

1056 Wind direction analysis provides a valuable supplement to the PMF model (Watson et al., 2008).
1057 Studies have shown that emissions from sources such as traffic, biomass burning, coal combustion,
1058 and salt lakes exhibit significant directional patterns, which can be effectively visualized using polar
1059 plots (Saraga et al., 2021). In this study, bivariate polar plots were generated for the concentrations
1060 of POC, SOC, char-EC, soot-EC, and selected ions/elements (Figure S21-S24), as well as for the
1061 source contributions resolved by the PMF model (Figure S25 and S26), to illustrate their directional
1062 provenance. Notably, the directional patterns of the various aerosol components exhibited distinct
1063 differences and did not fully align with the local prevailing wind directions.

1064 The polar plots of key tracer ions and elements (Figure S21-S24) showed patterns consistent
1065 with the corresponding PMF-resolved source factors (Figure S25 and S26), supporting the validity
1066 of the source apportionment. Specifically, the following pairs showed similar directional
1067 distributions: Total-ps and the salt-lake source; nps-K⁺, POC, and char-EC with biomass burning;
1068 nps-Ca²⁺ and Si with soil dust; nps-SO₄²⁻, nps-Cl⁻, and SOC with coal combustion; Fe and Cd with
1069 industry; Ni and Zn with vehicle combustion; Fe and Al with industry; and nps-SO₄²⁻ together with
1070 NO₃⁻ with secondary formation. These spatial consistencies reinforce that the selected chemical
1071 tracers are associated with their respective PMF-identified sources.

1072 Wind speeds in rural areas are generally higher than those in urban environments, with
1073 predominant wind directions between west (W) and north (N), indicating the potential long-distance
1074 transport of pollutants. Specifically, emissions from saline lakes primarily originate from the west-
1075 northwest (WNW) direction. Back trajectory modeling suggests that HP levels are mainly attributed
1076 to salt lake emissions from the northwestern QDB, while in NHP, sources include long-distance
1077 transport from salt lakes in the Tarim Basin (Figure S6, S7). For industrial emissions during the HP,
1078 sources primarily originate from medium- to short-distance transport in the W direction, with NHP
1079 periods showing contributions from both the west (W) and northwest-northwest (NNW) directions.
1080 In contrast, soil dust in HP is predominantly sourced from long-distance transport from the W
1081 direction, whereas in NHP, it is largely of local origin. Biomass burning during HP mainly arises
1082 from local sources, while its contribution during NHP is minimal and comes from both local and
1083 long-distance transport, consistent with PMF results.

1084 In urban areas, lower wind speeds and varying dominant wind directions between the HP and
1085 NHP lead to different sources of pollutants. During HP, emissions from saline lakes and coal

1086 combustion primarily originate from short-distance transport in the WNW direction, while biomass
1087 burning is sourced from the W. In contrast, industrial emissions, soil dust, and vehicle combustion
1088 are predominantly attributed to local sources. In NHP, pollutants demonstrate a dispersion trend
1089 from their sources to urban areas. Industrial emissions primarily come from the WNW to north-
1090 northeast (NNE) directions, soil dust from the southwest (SW), and vehicle emissions from the W
1091 direction. Notably, both salt lake and secondary formation sources exhibit similar directional
1092 patterns, indicating a common origin from the SW direction. The presence of processing enterprises
1093 near salt lakes suggests that secondary aerosols may form from emitted SO₂ and NO₂ (Hewitt, 2001).
1094 These findings align with previous analyses showing that urban industrial and traffic emissions
1095 mainly derive from local sources, while coal and biomass burning predominantly originate from
1096 surrounding rural areas, corroborating the role of nearby soil sources in salt lake and soil emissions.
1097

1098 **3.6 Environmental implication**

1099 The source apportionment analysis using the PMF model indicates that in the QDB, rural dust-
1100 fall predominantly originates from the combustion of solid fuels, including firewood, yak dung, and
1101 coal, accounting for approximately 72.05% of the total contribution. This proportion significantly
1102 exceeds contributions reported for rural areas in Beijing (41%) (Hua et al., 2018), Agra (54.3%)
1103 (Agarwal et al., 2020), and Beihai, Guangxi Province (66.7%) (Zhang et al., 2019).

1104 The higher contribution in this study likely reflects the local energy profile, as the sampling
1105 site in Haixi Mongol and Xizang Autonomous Prefecture, Qinghai Province, primarily relies on coal,
1106 yak dung, and firewood, constituting 58%, 23.5%, and 13% of rural energy consumption,
1107 respectively (Jiang et al., 2020; Shen et al., 2021). In contrast, solid biomass fuels, including wood
1108 and yak dung, account for over 70% of rural household energy consumption in Xizang, with yak
1109 dung alone representing 53% (Liu et al., 2008; Xiao et al., 2015). Similar patterns emerge in South
1110 and Central Asia, where biomass fuels dominate residential heating (firewood: 39%; dung: 29%)
1111 (Amacher et al., 1999; Heltberg et al., 2000; Hoeck et al., 2007; Foysal et al., 2012; Behera et al.,
1112 2015; Kerimray et al., 2018). In northern China, rural domestic heating primarily relies on coal
1113 (46%), firewood (23.8%), and electricity (15.1%) (Tao et al., 2018), further highlighting the unique
1114 energy composition of QDB.

1115 Recent studies have shown that South Asia, Central Asia, and Xizang contribute significantly
1116 to high concentrations of atmospheric PM, particularly BC, which accelerates glacier melting in the
1117 QXP (Ming et al., 2010; Xia et al., 2011; Chen et al., 2015). The QDB is recognized as a significant
1118 dust source affecting the glacier surfaces on the QXP, although it is often overlooked (Dong et al.,
1119 2014; Wei et al., 2017; Zheng et al., 2021). Compared to other dust sources, the QDB exhibits higher
1120 emissions from coal combustion, giving it a unique influence on the QXP. The organic matter and
1121 pollutants, such as PAHs, released from household solid fuel combustion, particularly coal (98%)
1122 and dung (94%), are substantially higher than those from firewood (Leavey et al., 2017; Secrest et
1123 al., 2017; Ye et al., 2020). Consequently, the impact of PM from coal combustion in the QDB on
1124 the QXP is significant. Specifically, the presence of BC in PM increases glacier albedo, accelerating
1125 the melting of glaciers and snow in the region (Kang et al., 2020) and impacting global freshwater
1126 resources (Huss and Hock, 2018). Additionally, BC enhances cloud condensation nuclei, ice number
1127 concentration, and cloud cover (Zhou et al., 2025), thereby influencing global climate change.
1128 Furthermore, coal combustion releases harmful emissions, including CO₂, NO_x, CO, SO₂ and sulfur
1129 trioxide (Munawer, 2018), adversely affecting local human health and exacerbating climate
1130 warming on the QXP (Liu et al., 2006; Li et al., 2023), with broader implications for global climate.
1131 Therefore, the atmospheric pollutants emission of the QDB deserves considerable attention.
1132 However, this study focuses primarily on larger particles, indicating a need for further research on
1133 the environmental impacts of carbonaceous aerosols in atmospheric PM within the QDB.

1134 In addition to the distinctive energy consumption structure in the rural QDB, which leads to
1135 significant contributions from coal and biomass burning during HP, atmospheric dust deposition in
1136 the QDB during the NHP primarily originates from traffic and industrial emissions. The contribution
1137 from traffic emissions during the NHP was twice that during the HP. Considering the larger particle
1138 size of the dust samples collected in this study, the traffic-related dust is likely derived mainly from
1139 vehicle non-exhaust emissions, such as road dust (Gondwal and Mandal, 2021). This indicates that
1140 NHP atmospheric conditions are significantly influenced by resource development and tourism.
1141 Sampling sites, such as Qarhan Salt Lake, along with GEM and LTC stations within approximately
1142 100 km (Figure 1), suggest that salt lake resource extraction has a lower impact on regional aerosols
1143 than traffic emissions, despite salt lakes being the primary resource. This is likely because salt lake
1144 development mainly involves solar evaporation and chemical processes like extraction and

1145 adsorption, which emit fewer pollutants compared to other mining methods (Zhen, 2010).
1146 Consequently, salt lake resource exploitation exerts a relatively minor effect on local atmospheric
1147 carbonaceous aerosol.

1148 Similar salt lakes with comparable environments to QDB, such as Salar de Uyuni in Bolivia,
1149 the Atacama Salt Lake in Chile, and Ombre Muerto in Argentina, are rich in lithium resources (Li
1150 et al., 2014), making them focal points for resource development. Additionally, Salar de Uyuni, the
1151 Atacama Salt Lake, Junggar Basin, and the Great Salt Lake are renowned tourist destinations. This
1152 suggests that, in arid basin salt lakes with similar climates and intensive human activity, atmospheric
1153 carbonaceous aerosols are likely influenced by resource exploitation and tourism, especially tourism.
1154 The study's findings can inform policy decisions regarding unexploited salt lakes in South America,
1155 such as Ombre Muerto and Salar de Uyuni. However, while QDB also hosts mineral resources such
1156 as copper, iron, and tin, this research focused on larger particles ($>100\ \mu\text{m}$), which are more
1157 indicative of local sources. Given that sampling was conducted around the salt lakes, potential
1158 impacts from other mineral resource developments may have been underestimated. Further research
1159 is necessary to fully assess the environmental effects of carbonaceous aerosols in QDB atmospheric
1160 particles.

1161 In conclusion, the localized source profiles developed in this study, such as OC/EC ratios for
1162 heating-period emissions and key heavy-metal tracers, provide critical input parameters for regional
1163 climate and air quality models. This enables more accurate simulation of the emission, transport,
1164 and deposition of carbonaceous aerosols in the QDB and supports quantitative assessment of their
1165 contribution to glacier retreat on the QXP. Based on that rural areas in arid and semi-arid basins
1166 such as QDB rely heavily on solid fuels for heating, with associated environmental impacts, we
1167 recommend that local governments implement targeted clean-energy transition policies. These
1168 should prioritize promoting clean heating alternatives (e.g., solar and electric heating) in rural
1169 regions, supported by financial subsidies and technical assistance. Simultaneously, the adoption of
1170 clean stoves and upgraded biomass fuels should be encouraged to reduce emissions from traditional
1171 biomass and coal combustion (Dickinson et al., 2015; Li et al., 2011; Shen et al., 2017). Given the
1172 close climatic and environmental linkage between QDB and QXP, we further propose integrating
1173 air pollution control in QDB into the broader environmental protection framework of QXP.
1174 Establishing a joint regional air pollution prevention and control mechanism for the “QDB–QXP”

1175 system would help align emission reduction in the basin with glacier protection goals on the plateau.
1176 To strengthen the scientific foundation of such a mechanism, future studies should focus on
1177 clarifying the key transport pathways, transformation processes, and quantitative impacts of air
1178 pollutants from QDB to QXP glaciers.

1179

1180 **4. Conclusion**

1181 This study analyzed the composition of dust deposition at six sampling sites in the southern
1182 QDB from January 2020 to March 2023 and examined DF, soluble ions, trace and carbonaceous
1183 element content in urban and rural samples during both domestic heating and non-domestic heating
1184 periods. Through integrated application of backward trajectory modeling, PMF, and carbon
1185 speciation indices, we identified dominant dust sources and evaluated domestic heating impacts on
1186 atmospheric processes in remote regions.

1187 The findings revealed that DF and carbon emissions were significantly higher in rural than in
1188 urban areas. Among carbon indicators, urban areas exhibited elevated EC levels (1.46 ± 1.60 mg/g),
1189 while OC levels were higher in rural (3.73 ± 2.61 mg/g). Economic development increase OC/EC
1190 ratios, but they are driven by different intrinsic factors. Char-EC was the dominant contributor to
1191 EC (80.44%), with urban char-EC levels (85.00%) showing a notable increase compared to rural
1192 levels (75.88%). Secondary organic carbon was the principal contributor to OC (72.61%), with rural
1193 SOC levels surpassing (78.44%) those in urban areas (67.78%). The OC/EC and char-EC/soot-EC
1194 ratios, along with PMF results, indicated that during HP, dust deposition in the QDB was primarily
1195 derived from coal combustion (26.85%) and biomass burning (24.04%), while traffic emissions
1196 accounted for 34.64% of dust during NHP. Coal and biomass burning were the main contributors to
1197 rural dust, strongly influenced by domestic heating, whereas urban dust predominantly originated
1198 from traffic (46.83%) and industrial emissions (16.12%). Compared to other dust sources in the
1199 QXP, coal consumption in the QDB is higher during the domestic heating period. The resulting
1200 emissions of BC and greenhouse gases may exacerbate glacier melting in the region, warranting
1201 increased attention. Given the distinctive carbonaceous aerosol signatures identified in the QDB,
1202 we recommend prioritizing their radiative forcing effects in regional environmental policymaking
1203 and climate modeling frameworks. Furthermore, findings of this study offer a valuable scientific

1204 basis for understanding atmospheric carbonaceous aerosols in arid basins and salt lake regions with
1205 climates similar to QDB. They can particularly inform policy decisions regarding unexploited salt
1206 lakes in South America, such as Ombre Muerto and Salar de Uyuni.

1207 However, this study primarily focused on larger-scale PM and examined the effects of heating
1208 on carbonaceous aerosols in the QDB. It lacks an investigation of aerosols with smaller particle
1209 sizes (e.g., PM₁₀, PM_{2.5}, PM₁), which is essential for a comprehensive understanding of
1210 carbonaceous aerosol characteristics in this unique region. Furthermore, in addition to offline
1211 observations, future research should incorporate online observations with high spatiotemporal
1212 resolution and utilize numerical air quality models such as CMAQ, CAMx, WRF-CHEM, and
1213 NAQPMS to analyze the spatiotemporal distribution and future trends of carbon aerosols in the
1214 QDB.

1215

1216 **Author contribution**

1217 HZ: Conceptualization, data curation, formal analysis, funding acquisition, investigation,
1218 methodology, project administration, validation, writing – original draft.

1219 LZ: Data curation, formal analysis, methodology.

1220 SZ: funding acquisition, validation, writing – review & edited.

1221 XZ: Supervision, conceptualization, funding acquisition, writing – review & edited.

1222

1223 **Acknowledgements**

1224 This research was funded by Major Science and Technology Project of Gansu Province
1225 (24ZD13FA003), and by Qinghai Provincial Innovation Platform Construction Special Program
1226 (Project No. 2024-ZJ-J03), and supported by Qinghai Provincial Key Laboratory of Geology and
1227 Environment of Salt Lakes (No. The Science and Technology Plan Project of Qinghai Province
1228 Incentive Fund 2024).

1229

1230 **Declaration of competing interest**

1231 The authors declare that there is no conflict of interest.

1232

1233 **Data availability**

1234 Datasets for this research has been uploaded in Zenodo and is available at
1235 <https://doi.org/10.5281/zenodo.14382853> (Zhu, 2024).

1236 **Reference**

- 1237 Abdollahi, S., Karimi, A., Madadi, M., Eslamian, S., Ostad-Ali-Askari, K., and Singh, V. P.: Lead
1238 concentration in dust fall in Zahedan, Sistan and Baluchistan Province, Iran, *Journal of Geography*
1239 and *Cartography*, 4, 6, <https://doi.org/10.24294/jgc.v4i2.601>, 2021.
- 1240 Adeniran, J. A., Yusuf, R. O., and Olajire, A. A.: Exposure to coarse and fine particulate matter at and
1241 around major intra-urban traffic intersections of Ilorin metropolis, Nigeria, *Atmospheric*
1242 *Environment*, 166, 383-392, <https://doi.org/10.1016/j.atmosenv.2017.07.041>, 2017.
- 1243 Agarwal, A., Satsangi, A., Lakhani, A., and Kumari, K. M.: Seasonal and spatial variability of secondary
1244 inorganic aerosols in PM_{2.5} at Agra: Source apportionment through receptor models, *Chemosphere*,
1245 242, 125132, <https://doi.org/10.1016/j.chemosphere.2019.125132>, 2020.
- 1246 Aiken, A. C., DeCarlo, P. F., Kroll, J. H., Worsnop, D. R., Huffman, J. A., Docherty, K. S., Ulbrich, I. M.,
1247 Mohr, C., Kimmel, J. R., Sueper, D., Sun, Y., Zhang, Q., Trimborn, A., Northway, M., Ziemann, P.
1248 J., Canagaratna, M. R., Onasch, T. B., Alfarra, M. R., Prevot, A. S. H., Dommen, J., Duplissy, J.,
1249 Metzger, A., Baltensperger, U., and Jimenez, J. L.: O/C and OM/OC ratios of primary, secondary,
1250 and ambient organic aerosols with High-Resolution Time-of-Flight Aerosol Mass Spectrometry,
1251 *Environmental Science & Technology*, 42, 4478-4485, <https://doi.org/10.1021/es703009q>, 2008.
- 1252 Almeida, S. M., Lage, J., Fernández, B., Garcia, S., Reis, M. A., and Chaves, P. C.: Chemical
1253 characterization of atmospheric particles and source apportionment in the vicinity of a steelmaking
1254 industry, *Science of The Total Environment*, 521-522, 411-420,
1255 <https://doi.org/10.1016/j.scitotenv.2015.03.112>, 2015.
- 1256 Alzahrani, A. J., Alghamdi, A. G., and Ibrahim, H. M.: Assessment of soil loss due to wind erosion and
1257 dust deposition: Implications for sustainable management in arid regions, *Applied Sciences*, 14(23),
1258 10822, <https://doi.org/10.3390/app142310822>, 2024.
- 1259 Amacher, G. S., Hyde, W. F., and Kanel, K. R.: Nepali fuelwood production and consumption: Regional
1260 and household distinctions, substitution and successful intervention, *The Journal of Development*
1261 *Studies*, 35, 138-163, <https://doi.org/10.1080/00220389908422584>, 1999.
- 1262 Ambade, B., Sankar, T. K., Sahu, L. K., and Dumka, U. C.: Understanding sources and composition of
1263 black carbon and PM_{2.5} in urban environments in East India, *Urban Science*, 6(3), 60,
1264 <https://doi.org/10.3390/urbansci6030060>, 2022.
- 1265 Amato, F., Alastuey, A., de la Rosa, J., Gonzalez Castanedo, Y., Sánchez de la Campa, A. M., Pandolfi,

1266 M., Lozano, A., Contreras González, J., and Querol, X.: Trends of road dust emissions contributions
1267 on ambient air particulate levels at rural, urban and industrial sites in southern Spain, *Atmospheric*
1268 *Chemistry and Physics*, 14, 3533-3544, <https://doi.org/10.5194/acp-14-3533-2014>, 2014.

1269 Arimoto, R., Duce, R. A., Savoie, D. L., Prospero, J. M., Talbot, R., Cullen, J. D., Tomza, U., Lewis, N.
1270 F., and Ray, B. J.: Relationships among aerosol constituents from Asia and the North Pacific during
1271 PEM-West A, *Journal of Geophysical Research: Atmospheres*, 101, 2011-2023,
1272 <https://doi.org/10.1029/95JD01071>, 1996.

1273 Ashrafi, K., Fallah, R., Hadei, M., Yarahmadi, M., and Shahsavani, A.: Source apportionment of Total
1274 Suspended Particles (TSP) by Positive Matrix Factorization (PMF) and Chemical Mass Balance
1275 (CMB) modeling in Ahvaz, Iran, *Archives of Environmental Contamination and Toxicology*, 75,
1276 278-294, <https://doi.org/10.1007/s00244-017-0500-z>, 2018.

1277 Bandowe, B. A. M., Nkansah, M. A., Leimer, S., Fischer, D., Lammel, G., and Han, Y.: Chemical (C, N,
1278 S, black carbon, soot and char) and stable carbon isotope composition of street dusts from a major
1279 West African metropolis: Implications for source apportionment and exposure, *Science of The Total*
1280 *Environment*, 655, 1468-1478, <https://doi.org/10.1016/j.scitotenv.2018.11.089>, 2019.

1281 Barjoe, S. S., Abadi, S. Z. M., Elmi, M. R., Varaoon, V. T., and Nikbakht, M.: Evaluation of trace
1282 elements pollution in deposited dust on residential areas and agricultural lands around Pb/Zn
1283 mineral areas using modified pollution indices, *Journal of Environmental Health Science and*
1284 *Engineering*, 19, 753-769, <https://doi.org/10.1007/s40201-021-00643-8>, 2021.

1285 Behera, B., Rahut, D. B., Jeetendra, A., and Ali, A.: Household collection and use of biomass energy
1286 sources in South Asia, *Energy*, 85, 468-480, <https://doi.org/10.1016/j.energy.2015.03.059>, 2015.

1287 Belis, C. A., Pernigotti, D., Karagulian, F., Pirovano, G., Larsen, B. R., Gerboles, M., and Hopke, P. K.:
1288 A new methodology to assess the performance and uncertainty of source apportionment models in
1289 intercomparison exercises, *Atmospheric Environment*, 119, 35-44,
1290 <https://doi.org/10.1016/j.atmosenv.2015.08.002>, 2015.

1291 Bibi, S., Alam, K., Chishtie, F., Bibi, H., and Rahman, S.: Temporal variation of Black Carbon
1292 concentration using Aethalometer observations and its relationships with meteorological variables
1293 in Karachi, Pakistan, *Journal of Atmospheric and Solar-Terrestrial Physics*, 157-158, 67-77,
1294 <https://doi.org/10.1016/j.jastp.2017.03.017>, 2017.

1295 Bond, T. C. and Bergstrom, R. W.: Light absorption by carbonaceous particles: An investigative review,

1296 Aerosol Science and Technology, 40, 27-67, <https://doi.org/10.1080/02786820500421521>, 2006.

1297 Bond, T. C., Streets, D. G., Yarber, K. F., Nelson, S. M., Woo, J. H., and Klimont, Z.: A technology-based
1298 global inventory of black and organic carbon emissions from combustion, *Journal of Geophysical*
1299 *Research: Atmospheres*, 109, <https://doi.org/10.1029/2003JD003697>, 2004.

1300 Bond, T. C., Doherty, S. J., Fahey, D. W., Forster, P. M., Berntsen, T., DeAngelo, B. J., Flanner, M. G.,
1301 Ghan, S., Kärcher, B., Koch, D., Kinne, S., Kondo, Y., Quinn, P. K., Sarofim, M. C., Schultz, M. G.,
1302 Schulz, M., Venkataraman, C., Zhang, H., Zhang, S., Bellouin, N., Guttikunda, S. K., Hopke, P. K.,
1303 Jacobson, M. Z., Kaiser, J. W., Klimont, Z., Lohmann, U., Schwarz, J. P., Shindell, D., Storelvmo,
1304 T., Warren, S. G., and Zender, C. S.: Bounding the role of black carbon in the climate system: A
1305 scientific assessment, *Journal of Geophysical Research: Atmospheres*, 118, 5380-5552,
1306 <https://doi.org/10.1002/jgrd.50171>, 2013.

1307 Boreddy, S. K. R., Kawamura, K., Okuzawa, K., Kanaya, Y., and Wang, Z.: Temporal and diurnal
1308 variations of carbonaceous aerosols and major ions in biomass burning influenced aerosols over Mt.
1309 Tai in the North China Plain during MTX2006, *Atmospheric Environment*, 154, 106-117,
1310 <https://doi.org/10.1016/j.atmosenv.2017.01.042>, 2017.

1311 Bowen, H. J. M.: *Environmental chemistry of the elements*. Academic Press,
1312 <https://doi.org/10.1002/9780470140451>, 1979.

1313 Brooks, J., Liu, D., Allan, J. D., Williams, P. I., Haywood, J., Highwood, E. J., Kompalli, S. K., Babu, S.
1314 S., Satheesh, S. K., Turner, A. G., and Coe, H.: Black carbon physical and optical properties across
1315 northern India during pre-monsoon and monsoon seasons, *Atmospheric Chemistry and Physics*, 19,
1316 13079-13096, <https://doi.org/10.5194/acp-19-13079-2019>, 2019.

1317 Butler, K. M. and Mulholland, G. W.: Generation and transport of smoke components, *Fire Technology*,
1318 40, 149-176, <https://doi.org/10.1023/B:FIRE.0000016841.07530.64>, 2004.

1319 Cachier, H. and Ducret, J.: Influence of biomass burning on equatorial African rains, *Nature*, 352, 228-
1320 230, <https://doi.org/10.1038/352228a0>, 1991.

1321 Cao, J. J., Wang, Q. Y., Chow, J. C., Watson, J. G., Tie, X.-X., Shen, Z. X., Wang, P., and An, Z. S.:
1322 Impacts of aerosol compositions on visibility impairment in Xi'an, China, *Atmospheric*
1323 *Environment*, 59, 559-566, <https://doi.org/10.1016/j.atmosenv.2012.05.036>, 2012a.

1324 Cao, J. J., Zhu, C. S., Chow, J. C., Watson, J. G., Han, Y. M., Wang, G. H., Shen, Z. X., and An, Z. S.:
1325 Black carbon relationships with emissions and meteorology in Xi'an, China, *Atmospheric Research*,

1326 94, 194-202, <https://doi.org/10.1016/j.atmosres.2009.05.009>, 2009.

1327 Cao, J.: Characteristics of carbonaceous aerosol in Pearl River Delta Region, China during 2001 winter
 1328 period, *Atmospheric Environment*, 37, 1451-1460, [https://doi.org/10.1016/s1352-2310\(02\)01002-6](https://doi.org/10.1016/s1352-2310(02)01002-6),
 1329 2003.

1330 Cao, J. J., Shen, Z. X., Chow, J. C., Watson, J. G., Lee, S. C., Tie, X. X., Ho, K. F., Wang, G. H., and
 1331 Han, Y. M.: Winter and summer PM_{2.5} chemical compositions in fourteen Chinese cities, *Journal of*
 1332 *Air Waste Manage Association*, 62, 1214-1226, <https://doi.org/10.1080/10962247.2012.701193>,
 1333 2012b.

1334 Cao, J. J., Zhu, C. S., Tie, X. X., Geng, F. H., Xu, H. M., Ho, S. S. H., Wang, G. H., Han, Y. M., and Ho,
 1335 K. F.: Characteristics and sources of carbonaceous aerosols from Shanghai, China, *Atmospheric*
 1336 *Chemistry and Physics*, 13, 803-817, <https://doi.org/10.5194/acp-13-803-2013>, 2013.

1337 Casotti Rienda, I. and Alves, C. A.: Road dust resuspension: A review, *Atmospheric Research*, 261,
 1338 105740, <https://doi.org/10.1016/j.atmosres.2021.105740>, 2021.

1339 Cesari, D., Amato, F., Pandolfi, M., Alastuey, A., Querol, X., and Contini, D.: An inter-comparison of
 1340 PM₁₀ source apportionment using PCA and PMF receptor models in three European sites,
 1341 *Environmental Science and Pollution Research*, 23, 15133-15148, [https://doi.org/10.1007/s11356-](https://doi.org/10.1007/s11356-016-6599-z)
 1342 [016-6599-z](https://doi.org/10.1007/s11356-016-6599-z), 2016.

1343 Chen, L., Zhang, X. Y., Tang, Q. L., Geng, Y., Wang, E. L., and Li, J. Y.: Heavy metal pollution and
 1344 source analysis of surface soil in the Qaidam Basin (in Chinese), *Environmental Science*, 42, 4880–
 1345 4888, <https://doi.org/10.13227/j.hjcx.202101052>, 2021.

1346 Chen, M., Li, M.-Y., Zhou, J. Y., Fu, R.-B., Wang, X. F., and Shen Z.: Characteristics and source analysis
 1347 of heavy metal pollution in dust in a heavy industrial area of Northwest China (in Chinese),
 1348 *Environmental Science and Technology*, 47(02), 155-164, [https://doi.org/10.19672/j.cnki.1003-](https://doi.org/10.19672/j.cnki.1003-6504.1004.23.338)
 1349 [6504.1004.23.338](https://doi.org/10.19672/j.cnki.1003-6504.1004.23.338), 2024.

1350 Chen, P., Kang, S., Bai, J., Sillanpää, M., and Li, C.: Yak dung combustion aerosols in the Tibetan Plateau:
 1351 Chemical characteristics and influence on the local atmospheric environment, *Atmospheric*
 1352 *Research*, 156, 58-66, <https://doi.org/10.1016/j.atmosres.2015.01.001>, 2015.

1353 Chen, W., Tong, D. Q., Dan, M., Zhang, S., Zhang, X., and Pan, Y.: Typical atmospheric haze during crop
 1354 harvest season in northeastern China: A case in the Changchun region, *Journal of Environmental*
 1355 *Sciences*, 54, 101-113, <https://doi.org/10.1016/j.jes.2016.03.031>, 2017.

1356 Cheng, X. and Lin, X.: Temporal and spatial distribution characteristics of dust in Shenyang and analysis
1357 of influencing factors (in Chinese). *Environmental Protection Science* 35(06), 1-3 + 58,
1358 <https://doi.org/10.16803/j.cnki.issn.1004-6216.2009.06.001>, 2009.

1359 Chow, J. C.: Measurement methods to determine compliance with ambient air quality standards for
1360 suspended particles, *Journal of the Air & Waste Management Association*, 45, 320-382,
1361 <https://doi.org/10.1080/10473289.1995.10467369>, 1995.

1362 Chow, J. C., Lowenthal, D. H., Chen, L. W. A., Wang, X., and Watson, J. G.: Mass reconstruction methods
1363 for PM_{2.5}: A review, *Air Quality, Atmosphere & Health*, 8, 243-263, [https://doi.org/10.1007/s11869-](https://doi.org/10.1007/s11869-015-0338-3)
1364 [015-0338-3](https://doi.org/10.1007/s11869-015-0338-3), 2015.

1365 Chow, J. C., Watson, J. G., Kuhns, H., Etyemezian, V., Lowenthal, D. H., Crow, D., Kohl, S. D.,
1366 Engelbrecht, J. P., and Green, M. C.: Source profiles for industrial, mobile, and area sources in the
1367 Big Bend Regional Aerosol Visibility and Observational study, *Chemosphere*, 54, 185-208,
1368 <https://doi.org/10.1016/j.chemosphere.2003.07.004>, 2004.

1369 Christie, J. A., Elliott, H. E., O'Connell-Lopez, S. M. O., Perry, K., Pratt, K. A., Hallar, A. G., Hrdina,
1370 A., Murphy, J. G., Riedel, T. P., Long, R. W., Mitroo, D., Haskins, J. D., and Gaston, C. J.: Halogen
1371 production from playa dust emitted from the Great Salt Lake: Implications of the shrinking Great
1372 Salt Lake on regional air quality, *ACS Earth and Space Chemistry*, 9, 480-493,
1373 <https://doi.org/10.1021/acsearthspacechem.4c00258>, 2025.

1374 Chuang, M. T., Lee, C. T., Chou, C. C. K., Lin, N.-H., Sheu, G. R., Wang, J. L., Chang, S. C., Wang,
1375 S.MH., Chi, K. H., Young, C. Y., Huang, H., Chen, H. W., Weng, G -H., Lai, S. Y., Hsu, S. P., Chang,
1376 Y. J., Chang, J. H., and Wu, X. C.: Carbonaceous aerosols in the air masses transported from
1377 Indochina to Taiwan: Long-term observation at Mt. Lulin, *Atmospheric Environment*, 89, 507-516,
1378 <https://doi.org/10.1016/j.atmosenv.2013.11.066>, 2014.

1379 Cichowicz, R. and Bochenek, A. D.: Assessing the effects of urban heat islands and air pollution on
1380 human quality of life, *Anthropocene*, 46, 100433, <https://doi.org/10.1016/j.ancene.2024.100433>,
1381 2024.

1382 Cong, Z., Kang, S., Luo, C., Li, Q., Huang, J., Gao, S., and Li, X.: Trace elements and lead isotopic
1383 composition of PM₁₀ in Lhasa, Tibet, *Atmospheric Environment*, 45, 6210-6215,
1384 <https://doi.org/10.1016/j.atmosenv.2011.07.060>, 2011.

1385 Dang, X., Chang, L., and Lu, N.: The impact of climatic warm-wet situation of the Tibetan Plateau on

1386 the water resources and environment in Qaidam Basin, *Geology of China*, 46, 359-368, 2019.

1387 Demir, T., Karakaş, D., and Yenisoay-Karakaş, S.: Source identification of exhaust and non-exhaust traffic
1388 emissions through the elemental carbon fractions and Positive Matrix Factorization method,
1389 *Environmental Research*, 204, 112399, <https://doi.org/10.1016/j.envres.2021.112399>, 2022.

1390 Deng Z. W., Fang, F. M., Jiang, P. L., Zhang J. Q. and Lin Y. S.: Distribution characteristics of black
1391 carbon content in surface dust in Wuhu city (in Chinese), *Journal of Anqing Normal University*
1392 (Natural Science Edition), 37(01), 58-62, <https://doi.org/10.14182/j.cnki.1001-2443.2014.01.009>,
1393 2014.

1394 Deshmukh, D. K., Deb, M. K., Tsai, Y. I., and Mkoma, S. L.: Water soluble ions in PM_{2.5} and PM₁
1395 aerosols in Durg City, Chhattisgarh, India, *Aerosol and Air Quality Research*, 11, 696-708,
1396 <https://doi.org/10.4209/aaqr.2011.03.0023>, 2011.

1397 Dickinson, K. L., Kanyomse, E., Piedrahita, R., Coffey, E., Rivera, I. J., Adoctor, J., Alirigia, R.,
1398 Muvandimwe, D., Dove, M., Dukic, V., Hayden, M. H., Diaz-Sanchez, D., Abisiba, A. V., Anaseba,
1399 D., Hagar, Y., Masson, N., Monaghan, A., Titiati, A., Steinhoff, D. F., Hsu, Y. Y., Kaspar, R., Brooks,
1400 B. A., Hodgson, A., Hannigan, M., Oduro, A. R., and Wiedinmyer, C.: Research on emissions, air
1401 quality, climate, and cooking technologies in Northern Ghana (Reacting): study rationale and
1402 protocol, *BMC Public Health*, 15, 126, <https://doi.org/10.1186/s12889-015-1414-1>, 2015.

1403 Donahue, N. M.: Chapter 3.2 - Air pollution and air quality, in: *Green chemistry*, Elsevier, 151-176,
1404 <https://doi.org/10.1016/B978-0-12-809270-5.00007-8>, 2018.

1405 Dong, Z., Qin, D., Kang, S., Ren, J., Chen, J., Cui, X., Du, Z., and Qin, X.: Physicochemical
1406 characteristics and sources of atmospheric dust deposition in snow packs on the glaciers of western
1407 Qilian Mountains, China, *Tellus B: Chemical and Physical Meteorology*, 66, 20956,
1408 <https://doi.org/10.3402/tellusb.v66.20956>, 2014.

1409 Duan, J. and Tan, J.: Atmospheric heavy metals and Arsenic in China: Situation, sources and control
1410 policies, *Atmospheric Environment*, 74, 93-101, <https://doi.org/10.1016/j.atmosenv.2013.03.031>,
1411 2013.

1412 Eivazzadeh, M., Hassanvand, M. S., Faridi, S., and Gholampour, A.: Source apportionment and
1413 deposition of dustfall-bound trace elements around Tabriz, Iran, *Environmental Science and*
1414 *Pollution Research International*, 28, 59403-59415, <https://doi.org/10.1007/s11356-020-12173-1>,
1415 2021.

1416 Fan, Q., Cheng, Y., Chen, T., and Xu, N.: Influence of water replenishment of lakes in the Northern
1417 Qaidam Basin on salt lake resources and ecological environment, *Journal of Salt Lake Research*, 30,
1418 11-18, <https://doi.org/10.18307/2024.0344> 2022.

1419 Fang, B., Zeng, H., Zhang, L., Wang, H., Liu, J., Hao, K., Zheng, G., Wang, M., Wang, Q., and Yang, W.:
1420 Toxic metals in outdoor/indoor airborne PM_{2.5} in port city of Northern, China: Characteristics,
1421 sources, and personal exposure risk assessment, *Environmental Pollution*, 279, 116937,
1422 <https://doi.org/10.1016/j.envpol.2021.116937>, 2021.

1423 Fang, H., Lowther, S. D., Zhu, M., Pei, C., Li, S., Fang, Z., Yu, X., Yu, Q., Wang, Y., Zhang, Y., Jones,
1424 K. C., and Wang, X.: PM_{2.5}-bound unresolved complex mixtures (UCM) in the Pearl River Delta
1425 region: Abundance, atmospheric processes and sources, *Atmospheric Environment*, 226,
1426 <https://doi.org/10.1016/j.atmosenv.2020.117407>, 2020.

1427 Feng, W., Guo, Z., Xiao, X., Peng, C., Shi, L., Ran, H., and Xu, W.: Atmospheric deposition as a source
1428 of cadmium and lead to soil-rice system and associated risk assessment, *Ecotoxicology and
1429 Environmental Safety*, 180, 160-167, <https://doi.org/10.1016/j.ecoenv.2019.04.090>, 2019.

1430 Filonchyk, M., Yan, H., Yang, S., and Lu, X.: Detection of aerosol pollution sources during sandstorms
1431 in Northwestern China using remote sensed and model simulated data, *Advances in Space Research*,
1432 61, 1035-1046, <https://doi.org/10.1016/j.asr.2017.11.037>, 2018.

1433 Foysal, M., Hossain, M., Rubaiyat, A., Sultana, S., Uddin, M. K., Sayem, M., and Akhter, J.: Household
1434 energy consumption pattern in rural areas of Bangladesh, *Indian Journal of Energy*, 1, 72-85, 2012.

1435 Fu, B.: Socio-economic data set of Qinghai-Tibet Plateau (1982-2018). National Tibetan Plateau / Third
1436 Pole Environment Data Center, <http://data.tpdc.ac.cn>, 2023.

1437 Gao, G. S., Song, L. M., and Ma, Z. T.: Temporal and spatial distribution of dust-fall in Qinghai Province
1438 and analysis of its influencing factors (in Chinese), *Chinese Journal of Desert Research*, 33(04),
1439 1124-1130, <https://doi.org/10.7522/j.issn.1000-694X.2013.00153>, 2013.

1440 Gao, H. and Washington, R.: Arctic oscillation and the interannual variability of dust emissions from the
1441 Tarim Basin: a TOMS AI based study, *Climate Dynamics*, 35, 511-522,
1442 <https://doi.org/10.1007/s00382-009-0687-4>, 2010.

1443 Gao, Y., Wang, H., Yuan, L., Jing, S., Yuan, B., Shen, G., Zhu, L., Koss, A., Li, Y., Wang, Q., Huang, D.
1444 D., Zhu, S., Tao, S., Lou, S., and Huang, C.: Measurement report: Underestimated reactive organic
1445 gases from residential combustion – insights from a near-complete speciation, *Atmospheric*

1446 Chemistry and Physics, 23, 6633-6646, <https://doi.org/10.5194/acp-23-6633-2023>, 2023.

1447 Garaga, R., Gokhale, S., and Kota, S. H.: Source apportionment of size-segregated atmospheric particles
 1448 and the influence of particles deposition in the human respiratory tract in rural and urban locations
 1449 of north-east India, *Chemosphere*, 255, <https://doi.org/10.1016/j.chemosphere.2020.126980>, 2020.

1450 Gertler, A., Kuhns, H., Abu-Allaban, M., Damm, C., Gillies, J., Etyemezian, V., Clayton, R., and Proffitt,
 1451 D.: A case study of the impact of Winter road sand/salt and street sweeping on road dust re-
 1452 entrainment, *Atmospheric Environment*, 40, 5976-5985,
 1453 <https://doi.org/10.1016/j.atmosenv.2005.12.047>, 2006.

1454 Gholampour, A., Nabizadeh, R., Hassanvand, M. S., Taghipour, H., Nazmara, S., and Mahvi, A. H.:
 1455 Characterization of saline dust emission resulted from Urmia Lake drying, *Journal of Environmental
 1456 Health Science & Engineering*, 13, 82, <https://doi.org/10.1186/s40201-015-0238-3>, 2015.

1457 Gonçalves, C., Alves, C., Evtugina, M., Mirante, F., Pio, C., Caseiro, A., Schmidl, C., Bauer, H., and
 1458 Carvalho, F.: Characterisation of PM₁₀ emissions from woodstove combustion of common woods
 1459 grown in Portugal, *Atmospheric Environment*, 44, 4474-4480, <https://doi.org/10.1016/j.atmosenv.2010.08.047>,
 1460 2010.

1461 Gondwal, T. K. and Mandal, P.: Review on classification, sources and management of road dust and
 1462 determination of uncertainty associated with measurement of particle size of road dust, *Mapan*, 36,
 1463 909-924, <https://doi.org/10.1007/s12647-021-00501-w>, 2021.

1464 Gong, M., Yin, S., Gu, X., Xu, Y., Jiang, N., and Zhang, R.: Refined 2013-based vehicle emission
 1465 inventory and its spatial and temporal characteristics in Zhengzhou, China, *Science of The Total
 1466 Environment*, 599-600, 1149-1159, <https://doi.org/10.1016/j.scitotenv.2017.03.299>, 2017.

1467 Goossens, D. and Offer, Z. Y. J. Z. F. G.: Eolian deposition of dust over symmetrical hills: an evaluation
 1468 of wind-tunnel data by means of terrain measurement, *Zeitschrift für Geomorphologie*, 37, 103-111,
 1469 <https://doi.org/10.1127/zfg/37/1993/103>, 1993. Gray, H. A., Cass, G. R., Huntzicker, J. J., Heyerdahl,
 1470 E. K., and Rau, J. A.: Characteristics of atmospheric organic and elemental carbon particle
 1471 concentrations in Los Angeles, *Environmental Science & Technology*, 20, 580-589,
 1472 <https://doi.org/10.1021/es00148a006>, 1986.

1473 Griffin, D. W., Kellogg, C. A., Garrison, V. H., and Shinn, E. A.: The global transport of dust: An
 1474 Intercontinental river of dust, microorganisms and toxic chemicals flows through the Earth's
 1475 atmosphere, *American Scientist*, 90, 228-235, <https://www.jstor.org/stable/27857658>, 2002.

1476 Guo, J., Miao, Y., Zhang, Y., Liu, H., Li, Z., Zhang, W., He, J., Lou, M., Yan, Y., Bian, L., and Zhai, P.:
1477 The climatology of planetary boundary layer height in China derived from radiosonde and
1478 reanalysis data, *Atmospheric Chemistry and Physics*, 16, 13309-13319, [https://doi.org/10.5194/acp-](https://doi.org/10.5194/acp-16-13309-2016)
1479 16-13309-2016, 2016.

1480 Guo, S., Wang, L., Zhou, P., Guo, S., Qin, W., An, S., Xiao, J. Y., Liu, J., and Ji, Y.: Characteristics and
1481 sources of organic carbon and elemental carbon in summer road dust in Shijiazhuang (in Chinese),
1482 *Environmental Engineering*, 36(04), 122-126, <https://doi.org/10.13205/j.hjgc.201804025>, 2018.

1483 Guo, W. T., Zhao, F. Q., and Chang, H. L.: Analysis of the trend of environmental air quality changes in
1484 the main urban area of Changzhi City (in Chinese), *Proceedings of Shanghai, China* 3, 2010.

1485 Gupta, A. and Dhir, A.: Assessment of air quality and chemical fingerprints for atmospheric fine aerosols
1486 in an Indian smart city, *Environmental Pollutants and Bioavailability*, 34, 21-33,
1487 <https://doi.org/10.1080/26395940.2021.2024091>, 2022.

1488 Hahnenberger, M. and Nicoll, K.: Meteorological characteristics of dust storm events in the eastern Great
1489 Basin of Utah, U.S.A, *Atmospheric Environment*, 60, 601-612, <https://doi.org/10.1016/j.atmosenv>,
1490 2012.

1491 Hama, S., Ouchen, I., Wyche, K. P., Cordell, R. L., and Monks, P. S.: Carbonaceous aerosols in five
1492 European cities: Insights into primary emissions and secondary particle formation, *Atmospheric*
1493 *Research*, 274, <https://doi.org/10.1016/j.atmosres>, 2022.

1494 Han, Y., Cao, J., An, Z., Chow, J. C., Watson, J. G., Jin, Z., Fung, K., and Liu, S.: Evaluation of the
1495 thermal/optical reflectance method for quantification of elemental carbon in sediments,
1496 *Chemosphere*, 69, 526-533, <https://doi.org/10.1016/j.chemosphere>, 2007a.

1497 Han, Y., Cao, J., Chow, J. C., Watson, J. G., An, Z., Jin, Z., Fung, K., and Liu, S.: Evaluation of the
1498 thermal/optical reflectance method for discrimination between char- and soot-EC, *Chemosphere*,
1499 69, 569-574, <https://doi.org/10.1016/j.chemosphere>, 2007b.

1500 Han, Y. M., Lee, S. C., Cao, J. J., Ho, K. F., and An, Z. S.: Spatial distribution and seasonal variation of
1501 char-EC and soot-EC in the atmosphere over China, *Atmospheric Environment*, 43, 6066-6073,
1502 <https://doi.org/10.1016/j.atmosenv>, 2009a.

1503 Han, Y. M., Cao, J. J., Chow, J. C., Watson, J. G., An, Z. S., and Liu, S. X.: Elemental carbon in urban
1504 soils and road dusts in Xi'an, China and its implication for air pollution, *Atmospheric Environment*,
1505 43, 2464-2470, <https://doi.org/10.1016/j.atmosenv>, 2009b.

1506 Han, Y. M., Han, Z. W., Cao, J. J., Chow, J. C., Watson, J. G., An, Z. S., Liu, S. X., and Zhang, R. J.:
1507 Distribution and origin of carbonaceous aerosol over a rural high-mountain lake area, Northern
1508 China and its transport significance, *Atmospheric Environment*, 42, 2405-2414,
1509 <https://doi.org/10.1016/j.atmosenv>, 2008.

1510 Han, Y. M., Cao, J. J., Yan, B. Z., Kenna, T. C., Jin, Z. D., Cheng, Y., Chow, J. C., and An, Z. S.:
1511 Comparison of elemental carbon in lake sediments measured by three different methods and 150-
1512 year pollution history in Eastern China, *Environmental Science & Technology*, 45, 5287-5293,
1513 <https://doi.org/10.1021/es103518c>, 2011.

1514 Han, Y. M., Chen, L. W. A., Huang, R. J., Chow, J. C., Watson, J. G., Ni, H. Y., Liu, S. X., Fung, K. K.,
1515 Shen, Z. X., Wei, C., Wang, Q. Y., Tian, J., Zhao, Z. Z., Prévôt, A. S. H., and Cao, J. J.: Carbonaceous
1516 aerosols in megacity Xi'an, China: Implications of thermal/optical protocols comparison,
1517 *Atmospheric Environment*, 132, 58-68, <https://doi.org/10.1016/j.atmosenv>, 2016.

1518 Hand, V. L., Capes, G., Vaughan, D. J., Formenti, P., Haywood, J. M., and Coe, H.: Evidence of internal
1519 mixing of African dust and biomass burning particles by individual particle analysis using electron
1520 beam techniques, *Journal of Geophysical Research: Atmospheres*, 115,
1521 <https://doi.org/10.1029/2009JD012938>, 2010.

1522 He, L. Y., Hu, M., Huang, X. F., Yu, B. D., Zhang, Y. H., and Liu, D. Q.: Measurement of emissions of
1523 fine particulate organic matter from Chinese cooking, *Atmospheric Environment*, 38, 6557-6564,
1524 <https://doi.org/10.1016/j.atmosenv>, 2004.

1525 Heltberg, R., Arndt, T. C., and Sekhar, N. U.: Fuelwood consumption and forest degradation: A household
1526 model for domestic energy substitution in rural India, *Land Economics*, 76, 213-232,
1527 <https://doi.org/10.2307/3147225>, 2000.

1528 Heo, J. B., Hopke, P., Yi, S. M. J. A. C., Source apportionment of PM_{2.5} in Seoul, Korea, *Atmospheric
1529 Chemistry and Physics*: 9, 4957-4971, <https://doi.org/10.5194/acp-9-4957-2009>, 2009.

1530 Hewitt, C. N.: The atmospheric chemistry of sulphur and nitrogen in power station plumes, *Atmospheric
1531 Environment*, 35, 1155-1170, [https://doi.org/10.1016/S1352-2310\(00\)00463-5](https://doi.org/10.1016/S1352-2310(00)00463-5), 2001.

1532 Hilary, U., Efeoghene, E. A., Issac, A. O., Sami, R., Baakdah, F., and Pareek, S.: Exposure to airborne
1533 pollutants in urban and rural areas: levels of metals and microorganisms in PM₁₀ and gaseous
1534 pollutants in ambient air, *Air Quality, Atmosphere & Health*, 18, 317-332,
1535 <https://doi.org/10.1007/s11869-024-01644-w>, 2025.

1536 Hoeck, T., Droux, R., Breu, T., Humi, H., and Maselli, D.: Rural energy consumption and land
1537 degradation in a post-Soviet setting – an example from the west Pamir mountains in Tajikistan,
1538 Energy for Sustainable Development, 11, 48-57, [https://doi.org/10.1016/S0973-0826\(08\)60563-3](https://doi.org/10.1016/S0973-0826(08)60563-3),
1539 2007.

1540 Hu, Y. N. and Liu, Y. L.: Characteristics and source analysis of heavy metal pollution in indoor dust in
1541 Jinan (in Chinese). Environmental Science and Technology 45(06), 179-184,
1542 <https://doi.org/10.19672/j.cnki.1003-6504.0043.22.338>, 2022.

1543 Hua, Y., Wang, S., Jiang, J., Zhou, W., Xu, Q., Li, X., Liu, B., Zhang, D., and Zheng, M.: Characteristics
1544 and sources of aerosol pollution at a polluted rural site southwest in Beijing, China, Science of The
1545 Total Environment, 626, 519-527, <https://doi.org/10.1016/j.scitotenv>, 2018.

1546 Huang, H., Xu, Z. Q., Yan, J. X., Zhao, X. G., and Wang, D. L.: Characteristics of heavy metal pollution
1547 and ecological risk evaluation of indoor dust from urban and rural areas in Taiyuan City during the
1548 heating season (in Chinese), Journal of Environmental Science, 42, 2143-2152,
1549 <https://doi.org/10.13227/j.hjx.202008045>, 2021a.

1550 Huang, X. and Gao, J.: A review of near-limit opposed fire spread, Fire Safety Journal, 120, 103141,
1551 <https://doi.org/10.1016/j.firesaf.2020.103141>, 2021a.

1552 Huang, X., Tang, G., Zhang, J., Liu, B., Liu, C., Zhang, J., Cong, L., Cheng, M., Yan, G., Gao, W., Wang,
1553 Y., and Wang, Y.: Characteristics of PM_{2.5} pollution in Beijing after the improvement of air quality,
1554 Journal of Environmental Sciences, 100, 1-10, <https://doi.org/10.1016/j.jes.2020.06.004>, 2021b.

1555 Ji, X., Xu, K., Liao, D., Chen, G., Liu, T., Hong, Y., Dong, S., Choi, S.-D., and Chen, J.: Spatial-temporal
1556 characteristics and source apportionment of ambient VOCs in Southeast Mountain Area of China,
1557 Aerosol And Air Quality Research, 22, 220016, <https://doi.org/10.4209/aaqr.220016>, 2022.

1558 Jia, H., Yan, C., and Xing, X.: Evaluation of eco-environmental quality in Qaidam Basin based on the
1559 Ecological Index (MRSEI) and GEE, Remote Sensing, 13, <https://doi.org/10.3390/rs13224543>,
1560 2021.

1561 Jia, S. M., Chen, M. H., Yang, P. F., Wang, L., Wang, G. Y., Liu, L. Y., and Ma, W. L.: Seasonal variations
1562 and sources of atmospheric EPFRs in a megacity in severe cold region: Implications for the
1563 influence of strong coal and biomass combustion, Environmental Research, 252,
1564 <https://doi.org/10.1016/j.envres.2024.119067>, 2024.

1565 Jian, X., Guan, P., Fu, S. T., Zhang, D. W., Zhang, W., and Zhang, Y.-S.: Miocene sedimentary

1566 environment and climate change in the northwestern Qaidam basin, northeastern Tibetan Plateau:
1567 Facies, biomarker and stable isotopic evidences, *Palaeogeography Palaeoclimatology*
1568 *Palaeoecology*, 414, 320-331, <https://doi.org/10.1016/j.palaeo.2014.09.011>, 2014.

1569 Jiang, L., Xue, B., Xing, R., Chen, X., Song, L., Wang, Y., Coffman, D. M., and Mi, Z.: Rural household
1570 energy consumption of farmers and herders in the Qinghai-Tibet Plateau, *Energy*, 192,
1571 <https://doi.org/10.1016/j.energy.2019.116649>, 2020.

1572 Jiang, Y., Shi, L., Guang, A. L., Mu, Z., Zhan, H., and Wu, Y.: Contamination levels and human health
1573 risk assessment of toxic heavy metals in street dust in an industrial city in Northwest China,
1574 *Environmental Geochemistry and Health*, 40, 2007-2020, [https://doi.org/10.1007/s10653-017-](https://doi.org/10.1007/s10653-017-0028-1)
1575 0028-1, 2018.

1576 Jiménez, L., Rühland, K. M., Jeziorski, A., Smol, J. P., and Pérez-Martínez, C.: Climate change and
1577 Saharan dust drive recent cladoceran and primary production changes in remote alpine lakes of
1578 Sierra Nevada, Spain, *Global Change Biology*, 24, e139-e158, <https://doi.org/10.1111/gcb.13878>,
1579 2018.

1580 Joshi, U. M., Vijayaraghavan, K., and Balasubramanian, R.: Elemental composition of urban street dusts
1581 and their dissolution characteristics in various aqueous media, *Chemosphere*, 77, 526-533,
1582 <https://doi.org/10.1016/j.chemosphere>, 2009.

1583 Kang, S., Zhang, Y., Qian, Y., and Wang, H.: A review of black carbon in snow and ice and its impact on
1584 the cryosphere, *Earth-Science Reviews*, 210, <https://doi.org/10.1016/j.earscirev.2020.103346>, 2020.

1585 Katakai, R., Goswami, K., Bordoloi, N. J., Narzari, R., Saikia, R., Sut, D., and Gogoi, L.: Biomass
1586 resources for biofuel production in Northeast India, in: *Bioprospecting of indigenous bioresources*
1587 *of North-East India*, Springer Singapore, Singapore, 127-151, [https://doi.org/10.1007/978-981-10-](https://doi.org/10.1007/978-981-10-0620-3_8)
1588 0620-3_8, 2016.

1589 Kerimray, A., Suleimenov, B., De Miglio, R., Rojas-Solórzano, L., Amouei Torkmahalleh, M., and Ó
1590 Gallachóir, B. P.: Investigating the energy transition to a coal free residential sector in Kazakhstan
1591 using a regionally disaggregated energy systems model, *Journal of Cleaner Production*, 196, 1532-
1592 1548, <https://doi.org/10.1016/j.jclepro>, 2018.

1593 Khan, A. J., Swami, K., Ahmed, T., Bari, A., Shareef, A., and Husain, L.: Determination of elemental
1594 carbon in lake sediments using a thermal-optical transmittance (TOT) method, *Atmospheric*
1595 *Environment*, 43, 5989-5995, <https://doi.org/10.1016/j.atmosenv.2009.08.030>, 2009.

1596 Kim, K. H., Sekiguchi, K., Kudo, S., and Sakamoto, K.: Characteristics of atmospheric elemental carbon
1597 (Char and Soot) in ultrafine and fine particles in a roadside environment, Japan, *Aerosol and Air*
1598 *Quality Research*, 11, 1-12, <https://doi.org/10.4209/aaqr.2010.07.0061>, 2011.

1599 Kong, L., Xin, J., Gao, W., Tang, G., Wang, X., Wang, Y., Zhang, W., Chen, W., and Jia, S.: A
1600 comprehensive evaluation of aerosol extinction apportionment in Beijing using a high-resolution
1601 time-of-flight aerosol mass spectrometer, *Science of The Total Environment*, 783, 146976,
1602 <https://doi.org/10.1016/j.scitotenv.2021.146976>, 2021.

1603 Kuang, Y., He, Y., Xu, W., Yuan, B., Zhang, G., Ma, Z., Wu, C., Wang, C., Wang, S., Zhang, S., Tao, J.,
1604 Ma, N., Su, H., Cheng, Y., Shao, M., and Sun, Y.: Photochemical aqueous-phase reactions induce
1605 rapid daytime formation of oxygenated organic aerosol on the North China Plain, *Environmental*
1606 *Science & Technology*, 54, 3849-3860, <https://doi.org/10.1021/acs.est.9b06836>, 2020.

1607 Kulmala, M., Vehkamäki, H., Petäjä, T., Dal Maso, M., Lauri, A., Kerminen, V. M., Birmili, W., and
1608 McMurry, P. H.: Formation and growth rates of ultrafine atmospheric particles: a review of
1609 observations, *Journal of Aerosol Science*, 35, 143-176,
1610 <https://doi.org/10.1016/j.jaerosci.2003.10.003>, 2004.

1611 Kumar, A.: Chemical characterization of mineral aerosols: Sources, transport and atmospheric
1612 transformations, Mohanlal Sukhadia University Udaipur, 2010.

1613 Kumar, N., Johnson, J., Yarwood, G., Woo, J. H., Kim, Y., Park, R. J., Jeong, J. I., Kang, S., Chun, S.,
1614 and Knipping, E.: Contributions of domestic sources to PM_{2.5} in South Korea, *Atmospheric*
1615 *Environment*, 287, 119273, <https://doi.org/10.1016/j.atmosenv.2022.119273>, 2022.

1616 Lai, S., Zhao, Y., Ding, A., Zhang, Y., Song, T., Zheng, J., Ho, K. F., Lee, S. C., and Zhong, L.:
1617 Characterization of PM_{2.5} and the major chemical components during a 1-year campaign in rural
1618 Guangzhou, Southern China, *Atmospheric Research*, 167, 208-215,
1619 <https://doi.org/10.1016/j.atmosres>, 2016.

1620 Leavey, A., Patel, S., Martinez, R., Mitroo, D., Fortenberry, C., Walker, M., Williams, B., and Biswas, P.:
1621 Organic and inorganic speciation of particulate matter formed during different combustion phases
1622 in an improved cookstove, *Environmental Research*, 158, 33-42, <https://doi.org/10.1016/j.envres>,
1623 2017.

1624 Lee, K. Y., Batmunkh, T., Joo, H. S., and Park, K.: Comparison of the physical and chemical
1625 characteristics of fine road dust at different urban sites, *Journal of the Air & Waste Management*

1626 Association, 68, 812-823, <https://doi.org/10.1080/10962247.2018.1443855>, 2018.

1627 Li, J. K., Liu, X. F. and Wang, D. H.: Overview of mineralization laws of lithium deposits in China (in
1628 Chinese). *Acta Geologica Sinica*, 88: 2269-2283. <https://doi.org/10.19762/j.cnki.dizhixuebao>, 2014.

1629 Li, L., Ni, W., Cheng, Y., Wang, H., Yuan, K., and Zhou, B.: Evaluation of the eco-geo-environment in
1630 the Qaidam Basin, China, *Environmental Earth Sciences*, 80, [https://doi.org/10.1007/s12665-020-](https://doi.org/10.1007/s12665-020-09312-9)
1631 [09312-9](https://doi.org/10.1007/s12665-020-09312-9), 2021a.

1632 Li, M., Liu, Z., Chen, J., Huang, X., Liu, J., Xie, Y., Hu, B., Xu, Z., Zhang, Y., and Wang, Y.:
1633 Characteristics and source apportionment of metallic elements in PM_{2.5} at urban and suburban sites
1634 in Beijing: Implication of emission reduction, *Atmosphere*, 10,
1635 <https://doi.org/10.3390/atmos10030105>, 2019a.

1636 Li, P. H., Wang, Y., Li, T., Sun, L., Yi, X., Guo, L. Q., and Su, R. H.: Characterization of carbonaceous
1637 aerosols at Mount Lu in South China: implication for secondary organic carbon formation and long-
1638 range transport, *Environmental Science and Pollution Research*, 22, 14189-14199,
1639 <https://doi.org/10.1007/s11356-015-4654-9>, 2015b.

1640 Li, Q. L and Sha, Z. J.: Remote sensing monitoring of ecological environment quality in the Qaidam
1641 Basin under climate warming (in Chinese), *Ecological Science*, 41(06), 92-99,
1642 <https://doi.org/10.14108/j.cnki.1008-8873>, 2022.

1643 Li, R., Li, C., Zhuang, J., Zhu, H., Fang, L., and Sun, D.: Mechanistic influence of chemical
1644 agglomeration agents on removal of inhalable particles from coal combustion, *ACS Omega*, 5,
1645 25906-25912, <https://doi.org/10.1021/acsomega.0c03263>, 2020.

1646 Li, Y., Ma, L., Ge, Y., and Abuduwaili, J.: Health risk of heavy metal exposure from dustfall and source
1647 apportionment with the PCA-MLR model: A case study in the Ebinur Lake Basin, China,
1648 *Atmospheric Environment*, 272, 118950, <https://doi.org/10.1016/j.atmosenv>, 2022.

1649 Li, Y., Song, Y., Kaskaoutis, D. G., Chen, X., Mamadjanov, Y., and Tan, L.: Atmospheric dust dynamics
1650 in southern Central Asia: Implications for buildup of Tajikistan loess sediments, *Atmospheric*
1651 *Research*, 229, 74-85, <https://doi.org/10.1016/j.atmosres.2019.06.013>, 2019b.

1652 Li, Z., Sjödin, A., Romanoff, L. C., Horton, K., Fitzgerald, C. L., Eppler, A., Aguilar-Villalobos, M., and
1653 Naeher, L. P.: Evaluation of exposure reduction to indoor air pollution in stove intervention projects
1654 in Peru by urinary biomonitoring of polycyclic aromatic hydrocarbon metabolites, *Environment*
1655 *International*, 37, 1157-1163, <https://doi.org/10.1016/j.envint.2011.03.024>, 2011.

1656 Li, Z., Liu, J., Zhai, Z., Liu, C., Ren, Z., Yue, Z., Yang, D., Hu, Y., Zheng, H., and Kong, S.:
1657 Heterogeneous changes of chemical compositions, sources and health risks of PM_{2.5} with the "Clean
1658 Heating" policy at urban/suburban/industrial sites, *Science of The Total Environment*, 854, 158871,
1659 <https://doi.org/10.1016/j.scitotenv.2022.158871>, 2023.

1660 Li, Z., Yue, Z., Yang, D., Wang, L., Wang, X., Li, Z., Wang, Y., Chen, L., Guo, S., Yao, J., Lou, X., Xu,
1661 X., and Wei, J.: Levels, chemical compositions, and sources of PM_{2.5} of rural and urban area under
1662 the impact of wheat harvest, *Aerosol and Air Quality Research*, 21,
1663 <https://doi.org/10.4209/aaqr.210026>, 2021.

1664 Lin, Y., Mu, G., Chen, L., Wu, C., and Xu, L.: Sorting characteristics and implications indicated by the
1665 grain size of near-surface atmospheric dust fall in the Qira Oasis (in Chinese), *Journal of Desert
1666 Research*, 42, 139-146, <https://doi.org/10.7522/j.issn.1000-694X>, 2022a.

1667 Lin, Y., Mu, G., and Xu, L.: Grain size and sedimentary sorting characteristics of atmospheric dust in the
1668 Cele Oasis, Southern Margin of Taklimakan Desert, 14(13), 8093,
1669 <https://doi.org/10.3390/su14138093>, 2022b.

1670 Lin, Y. C., Tsai, C. J., Wu, Y. C., Zhang, R., Chi, K. H., Huang, Y. T., Lin, S. H., and Hsu, S. C.:
1671 Characteristics of trace metals in traffic-derived particles in Hsuehshan Tunnel, Taiwan: size
1672 distribution, potential source, and fingerprinting metal ratio, *Atmospheric Chemistry and Physics*,
1673 15, 4117-4130, <https://doi.org/10.5194/acp-15-4117-2015>, 2015.

1674 Liu, B., Song, N., Dai, Q., Mei, R., Sui, B., Bi, X., and Feng, Y.: Chemical composition and source
1675 apportionment of ambient PM_{2.5} during the non-heating period in Taian, China, *Atmospheric
1676 Research*, 170, 23-33, <https://doi.org/10.1016/j.atmosres>, 2016a.

1677 Liu, G., Lucas, M., and Shen, L.: Rural household energy consumption and its impacts on eco-
1678 environment in Tibet: Taking Taktse county as an example, *Renewable and Sustainable Energy
1679 Reviews*, 12, 1890-1908, <https://doi.org/10.1016/j.rser>, 2008.

1680 Liu, G., Li, J., Wu, D., and Xu, H.: Chemical composition and source apportionment of the ambient PM_{2.5}
1681 in Hangzhou, China, *Particuology*, 18, 135-143, <https://doi.org/10.1016/j.partic>, 2015.

1682 Liu, G., Yin, G., Kurban, A., Aishan, T., and You, H.: Spatiotemporal dynamics of land cover and their
1683 impacts on potential dust source regions in the Tarim Basin, NW China, *Environmental Earth
1684 Sciences*, 75, 1477, <https://doi.org/10.1007/s12665-016-6269-y>, 2016b.

1685 Liu, H., Hu, B., Zhang, L., Zhao, X. J., Shang, K. Z., Wang, Y. S., and Wang, J.: Ultraviolet radiation

1686 over China: Spatial distribution and trends, *Renewable and Sustainable Energy Reviews*, 76, 1371-
1687 1383, [https://doi.org/10.1016/j.rser, 2017](https://doi.org/10.1016/j.rser.2017).

1688 Liu, H., Jia, M., Tao, J., Yao, D., Li, J., Zhang, R., Li, L., Xu, M., Fan, Y., Liu, Y., and Cheng, K.:
1689 Elucidating pollution characteristics, temporal variation and source origins of carbonaceous species
1690 in Xinxiang, a heavily polluted city in North China, *Atmospheric Environment*, 298, 119626,
1691 <https://doi.org/10.1016/j.atmosenv.2023.119626>, 2023a.

1692 Liu, P., Zhou, H., Chun, X., Wan, Z., Liu, T., Sun, B., Wang, J., and Zhang, W.: Characteristics of fine
1693 carbonaceous aerosols in Wuhai, a resource-based city in Northern China: Insights from energy
1694 efficiency and population density, *Environmental Pollution*, 292, 118368,
1695 [https://doi.org/10.1016/j.envpol, 2022](https://doi.org/10.1016/j.envpol.2022).

1696 Liu, T., Zhao, C., Chen, Q., Li, L., Si, G., Li, L., and Guo, B.: Characteristics and health risk assessment
1697 of heavy metal pollution in atmospheric particulate matter in different regions of the Yellow River
1698 Delta in China, *Environmental Geochemistry and Health*, 45, 2013-2030,
1699 <https://doi.org/10.1007/s10653-022-01318-5>, 2023b.

1700 Liu, W., Hopke, P. K., Han, Y. J., Yi, S. M., Holsen, T. M., Cybart, S., Kozłowski, K., and Milligan, M.:
1701 Application of receptor modeling to atmospheric constituents at Potsdam and Stockton, NY,
1702 *Atmospheric Environment*, 37, 4997-5007, <https://doi.org/10.1016/j.atmosenv.2003.08.036>, 2003.

1703 Liu, X., Wang, Y., Liu, R., Zhang, Y., Shao, L., Han, K., and Zhang, Y.: Pollution characteristics, source
1704 identification and potential ecological risk of 50 elements in atmospheric particulate matter during
1705 winter in Qingdao, *Arabian Journal of Geosciences*, 15, [https://doi.org/10.1007/s12517-022-09521-](https://doi.org/10.1007/s12517-022-09521-5)
1706 5, 2022b.

1707 Liu, Y., Liu, G., Yousaf, B., Zhang, J., and Zhou, L.: Carbon fractionation and stable carbon isotopic
1708 fingerprint of road dusts near coal power plant with emphases on coal-related source apportionment,
1709 *Ecotoxicology and Environmental Safety*, 202, 110888, [https://doi.org/10.1016/j.ecoenv, 2020a](https://doi.org/10.1016/j.ecoenv.2020a).

1710 Liu, Y., Wu, G., Duan, A. and Zhang, Q.: New evidence that climate warming in the Tibetan Plateau is a
1711 result of intensified greenhouse gas emissions (in Chinese), *Chinese Science Bulletin*, 51(8), 989-
1712 992, <https://doi.org/10.1360/csb2006-51-8-989>, 2006.

1713 Liu, Y., Zhu, Q., Huang, J., Hua, S., and Jia, R.: Impact of dust-polluted convective clouds over the
1714 Tibetan Plateau on downstream precipitation, *Atmospheric Environment*, 209, 67-77,
1715 <https://doi.org/10.1016/j.atmosenv>, 2019.

1716 Liu, Y., Zhu, Q., Hua, S., Alam, K., Dai, T., and Cheng, Y.: Tibetan Plateau driven impact of Taklimakan
1717 dust on northern rainfall, *Atmospheric Environment*, 234, 117583,
1718 [https://doi.org/10.1016/j.atmosenv, 2020b](https://doi.org/10.1016/j.atmosenv.2020b).

1719 Liu, Z. Y., Cheng, J. L., Li, C. Y., Gao, Y., Zhan, C. L., Liu, S., Zhang, J. Q., and Liu, H. X.: Pollution
1720 characteristics and source analysis of carbon components in road dust from Qingshan District,
1721 Wuhan (in Chinese), *Environmental Chemistry*, 40, 772–778, [https://doi.org/10.7524/j.issn.0254-](https://doi.org/10.7524/j.issn.0254-6108.2020061305)
1722 [6108.2020061305](https://doi.org/10.7524/j.issn.0254-6108.2020061305), 2021.

1723 Lonati, G., Ozgen, S., and Giugliano, M.: Primary and secondary carbonaceous species in PM_{2.5} samples
1724 in Milan (Italy), *Atmospheric Environment*, 41, 4599-4610, [https://doi.org/10.1016/j.atmosenv,](https://doi.org/10.1016/j.atmosenv.2007)
1725 [2007](https://doi.org/10.1016/j.atmosenv.2007).

1726 Löw, F., Navratil, P., Kotte, K., Schöler, H. F., and Bubenzer, O.: Remote-sensing-based analysis of
1727 landscape change in the desiccated seabed of the Aral Sea—a potential tool for assessing the hazard
1728 degree of dust and salt storms, *Environmental Monitoring and Assessment*, 185, 8303-8319,
1729 <https://doi.org/10.1007/s10661-013-3174-7>, 2013.

1730 Luo, M., Liu, Y., Zhu, Q., Tang, Y., and Alam, K.: Role and mechanisms of black carbon affecting water
1731 vapor transport to Tibet, *Remote Sensing*, 12(2), 0231, <https://doi.org/10.3390/rs12020231>, 2020.

1732 Ma, Q., Wu, Y., Tao, J., Xia, Y., Liu, X., Zhang, D., Han, Z., Zhang, X., and Zhang, R.: Variations of
1733 chemical composition and source apportionment of PM_{2.5} during winter haze episodes in Beijing,
1734 *Aerosol and Air Quality Research*, 17, 2791-2803, <https://doi.org/10.4209/aaqr.2017.10.0366>, 2017.

1735 Ma, Y., Ji, Y. Q., Guo, J. J., Zhao, J. Q., Li, Y. Y., Wang, S. B. and Zhang, L.: Characteristics of carbon
1736 components and source analysis of road dust during spring in Tianjin (in Chinese), *Acta Scientiae*
1737 *Circumstantiae* 40(06), 2540-2545, <https://doi.org/10.13227/j.hjcx>, 2019.

1738 Mahowald, N. M., Engelstaedter, S., Luo, C., Sealy, A., Artaxo, P., Benitez-Nelson, C., Bonnet, S., Chen,
1739 Y., Chuang, P. Y., Cohen, D. D., Dulac, F., Herut, B., Johansen, A. M., Kubilay, N., Losno, R.,
1740 Maenhaut, W., Paytan, A., Prospero, J. M., Shank, L. M., and Siefert, R. L.: Atmospheric iron
1741 deposition: Global distribution, variability, and human perturbations, *Annual Review of Marine*
1742 *Science*, 1, 245-278, <https://doi.org/10.1146/annurev.marine.010908.163727>, 2009.

1743 Manousakas, M., Papaefthymiou, H., Diapouli, E., Migliori, A., Karydas, A. G., Bogdanovic-Radovic,
1744 I., and Eleftheriadis, K.: Assessment of PM_{2.5} sources and their corresponding level of uncertainty
1745 in a coastal urban area using EPA PMF 5.0 enhanced diagnostics, *Science of The Total Environment*,

1746 574, 155-164, <https://doi.org/10.1016/j.scitotenv.2016.09.047>, 2017.

1747 Mbengue, S., Fusek, M., Schwarz, J., Vodička, P., Šmejkalová, A. H., and Holoubek, I.: Four years of
1748 highly time resolved measurements of elemental and organic carbon at a rural background site in
1749 Central Europe, *Atmospheric Environment*, 182, 335-346, <https://doi.org/10.1016/j.atmosenv>,
1750 2018. Meng, C. C., Wang, L. T., Zhang, F. F., Wei, Z., Ma, S. M., Ma, X., and Yang, J.: Characteristics
1751 of concentrations and water-soluble inorganic ions in PM_{2.5} in Handan City, Hebei province, China,
1752 *Atmospheric Research*, 171, 133-146, <https://doi.org/10.1016/j.atmosres.2015.12.013>, 2016.

1753 Meng, J. H., Shi, X. F., Xiang, Y. and Ren, Y. F.: Current status and sources of heavy metal pollution in
1754 the atmosphere (in Chinese). *Environmental Science and Management* 42(08), 51-53,
1755 <https://doi.org/10.3969/j.issn.1673-1212.2017.08.011>, 2017.

1756 Meng, W., Zhong, Q., Chen, Y., Shen, H., Yun, X., Smith, K. R., Li, B., Liu, J., Wang, X., Ma, J., Cheng,
1757 H., Zeng, E. Y., Guan, D., Russell, A. G., and Tao, S.: Energy and air pollution benefits of household
1758 fuel policies in northern China, *Proceedings of the National Academy of Sciences*, 116, 16773-
1759 16780, <https://doi.org/10.1073/pnas.1904182116>, 2019.

1760 Meng, W., Shen, H., Yun, X., Chen, Y., Zhong, Q., Zhang, W., Yu, X., Xu, H., Ren, Y. a., Shen, G., Ma,
1761 J., Liu, J., Cheng, H., Wang, X., Zhu, D., and Tao, S.: Differentiated-rate clean heating strategy with
1762 superior environmental and health benefits in Northern China, *Environmental Science &*
1763 *Technology*, 54, 13458-13466, <https://doi.org/10.1021/acs.est.0c04019>, 2020.

1764 Miller, M. B., Fine, R., Pierce, A. M., and Gustin, M. S.: Identifying sources of ozone to three rural
1765 locations in Nevada, USA, using ancillary gas pollutants, aerosol chemistry, and mercury, *Science*
1766 *of The Total Environment*, 530-531, 483-492, <https://doi.org/10.1016/j.scitotenv>, 2015.

1767 Millet, D. B., Donahue, N. M., Pandis, S. N., Polidori, A., Stanier, C. O., Turpin, B. J., and Goldstein, A.
1768 H.: Atmospheric volatile organic compound measurements during the Pittsburgh Air Quality Study:
1769 Results, interpretation, and quantification of primary and secondary contributions, *Journal of*
1770 *Geophysical Research: Atmospheres*, 110, <https://doi.org/10.1029/2004JD004601>, 2005.

1771 Ming, J., Xiao, C., Sun, J., Kang, S., and Bonasoni, P.: Carbonaceous particles in the atmosphere and
1772 precipitation of the Nam Co region, central Tibet, *Journal of Environmental Sciences*, 22, 1748-
1773 1756, [https://doi.org/10.1016/S1001-0742\(09\)60315-6](https://doi.org/10.1016/S1001-0742(09)60315-6), 2010.

1774 Mishra, M. and Kulshrestha, U.: Chemical characteristics and deposition fluxes of dust-carbon mixed
1775 coarse aerosols at three sites of Delhi, NCR, *Journal of Atmospheric Chemistry*, 74, 399-421,

1776 <https://doi.org/10.1007/s10874-016-9349-1>, 2017.

1777 Moravek, A., Murphy, J. G., Hrdina, A., Lin, J. C., Pennell, C., Franchin, A., Middlebrook, A. M., Fibiger,
1778 D. L., Womack, C. C., McDuffie, E. E., Martin, R., Moore, K., Baasandorj, M., and Brown, S. S.:
1779 Wintertime spatial distribution of ammonia and its emission sources in the Great Salt Lake region,
1780 Atmospheric Chemistry and Physics, 19, 15691-15709, <https://doi.org/10.5194/acp-19-15691-2019>,
1781 2019.

1782 Munawer, M. E.: Human health and environmental impacts of coal combustion and post-combustion
1783 wastes, Journal of Sustainable Mining, 17, 87-96, <https://doi.org/10.1016/j.jsm>, 2018.

1784 Na, K., Sawant, A. A., Song, C., and Cocker, D. R.: Primary and secondary carbonaceous species in the
1785 atmosphere of Western Riverside County, California, Atmospheric Environment, 38, 1345-1355,
1786 <https://doi.org/10.1016/j.atmosenv>, 2004.

1787 Noll, K. E. and Fang, K. Y. P.: Development of a dry deposition model for atmospheric coarse particles,
1788 Atmospheric Environment (1967), 23, 585-594, [https://doi.org/10.1016/0004-6981\(89\)90007-3](https://doi.org/10.1016/0004-6981(89)90007-3),
1789 1989.

1790 Norris, G., Duvall, R., Brown, S., and Bai, S.: EPA Positive Matrix Factorization (PMF) 5.0 fundamentals
1791 and user guide, The United States Environmental Protection Agency, <https://www.epa.gov>,
1792 2014. Nuralkyzy, B., Wang, P., Deng, X., An, S., and Huang, Y.: Heavy metal contents and
1793 assessment of soil contamination in different land-use types in the Qaidam Basin, Sustainability,
1794 13(21), 12020, <https://doi.org/10.3390/su132112020>, 2021.

1795 Offer, Z. Y., Goossens, D., and Shachak, M.: Aeolian deposition of nitrogen to sandy and loessial
1796 ecosystems in the Negev Desert, Journal of Arid Environments, 23, 355-363,
1797 [https://doi.org/10.1016/S0140-1963\(18\)30609-8](https://doi.org/10.1016/S0140-1963(18)30609-8), 1992.

1798 Oliveira, T., Pio, C., Alves, C., Silvestre, A., Evtyugina, M., Afonso, J., Caseiro, A., and Legrand, M.:
1799 Air quality and organic compounds in aerosols from a coastal rural area in the Western Iberian
1800 Peninsula over a year long period: Characterisation, loads and seasonal trends, Atmospheric
1801 Environment, 41, 3631-3643, <https://doi.org/10.1016/j.atmosenv>, 2007.

1802 Pacyna, J. M. and Pacyna, E. G.: An assessment of global and regional emissions of trace metals to the
1803 atmosphere from anthropogenic sources worldwide, Environmental Reviews, 9, 269-298,
1804 <https://doi.org/10.1139/a01-012>, 2001.

1805 Pandolfi, M., Gonzalez-Castanedo, Y., Alastuey, A., de la Rosa, J. D., Mantilla, E., de la Campa, A. S.,

1806 Querol, X., Pey, J., Amato, F., and Moreno, T.: Source apportionment of PM₁₀ and PM_{2.5} at multiple
1807 sites in the strait of Gibraltar by PMF: impact of shipping emissions, *Environmental Science and*
1808 *Pollution Research*, 18, 260-269, <https://doi.org/10.1007/s11356-010-0373-4>, 2010.

1809 Parajuli, S. P., Stenchikov, G. L., Ukhov, A., Mostamandi, S., Kucera, P. A., Axisa, D., Gustafson Jr, W.
1810 I., and Zhu, Y.: Effect of dust on rainfall over the Red Sea coast based on WRF-Chem model
1811 simulations, *Atmospheric Chemistry and Physics*, 22, 8659-8682, [https://doi.org/10.5194/acp-22-](https://doi.org/10.5194/acp-22-8659-2022)
1812 [8659-2022](https://doi.org/10.5194/acp-22-8659-2022), 2022.

1813 Peng, T., Sun, C., Zhang, Y., and Fan, F.: Spatiotemporal variation of anthropogenic heat emission
1814 landscape pattern in the central urban area of Guangzhou, *Journal of South China Normal University*
1815 *(Natural Science Edition)*, 53, 92–102, <https://doi.org/10.6054/j.jscnun.2021080>, 2021.

1816 Pervez, S., Bano, S., Watson, J. G., Chow, J. C., Matawle, J. L., Shrivastava, A., Tiwari, S., and Pervez,
1817 Y. F.: Source profiles for PM_{10-2.5} resuspended dust and vehicle exhaust emissions in Central India,
1818 *Aerosol and Air Quality Research*, 18, 1660-1672, <https://doi.org/10.4209/aaqr>, 2018.

1819 Phairuang, W., Hongtieab, S., Suwattiga, P., Furuuchi, M., and Hata, M.: Atmospheric Ultrafine
1820 Particulate Matter (PM_{0.1})-bound carbon composition in Bangkok, Thailand, *Atmosphere*, 13,
1821 <https://doi.org/10.3390/atmos13101676>, 2022.

1822 Pio, C., Cerqueira, M., Harrison, R. M., Nunes, T., Mirante, F., Alves, C., Oliveira, C., Sanchez de la
1823 Campa, A., Artífano, B., and Matos, M.: OC/EC ratio observations in Europe: Re-thinking the
1824 approach for apportionment between primary and secondary organic carbon, *Atmospheric*
1825 *Environment*, 45, 6121-6132, <https://doi.org/10.1016/j.atmosenv>, 2011.

1826 Pipal, A. S., Singh, S., and Satsangi, G. P.: Study on bulk to single particle analysis of atmospheric
1827 aerosols at urban region, *Urban Climate*, 27, 243-258, <https://doi.org/10.1016/j.uclim.2018.12.008>,
1828 2019.

1829 Popovicheva, O. B., Engling, G., Diapouli, E., Saraga, D., Persiantseva, N. M., Timofeev, M. A., Kireeva,
1830 E. D., Shonija, N. K., Chen, S. H., Nguyen, D. L., Eleftheriadis, K., and Lee, C. T.: Impact of smoke
1831 intensity on size-resolved aerosol composition and microstructure during the biomass burning
1832 season in Northwest Vietnam, *Aerosol and Air Quality Research*, 16, 2635-2654,
1833 <https://doi.org/10.4209/aaqr>, 2016.

1834 Qi, D. L., Zhao, Q. N., Zhao, H. F., Han, T. F. and Su, W. J.: Temporal and spatial characteristics and
1835 regional differences of dust-fall in Qinghai Province from 2004 to 2017 (in Chinese), *Arid*

1836 Meteorology, 36(06), 927-935, <http://www.ghqx.org.cn/CN/Y2018/V36/I6/927>, 2018.

1837 Qian, G. Q. and Dong, Z. B.: Research on methods and related issues of atmospheric dust collection (in
1838 Chinese), Chinese Journal of Desert Research, (06), 119-122, [https://doi.org/1000-694X9\(2004\)06-](https://doi.org/1000-694X9(2004)06-0779-04)
1839 0779-04, 2014.

1840 Qian, Y., Yasunari, T. J., Doherty, S. J., Flanner, M. G., Lau, W. K. M., Ming, J., Wang, H., Wang, M.,
1841 Warren, S. G., and Zhang, R.: Light-absorbing particles in snow and ice: Measurement and
1842 modeling of climatic and hydrological impact, Advances in Atmospheric Sciences, 32, 64-91,
1843 <https://doi.org/10.1007/s00376-014-0010-0>, 2015.

1844 Qiao, Q., Huang, B., Zhang, C., Piper, J. D. A., Pan, Y., and Sun, Y.: Assessment of heavy metal
1845 contamination of dustfall in northern China from integrated chemical and magnetic investigation,
1846 Atmospheric Environment, 74, 182-193, <https://doi.org/10.1016/j.atmosenv>, 2013.

1847 Rabha, S., Saikia, B. K., Singh, G. K., and Gupta, T.: Meteorological influence and chemical
1848 compositions of atmospheric particulate matters in an Indian Urban Area, ACS Earth and Space
1849 Chemistry, 5, 1686-1694, <https://doi.org/10.1021/acsearthspacechem.1c00037>, 2021.

1850 Ramanathan, V. and Carmichael, G.: Global and regional climate changes due to black carbon, Nature
1851 Geoscience, 1, 221-227, <https://doi.org/10.1038/ngeo156>, 2008.

1852 Rogge, W. F., Hildemann, L. M., Mazurek, M. A., Cass, G. R., and Simoneit, B. R. T.: Sources of fine
1853 organic aerosol. 3. Road dust, tire debris, and organometallic brake lining dust: roads as sources and
1854 sinks, Environmental Science & Technology, 27, 1892-1904, <https://doi.org/10.1021/es00046a019>,
1855 1993.

1856 Rörig-Dalgaard, I.: Direct measurements of the deliquescence relative humidity in salt mixtures
1857 including the contribution from metastable phases, ACS Omega, 6, 16297-16306,
1858 <https://doi.org/10.1021/acsomega.1c00538>, 2021.

1859 Safai, P. D., Raju, M. P., Rao, P. S. P., and Pandithurai, G.: Characterization of carbonaceous aerosols
1860 over the urban tropical location and a new approach to evaluate their climatic importance,
1861 Atmospheric Environment, 92, 493-500, <https://doi.org/10.1016/j.atmosenv.2014.04.055>, 2014.

1862 Saha, A. and Despiou, S.: Seasonal and diurnal variations of black carbon aerosols over a Mediterranean
1863 coastal zone, Atmospheric Research, 92, 27-41, <https://doi.org/10.1016/j.atmosres.2008.07.007>,
1864 2009.

1865 Sandrini, S., Fuzzi, S., Piazzalunga, A., Prati, P., Bonasoni, P., Cavalli, F., Bove, M. C., Calvello, M.,

1866 Cappelletti, D., Colombi, C., Contini, D., de Gennaro, G., Di Gilio, A., Fermo, P., Ferrero, L.,
1867 Gianelle, V., Giugliano, M., Ielpo, P., Lonati, G., Marinoni, A., Massabò, D., Molteni, U., Moroni,
1868 B., Pavese, G., Perrino, C., Perrone, M. G., Perrone, M. R., Putaud, J.-P., Sargolini, T., Vecchi, R.,
1869 and Gilardoni, S.: Spatial and seasonal variability of carbonaceous aerosol across Italy, *Atmospheric*
1870 *Environment*, 99, 587-598, <https://doi.org/10.1016/j.atmosenv.2014.10.032>, 2014.

1871 Saraga, D., Maggos, T., Degrendele, C., Klánová, J., Horvat, M., Kocman, D., Kanduč, T., Garcia Dos
1872 Santos, S., Franco, R., Gómez, P. M., Manousakas, M., Bairachtari, K., Eleftheriadis, K.,
1873 Kermenidou, M., Karakitsios, S., Gotti, A., and Sarigiannis, D.: Multi-city comparative PM_{2.5}
1874 source apportionment for fifteen sites in Europe: The ICARUS project, *Science of The Total*
1875 *Environment*, 751, 141855, <https://doi.org/10.1016/j.scitotenv.2020.141855>, 2021.

1876 Schepanski, K.: Transport of mineral dust and its impact on climate, *Geosciences*, 2018, 8(5), 151,
1877 <https://doi.org/10.3390/geosciences8050151>, 2018.

1878 Schmidl, C., Marr, I. L., Caseiro, A., Kotianová, P., Berner, A., Bauer, H., Kasper-Giebl, A., and Puxbaum,
1879 H.: Chemical characterisation of fine particle emissions from wood stove combustion of common
1880 woods growing in mid-European Alpine regions, *Atmospheric Environment*, 42, 126-141,
1881 <https://doi.org/10.1016/j.atmosenv.2008>.

1882 Secrest, M. H., Schauer, J. J., Carter, E. M., and Baumgartner, J.: Particulate matter chemical component
1883 concentrations and sources in settings of household solid fuel use, *Indoor Air*, 27, 1052-1066,
1884 <https://doi.org/10.1111/ina.12389>, 2017.

1885 Seinfeld, J. H., Pandis, S. N., and Noone, K. J. J. P. T.: *Atmospheric chemistry and physics: From air*
1886 *pollution to climate change*, 51, 88-90, 1998.

1887 Shahram, N., Majid, K., Mehdi, F., Soodabeh, M., and Ahmad, Y.: The origins and sources of dust
1888 particles, their effects on environment and health, and control strategies: A review, *Journal of Air*
1889 *Pollution and Health*, 1(2):137-152, <https://api.semanticscholar.org/CorpusID:56256748>, 2016.

1890 Sharma, S., Brook, J. R., Cachier, H., Chow, J., Gaudenzi, A., and Lu, G.: Light absorption and thermal
1891 measurements of black carbon in different regions of Canada, *Journal of Geophysical Research:*
1892 *Atmospheres*, 107, AAC 11-11, <https://doi.org/10.1029/2002JD002496>, 2002.

1893 Sheehan, P. E. and Bowman, F. M.: Estimated effects of temperature on secondary organic aerosol
1894 concentrations, *Environmental Science & Technology*, 35, 2129-2135,
1895 <https://doi.org/10.1021/es001547g>, 2001.

1896 Shen, J. and Dai, B. L.: Development and utilization of salt lake brine lithium resources and its prospects
1897 (in Chinese), *Industrial Minerals & Processing*, 38, 1–4+7,
1898 <https://doi.org/10.16283/j.cnki.hgkwyjg.2009.04.004>, 2009.

1899 Shen, G. F., Xiong, R., Cheng, H. F. and Tao, S.: Estimation of residential energy structure and primary
1900 PM_{2.5} emissions in rural Tibet (in Chinese), *Science Bulletin*, 66(15), 1900-1911,
1901 <https://doi.org/10.1360/TB-2020-0408>, 2021.

1902 Shen, L., Wang, H., Kong, X., Zhang, C., Shi, S., and Zhu, B.: Characterization of black carbon aerosol
1903 in the Yangtze River Delta, China: Seasonal variation and source apportionment, *Atmospheric
1904 Pollution Research*, 12, 195-209, <https://doi.org/10.1016/j.apr.2020.08.035>, 2021.

1905 Shen, Z., Arimoto, R., Cao, J., Zhang, R., Li, X., Du, N., Okuda, T., Nakao, S., and Tanaka, S.: Seasonal
1906 variations and evidence for the effectiveness of pollution controls on water-soluble inorganic species
1907 in total suspended particulates and fine particulate matter from Xi'an, China, *Journal of the Air &
1908 Waste Management Association*, 58, 1560-1570, <https://doi.org/10.3155/1047-3289.58.12.1560>,
1909 2008.

1910 Shen, Z., Zhang, Q., Cao, J., Zhang, L., Lei, Y., Huang, Y., Huang, R. J., Gao, J., Zhao, Z., Zhu, C., Yin,
1911 X., Zheng, C., Xu, H., and Liu, S.: Optical properties and possible sources of brown carbon in PM_{2.5}
1912 over Xi'an, China, *Atmospheric Environment*, 150, 322-330,
1913 <https://doi.org/10.1016/j.atmosenv.2016.11.024>, 2017.

1914 Shi, G., Chen, Z., Teng, J., Bi, C., Zhou, D., Sun, C., Li, Y., and Xu, S.: Fluxes, variability and sources
1915 of cadmium, lead, arsenic and mercury in dry atmospheric depositions in urban, suburban and rural
1916 areas, *Environmental Research*, 113, 28-32, <https://doi.org/10.1016/j.envres.2012.01.001>, 2012.

1917 Shi, X., Zhao, Y., Dai, S., Xu, L., Li, Y., Jia, H., and Zhang, Q.: Research on climatic change of Qaidam
1918 Basin since 1961, *Journal of Desert Research*, 25, 123-128,
1919 <http://www.desert.ac.cn/CN/Y2005/V25/I1/123>, 2005.

1920 Shi, Z., Vu, T., Kotthaus, S., Harrison, R. M., Grimmond, S., Yue, S., Zhu, T., Lee, J., Han, Y., Demuzere,
1921 M., Dunmore, R. E., Ren, L., Liu, D., Wang, Y., Wild, O., Allan, J., Acton, W. J., Barlow, J., Barratt,
1922 B., Beddows, D., Bloss, W. J., Calzolari, G., Carruthers, D., Carslaw, D. C., Chan, Q., Chatzidiakou,
1923 L., Chen, Y., Crilley, L., Coe, H., Dai, T., Doherty, R., Duan, F., Fu, P., Ge, B., Ge, M., Guan, D.,
1924 Hamilton, J. F., He, K., Heal, M., Heard, D., Hewitt, C. N., Hollaway, M., Hu, M., Ji, D., Jiang, X.,
1925 Jones, R., Kalberer, M., Kelly, F. J., Kramer, L., Langford, B., Lin, C., Lewis, A. C., Li, J., Li, W.,

1926 Liu, H., Liu, J., Loh, M., Lu, K., Lucarelli, F., Mann, G., McFiggans, G., Miller, M. R., Mills, G.,
1927 Monk, P., Nemitz, E., O'Connor, F., Ouyang, B., Palmer, P. I., Percival, C., Popoola, O., Reeves, C.,
1928 Rickard, A. R., Shao, L., Shi, G., Spracklen, D., Stevenson, D., Sun, Y., Sun, Z., Tao, S., Tong, S.,
1929 Wang, Q., Wang, W., Wang, X., Wang, X., Wang, Z., Wei, L., Whalley, L., Wu, X., Wu, Z., Xie, P.,
1930 Yang, F., Zhang, Q., Zhang, Y., Zhang, Y., and Zheng, M.: Introduction to the special issue “In-depth
1931 study of air pollution sources and processes within Beijing and its surrounding region (APHH-
1932 Beijing)”, *Atmospheric Chemistry and Physics*, 19, 7519-7546, [https://doi.org/10.5194/acp-19-](https://doi.org/10.5194/acp-19-7519-2019)
1933 7519-2019, 2019.

1934 Shrivastava, M., Lou, S., Zelenyuk, A., Easter, R. C., Corley, R. A., Thrall, B. D., Rasch, P. J., Fast, J. D.,
1935 Massey Simonich, S. L., Shen, H., and Tao, S.: Global long-range transport and lung cancer risk
1936 from polycyclic aromatic hydrocarbons shielded by coatings of organic aerosol, *Proceedings of the*
1937 *National Academy of Sciences*, 114, 1246-1251, <https://doi.org/10.1073/pnas.1618475114>, 2017.

1938 Simoneit, B. R. T.: Biomass burning — a review of organic tracers for smoke from incomplete
1939 combustion, *Applied Geochemistry*, 17, 129-162, [https://doi.org/10.1016/S0883-2927\(01\)00061-0](https://doi.org/10.1016/S0883-2927(01)00061-0),
1940 2002.

1941 Smichowski, P., Gómez, D., Frazzoli, C., and Caroli, S.: Traffic-related elements in airborne particulate
1942 matter, *Applied Spectroscopy Reviews*, 43, 23-49, <https://doi.org/10.1080/05704920701645886>,
1943 2007.

1944 Smith, R. M. and Twiss, P. C.: Extensive gaging of dust deposition rates, *Kansas Acad.*, 68:2,
1945 <https://doi.org/10.2307/3626489>, 1965.

1946 Song, P. S., Li, W., Sun, B., Nie, Z., Bu, L. Z., and Wang, Y. S.: Progress in the development and
1947 utilization of salt lake resources (in Chinese), *Journal of Inorganic Chemistry*, 27, 801–815, 2011.

1948 Sow, M., Goossens, D., and Rajot, J. L.: Calibration of the MDCO dust collector and of four versions of
1949 the inverted frisbee dust deposition sampler, *Geomorphology*, 82, 360-375,
1950 <https://doi.org/10.1016/j.geomorph.2006.05.013>, 2006.

1951 Strader, R., Lurmann, F., and Pandis, S. N.: Evaluation of secondary organic aerosol formation in winter,
1952 *Atmospheric Environment*, 33, 4849-4863, [https://doi.org/10.1016/S1352-2310\(99\)00310-6](https://doi.org/10.1016/S1352-2310(99)00310-6), 1999.

1953 Sulong, N. A., Latif, M. T., Sahani, M., Khan, M. F., Fadzil, M. F., Tahir, N. M., Mohamad, N., Sakai,
1954 N., Fujii, Y., Othman, M., and Tohno, S.: Distribution, sources and potential health risks of
1955 polycyclic aromatic hydrocarbons (PAHs) in PM_{2.5} collected during different monsoon seasons and

1956 haze episode in Kuala Lumpur, *Chemosphere*, 219, 1-14, <https://doi.org/10.1016/j.chemosphere>,

1957 2019.

1958 Tang, Y., Han, G. L. and Xu, Z. F.: Characteristics of black carbon content in atmospheric dust in Beijing

1959 and its northern regions (in Chinese), *Acta Scientiae Circumstantiae*, 33(02), 332-338,

1960 <https://doi.org/10.13671/j.hjkxxb.2013.02.033>, 2013.

1961 Tao, J., Cheng, T., Zhang, R., Cao, J., Zhu, L., Wang, Q., Luo, L., and Zhang, L.: Chemical composition

1962 of PM_{2.5} at an urban site of Chengdu in southwestern China, *Advances in Atmospheric Sciences*, 30,

1963 1070-1084, <https://doi.org/10.1007/s00376-012-2168-7>, 2013.

1964 Tao, S., Ru, M. Y., Du, W., Zhu, X., Zhong, Q. R., Li, B. G., Shen, G. F., Pan, X. L., Meng, W. J., Chen,

1965 Y. L., Shen, H. Z., Lin, N., Su, S., Zhuo, S. J., Huang, T. B., Xu, Y., Yun, X., Liu, J. F., Wang, X. L.,

1966 Liu, W. X., Cheng, H. F., and Zhu, D. Q.: Quantifying the rural residential energy transition in China

1967 from 1992 to 2012 through a representative national survey, *Nature Energy*, 3, 567-573,

1968 <https://doi.org/10.1038/s41560-018-0158-4>, 2018.

1969 Tian, M., Gao, J., Zhang, L., Zhang, H., Feng, C., and Jia, X.: Effects of dust emissions from wind erosion

1970 of soil on ambient air quality, *Atmospheric Pollution Research*, 12,

1971 <https://doi.org/10.1016/j.apr.2021.101108>, 2021.

1972 Tian, S. L., Pan, Y. P., and Wang, Y. S.: Size-resolved source apportionment of particulate matter in urban

1973 Beijing during haze and non-haze episodes, *Atmospheric Chemistry and Physics*, 16, 1-19,

1974 <https://doi.org/10.5194/acp-16-1-2016>, 2016.

1975 Tiwari, S., Pandithurai, G., Attri, S. D., Srivastava, A. K., Soni, V. K., Bisht, D. S., Anil Kumar, V., and

1976 Srivastava, M. K.: Aerosol optical properties and their relationship with meteorological parameters

1977 during wintertime in Delhi, India, *Atmospheric Research*, 153, 465-479,

1978 <https://doi.org/10.1016/j.atmosres.2014.10.003>, 2015.

1979 Turpin, B. J. and Huntzicker, J. J.: Identification of secondary organic aerosol episodes and quantitation

1980 of primary and secondary organic aerosol concentrations during SCAQS, *Atmospheric Environment*,

1981 29, 3527-3544, [https://doi.org/10.1016/1352-2310\(94\)00276-Q](https://doi.org/10.1016/1352-2310(94)00276-Q), 1995.

1982 Turpin, B. J., Huntzicker, J. J., and Hering, S. V.: Investigation of organic aerosol sampling artifacts in

1983 the los angeles basin, *Atmospheric Environment*, 28, 3061-3071, <https://doi.org/10.1016/1352->

1984 2310(94)00133-6, 1994.

1985 VanCuren, R. and Gustin, M. S.: Identification of sources contributing to PM_{2.5} and ozone at elevated

1986 sites in the western U.S. by receptor analysis: Lassen Volcanic National Park, California, and Great
1987 Basin National Park, Nevada, *Science of The Total Environment*, 530-531, 505-518,
1988 <https://doi.org/10.1016/j.scitotenv>, 2015.

1989 Venkataraman, C., Brauer, M., Tibrewal, K., Sadavarte, P., Ma, Q., Cohen, A., Chaliyakunnel, S., Frostad,
1990 J., Klimont, Z., Martin, R. V., Millet, D. B., Philip, S., Walker, K., and Wang, S.: Source influence
1991 on emission pathways and ambient PM_{2.5} pollution over India (2015–2020), *Atmospheric Chemistry
1992 and Physics*, 18, 8017-8039, <https://doi.org/10.5194/acp-18-8017-2018>, 2018.

1993 Wang, F.: The mechanism and timescales of soil formation in the hyper-arid Atacama Desert, Chile,
1994 Purdue University, 2013.

1995 Wang, F., Michalski, G., Seo, J.-h., and Ge, W.: Geochemical, isotopic, and mineralogical constraints on
1996 atmospheric deposition in the hyper-arid Atacama Desert, Chile, *Geochimica et Cosmochimica Acta*,
1997 135, 29-48, <https://doi.org/10.1016/j.gca>, 2014.

1998 Wang, M., Duan, Y., Xu, W., Wang, Q., Zhang, Z., Yuan, Q., Li, X., Han, S., Tong, H., Huo, J., Chen, J.,
1999 Gao, S., Wu, Z., Cui, L., Huang, Y., Xiu, G., Cao, J., Fu, Q., and Lee, S.: Measurement report:
2000 Characterisation and sources of the secondary organic carbon in a Chinese megacity over 5 years
2001 from 2016 to 2020, *Atmospheric Chemistry and Physics*, 22, 12789-12802,
2002 <https://doi.org/10.5194/acp-22-12789-2022>, 2022.

2003 Watson, J. G., Antony Chen, L. W., Chow, J. C., Doraiswamy, P., and Lowenthal, D. H.: Source
2004 apportionment: Findings from the U.S. supersites program, *Journal of the Air & Waste Management
2005 Association*, 58, 265-288, <https://doi.org/10.3155/1047-3289.58.2.265>, 2008.

2006 Wei, C., Bandowe, B. A. M., Han, Y., Cao, J., Zhan, C., and Wilcke, W.: Polycyclic aromatic
2007 hydrocarbons (PAHs) and their derivatives (alkyl-PAHs, oxygenated-PAHs, nitrated-PAHs and
2008 azaarenes) in urban road dusts from Xi'an, Central China, *Chemosphere*, 134, 512-520,
2009 <https://doi.org/10.1016/j.chemosphere.2014.11.052>, 2015.

2010 Wei, T., Dong, Z., Kang, S., Qin, X., and Guo, Z.: Geochemical evidence for sources of surface dust
2011 deposited on the Laohugou glacier, Qilian Mountains, *Applied Geochemistry*, 79, 1-8,
2012 <https://doi.org/10.1016/j.apgeochem>, 2017.

2013 Wei, Y., Xie, Y., Dang, X., Guo, J., Liu, M., and Wu, H.: Characteristics of atmospheric dust deposition
2014 and influencing factors in different protection functional areas of the Jilantai Salt Lake Protection
2015 system, *Research of Soil and Water Conservation*, 30, 201-208,

2016 <https://doi.org/10.13869/j.cnki.rswc.2023.05.027>, 2023.

2017 Wu, C. and Yu, J. Z.: Determination of primary combustion source organic carbon-to-elemental carbon
2018 (OC/EC) ratio using ambient OC and EC measurements: secondary OC-EC correlation
2019 minimization method, *Atmospheric Chemistry and Physics*, 16, 5453-5465,
2020 <https://doi.org/10.5194/acp-16-5453-2016>, 2016.

2021 Wu, C., Wu, D., and Yu, J. Z.: Quantifying black carbon light absorption enhancement with a novel
2022 statistical approach, *Atmospheric Chemistry and Physics*, 18, 289-309, [https://doi.org/10.5194/acp-](https://doi.org/10.5194/acp-18-289-2018)
2023 18-289-2018, 2018a.

2024 Wu, Y., Zhang, R., Tian, P., Tao, J., Hsu, S. C., Yan, P., Wang, Q., Cao, J., Zhang, X., and Xia, X.: Effect
2025 of ambient humidity on the light absorption amplification of black carbon in Beijing during January
2026 2013, *Atmospheric Environment*, 124, 217-223, <https://doi.org/10.1016/j.atmosenv.2015.04.041>,
2027 2016.

2028 Xia, X., Zong, X., Cong, Z., Chen, H., Kang, S., and Wang, P.: Baseline continental aerosol over the
2029 central Tibetan plateau and a case study of aerosol transport from South Asia, *Atmospheric*
2030 *Environment*, 45, 7370-7378, <https://doi.org/10.1016/j.atmosenv.2011.07.067>, 2011.

2031 Xiao, Q., Saikawa, E., Yokelson, R. J., Chen, P., Li, C., and Kang, S.: Indoor air pollution from burning
2032 yak dung as a household fuel in Tibet, *Atmospheric Environment*, 102, 406-412,
2033 <https://doi.org/10.1016/j.atmosenv>, 2015.

2034 Xie, F., Guo, L., Wang, Z., Tian, Y., Yue, C., Zhou, X., Wang, W., Xin, J., and Lu, C.: Geochemical
2035 characteristics and socioeconomic associations of carbonaceous aerosols in coal-fueled cities with
2036 significant seasonal pollution pattern, *Environmental International*, 179, 108179,
2037 <https://doi.org/10.1016/j.envint.2023.108179>, 2023.

2038 Xu, L., Chen, X., Chen, J., Zhang, F., He, C., Zhao, J., and Yin, L.: Seasonal variations and chemical
2039 compositions of PM_{2.5} aerosol in the urban area of Fuzhou, China, *Atmospheric Research*, 104-
2040 105, 264-272, <https://doi.org/10.1016/j.atmosres>, 2012.

2041 Xu, M., Liu, Z., Hu, B., Yan, G., Zou, J., Zhao, S., Zhou, J., Liu, X., Zheng, X., Zhang, X., Cao, J., Guan,
2042 M., Lv, Y., and Zhang, Y.: Chemical characterization and source identification of PM_{2.5} in Luoyang
2043 after the clean air actions, *Journal of Environmental Sciences*, 115, 265-276,
2044 <https://doi.org/10.1016/j.jes.2021.06.021>, 2022.

2045 Xu, R., Tie, X., Li, G., Zhao, S., Cao, J., Feng, T., and Long, X.: Effect of biomass burning on black

2046 carbon (BC) in South Asia and Tibetan Plateau: The analysis of WRF-Chem modeling, *Science of*
2047 *The Total Environment*, 645, 901-912, <https://doi.org/10.1016/j.scitotenv.2018.07.165>, 2018b.

2048 Xu, Z., Wang, J., and Han, J.: Ecological vulnerability assessment of the Qaidam Basin based on the SRP
2049 Model, *Salt Lake Research*, 32, 53-60, <https://doi.org/10.3724/j.yhyj.2024009>, 2024.

2050 Xu, Z.: Airborne particles in outdoor air: Atmospheric dust, in: *Fundamentals of air cleaning technology*
2051 *and its application in cleanrooms*, Springer Berlin Heidelberg, 47-132, [https://doi.org/10.1007/978-](https://doi.org/10.1007/978-3-642-39374-7_2)
2052 [3-642-39374-7_2](https://doi.org/10.1007/978-3-642-39374-7_2), 2014.

2053 Xue, W., Wang, L., Yang, Z., Xiong, Z., Li, X., Xu, Q., and Cai, Z.: Can clean heating effectively alleviate
2054 air pollution: An empirical study based on the plan for cleaner winter heating in northern China,
2055 *Applied Energy*, 351, 121923, <https://doi.org/10.1016/j.apenergy>, 2023.

2056 Yan, B., Zheng, M., Hu, Y., Ding, X., Sullivan, A. P., Weber, R. J., Baek, J., Edgerton, E. S., and Russell,
2057 A. G.: Roadside, urban, and rural comparison of primary and secondary organic molecular markers
2058 in ambient PM_{2.5}, *Environmental Science & Technology*, 43, 4287-4293,
2059 <https://doi.org/10.1021/es900316g>, 2009.

2060 Yang, F., He, K., Ye, B., Chen, X., Cha, L., Cadle, S. H., Chan, T., and Mulawa, P. A.: One-year record
2061 of organic and elemental carbon in fine particles in downtown Beijing and Shanghai, *Atmospheric*
2062 *Chemistry and Physics*, 5, 1449-1457, <https://doi.org/10.5194/acp-5-1449-2005>, 2005.

2063 Yang, Q. L., Wang, J. X. and Zhao, Z. X.: Temporal and spatial distribution characteristics and source
2064 analysis of heavy metals in atmospheric dust in typical industrial cities in Northeast China during
2065 winter and spring (in Chinese), *Acta Scientiae Circumstantiae*, 1-9,
2066 <https://doi.org/10.13671/j.hjkxxb.2024.0254>, 2024.

2067 Yao, L., Yang, L., Yuan, Q., Yan, C., Dong, C., Meng, C., Sui, X., Yang, F., Lu, Y., and Wang, W.: Sources
2068 apportionment of PM_{2.5} in a background site in the North China Plain, *Science of the Total*
2069 *Environment*, 541, 590-598, <https://doi.org/10.1016/j.scitotenv>, 2016.

2070 Ye, W., Saikawa, E., Avramov, A., Cho, S. H., and Chartier, R.: Household air pollution and personal
2071 exposure from burning firewood and yak dung in summer in the eastern Tibetan Plateau,
2072 *Environmental Pollution*, 263, 114531, <https://doi.org/10.1016/j.envpol>, 2020.

2073 Yoo, H. Y., Kim, K. A., Kim, Y. P., Jung, C. H., Shin, H. J., Moon, K. J., Park, S. M., and Lee, J. Y.:
2074 Validation of SOC estimation using OC and EC concentration in PM_{2.5} measured at Seoul, *Aerosol*
2075 *and Air Quality Research*, 22, 210388, <https://doi.org/10.4209/aaqr.210388>, 2022.

2076 You, S., Yao, Z., Dai, Y., and Wang, C. H.: A comparison of PM exposure related to emission hotspots in
2077 a hot and humid urban environment: Concentrations, compositions, respiratory deposition, and
2078 potential health risks, *Science of The Total Environment*, 599-600, 464-473,
2079 <https://doi.org/10.1016/j.scitotenv.2017.04.217>, 2017.

2080 Yu, H., Yang, W., Wang, X., Yin, B., Zhang, X., Wang, J., Gu, C., Ming, J., Geng, C., and Bai, Z.: A
2081 seriously sand storm mixed air-polluted area in the margin of Tarim Basin: Temporal-spatial
2082 distribution and potential sources, *Science of The Total Environment*, 676, 436-446,
2083 <https://doi.org/10.1016/j.scitotenv>, 2019.

2084 Yu, L. P., Li, D., Meng, L., Du, C. Y. and Zhao, P.: Observation and data processing methods for
2085 atmospheric dust deposition (in Chinese), *Anhui Agricultural Sciences*, 44: 185-186,
2086 <https://doi.org/10.13989/j.cnki.0517-6611.2016.31.064>, 2016.

2087 Yu, L., Wang, G., Zhang, R., Zhang, L., Song, Y., Wu, B., Li, X., An, K., and Chu, J.: Characterization
2088 and source apportionment of PM_{2.5} in an urban environment in Beijing, *Aerosol and Air Quality
2089 Research*, 13, 574-583, <https://doi.org/10.4209/aaqr.2012.07.0192>, 2013.

2090 Yue, D., Zhong, L., Zhang, T., Shen, J., Zhou, Y., Zeng, L., Dong, H., and Ye, S.: Pollution properties of
2091 water-soluble secondary inorganic ions in atmospheric PM_{2.5} in the Pearl River Delta Region,
2092 *Aerosol and Air Quality Research*, 15, 1737-1747, <https://doi.org/10.4209/aaqr.2014.12.0333>, 2015.

2093 Zan, J., Maher, B. A., Fang, X., Stevens, T., Ning, W., Wu, F., Yang, Y., Kang, J., and Hu, Z.: Global dust
2094 impacts on biogeochemical cycles and climate, *Nature Reviews Earth & Environment*, 6, 789-807,
2095 <https://doi.org/10.1038/s43017-025-00734-2>, 2025.

2096 Zang, L., Zhang, Y., Zhu, B., Mao, F., Zhang, Y., and Wang, Z.: Characteristics of water-soluble inorganic
2097 aerosol pollution and its meteorological response in Wuhan, Central China, *Atmospheric Pollution
2098 Research*, 12, 362-369, <https://doi.org/10.1016/j.apr.2021.01.003>, 2021.

2099 Zhan, C., Han, Y., Cao, J., Wei, C., Zhang, J., and An, Z.: Validation and application of a thermal–optical
2100 reflectance (TOR) method for measuring black carbon in loess sediments, *Chemosphere*, 91, 1462-
2101 1470, <https://doi.org/10.1016/j.chemosphere.2012.12.011>, 2013.

2102 Zhan, C. L., Zhan, J. W., Ke, Z. D., Liu, S., Zhang, J. Q. and Liu, H. X.: Pollution characteristics and
2103 source analysis of black carbon in different types of dust in Xiaogan, Hubei (in Chinese),
2104 *Environmental Pollution and Control* 44(01), 14-19 + 26, <https://doi.org/10.15985/j.cnki.1001-3865>,
2105 2022.

2106 Zhan, C. L., Zhang, J. Q., Zheng, J. G., Yao, R. Z., Xiao, W. S. and Cao, J. J.: Pollution characteristics
2107 and source analysis of black carbon in atmospheric dust along National Highway 316 (in Chinese),
2108 Environmental Science and Technology, 39(04), 154-160, [https://doi.org/10.3969-j.issn.1003-](https://doi.org/10.3969-j.issn.1003-6504.20169)
2109 6504.20169, 2016.

2110 Zhang, B., Shen, Z., Sun, J., He, K., Zou, H., Zhang, Q., Li, J., Xu, H., Liu, S., Ho, K.-F., and Cao, J.:
2111 County-level of particle and gases emission inventory for animal dung burning in the Qinghai–
2112 Tibetan Plateau, China, Journal of Cleaner Production, 367,
2113 <https://doi.org/10.1016/j.jclepro.2022.133051>, 2022.

2114 Zhang, F.: Study on the dry deposition of organic carbon and elemental carbon in the atmosphere of
2115 Nanchang (in Chinese), Master's Thesis, 2014.

2116 Zhang, F., Wang, Z. W., Cheng, H. R., Lv, X. P., Gong, W., Wang, X. M., and Zhang, G.: Seasonal
2117 variations and chemical characteristics of PM_{2.5} in Wuhan, central China, Science of the Total
2118 Environment, 518-519, 97-105, <https://doi.org/10.1016/j.scitotenv>, 2015a.

2119 Zhang, J., Liu, H. N., Zheng, Q. P., and Tang, L. J.: Correlation study between particulate matter and
2120 visibility in Suzhou, Proceedings of the 7th Annual Conference of Chinese Society of Particuology
2121 cum Symposium on Particle Technology across Taiwan Straits, Xi'an, Shaanxi, China, 1, 2010.

2122 Zhang, H. and Han, F.: The preliminary remote sensing interpretation of salt lake and its environments
2123 in the Central Qaidam Basin, Northwest China, Journal of Salt Lake Research, 10, 28-34, 2002.

2124 Zhang, J., Smith, K. R., Ma, Y., Ye, S., Jiang, F., Qi, W., Liu, P., Khalil, M. A. K., Rasmussen, R. A., and
2125 Thorneloe, S. A.: Greenhouse gases and other airborne pollutants from household stoves in China:
2126 a database for emission factors, Atmospheric Environment, 34, 4537-4549,
2127 [https://doi.org/10.1016/S1352-2310\(99\)00450-1](https://doi.org/10.1016/S1352-2310(99)00450-1), 2000.

2128 Zhang, J., Huang, X., Li, J., Chen, L., Zhao, R., Wang, R., Sun, W., Chen, C., Su, Y., Wang, F., Huang,
2129 Y., and Lin, C.: Chemical composition, sources and evolution of PM_{2.5} during wintertime in the city
2130 cluster of southern Sichuan, China, Atmospheric Pollution Research, 14, 101635,
2131 <https://doi.org/10.1016/j.apr.2022.101635>, 2023.

2132 Zhang, K., Shang, X., Herrmann, H., Meng, F., Mo, Z., Chen, J., and Lv, W.: Approaches for identifying
2133 PM_{2.5} source types and source areas at a remote background site of South China in spring, Science
2134 of The Total Environment, 691, 1320-1327, <https://doi.org/10.1016/j.scitotenv>, 2019.

2135 Zhang, N., Cao, J., Liu, S., Zhao, Z., Xu, H., and Xiao, S.: Chemical composition and sources of PM_{2.5}

2136 and TSP collected at Qinghai Lake during summertime, *Atmospheric Research*, 138, 213-222,
2137 <https://doi.org/10.1016/j.atmosres>, 2014.

2138 Zhang, P. X.: Salt lakes in the Qaidam Basin (in Chinese), Beijing: Science Press, 1987.

2139 Zhang, R., Wang, H., Qian, Y., Rasch, P. J., Easter, R. C., Ma, P. L., Singh, B., Huang, J., and Fu, Q.:
2140 Quantifying sources, transport, deposition, and radiative forcing of black carbon over the Himalayas
2141 and Tibetan Plateau, *Atmospheric Chemistry and Physics*, 15, 6205-6223,
2142 <https://doi.org/10.5194/acp-15-6205-2015>, 2015b.

2143 Zhang, R., Jing, J., Tao, J., Hsu, S. C., Wang, G., Cao, J., Lee, C. S. L., Zhu, L., Chen, Z., Zhao, Y., and
2144 Shen, Z.: Chemical characterization and source apportionment of PM_{2.5} in Beijing: seasonal
2145 perspective, *Atmospheric Chemistry and Physics*, 13, 7053-7074, [https://doi.org/10.5194/acp-13-](https://doi.org/10.5194/acp-13-7053-2013)
2146 [7053-2013](https://doi.org/10.5194/acp-13-7053-2013), 2013.

2147 Zhang, S.: Spatial and temporal variation characteristics of atmospheric dust deposition flux in Hebei
2148 Province over the Recent 20 Years, Master's thesis, Hebei Normal University, 2010.

2149 Zhang, X. Y., Wang, Y. Q., Zhang, X. C., Guo, W., and Gong, S. L.: Carbonaceous aerosol composition
2150 over various regions of China during 2006, *Journal of Geophysical Research: Atmospheres*, 113,
2151 <https://doi.org/10.1029/2007jd009525>, 2008.

2152 Zhang, X. Y., Wang, Y. Q., Wang, D., Gong, S. L., Arimoto, R., Mao, L. J., and Li, J.: Characterization
2153 and sources of regional-scale transported carbonaceous and dust aerosols from different pathways
2154 in coastal and sandy land areas of China, *Journal of Geophysical Research: Atmospheres*, 110,
2155 <https://doi.org/10.1029/2004jd005457>, 2005.

2156 Zhang, Y.: Satellite Observation and ground validation of volatile organic compounds emissions from
2157 biomass combustion, Master's thesis, Yunnan University,
2158 <https://doi.org/10.27456/d.cnki.gyndu.2024.002784>, 2024.

2159 Zhang, Z., Zhou, Y., Zhao, N., Li, H., Tohniyaz, B., Mperejekumana, P., Hong, Q., Wu, R., Li, G., Sultan,
2160 M., Zayan, A. M. I., Cao, J., Ahmad, R., and Dong, R.: Clean heating during winter season in
2161 Northern China: A review, *Renewable and Sustainable Energy Reviews*, 149, 111339,
2162 <https://doi.org/10.1016/j.rser>, 2021.

2163 Zhang, Z. C., Xie, Y. Q., Zhang, Z. J., Gao, G. S., Xu, B., Tian, X., Xu, H., Wie, Y. T., Shi, G. L. and
2164 Feng, Y. C.: Source analysis and seasonal variation characteristics of atmospheric dust deposition
2165 in Taiyuan City based on two receptor models (in Chinese), *China Environmental Science*, 42, 2577-

2166 2586, <https://doi.org/10.3969/j.issn.1000-6923>, 2022.

2167 Zhao, Z., Cao, J., Shen, Z., Xu, B., Zhu, C., Chen, L. W. A., Su, X., Liu, S., Han, Y., Wang, G., and Ho,
2168 K.: Aerosol particles at a high-altitude site on the Southeast Tibetan Plateau, China: Implications
2169 for pollution transport from South Asia, *Journal of Geophysical Research: Atmospheres*, 118,
2170 <https://doi.org/10.1002/jgrd.50599>, 2013.

2171 Zheng, J., Hu, M., Du, Z., Shang, D., Gong, Z., Qin, Y., Fang, J., Gu, F., Li, M., Peng, J., Li, J., Zhang,
2172 Y., Huang, X., He, L., Wu, Y., and Guo, S.: Influence of biomass burning from South Asia at a high-
2173 altitude mountain receptor site in China, *Atmospheric Chemistry and Physics*, 17, 6853-6864,
2174 <https://doi.org/10.5194/acp-17-6853-2017>, 2017.

2175 Zheng, K., Li, Y., Li, Z., and Huang, J.: Provenance tracing of dust using rare earth elements in recent
2176 snow deposited during the pre-monsoon season from mountain glaciers in the central to northern
2177 Tibetan Plateau, *Environmental Science and Pollution Research*, 28, 45765-45779,
2178 <https://doi.org/10.1007/s11356-021-13561-x>, 2021.

2179 Zheng, M. P.: Geological report on salt lake resources and ecological environment in China (in Chinese),
2180 *Acta Geologica Sinica*, 84: 1613-1622. <https://doi.org/10.19762/j.cnki.dizhixuebao>, 2017.

2181 Zhou, Y., Gao, X., and Lei, J.: Characteristics of dust weather in the Tarim Basin from 1989 to 2021 and
2182 its impact on the atmospheric environment, <https://doi.org/10.3390/rs15071804>, 2023.

2183 Zhou, Y., Yang, J., Kang, S., Hu, Y., Chen, X., Xu, M., and Ma, M.: Black carbon aerosols impact
2184 snowfall over the Tibetan Plateau, *Geoscience Frontiers*, 16, 101978, <https://doi.org/10.1016/j.gsf>,
2185 2025.

2186 Zhu, C. S., Chen, C. C., Cao, J. J., Tsai, C. J., Chou, C. C. K., Liu, S. C., and Roam, G. D.:
2187 Characterization of carbon fractions for atmospheric fine particles and nanoparticles in a highway
2188 tunnel, *Atmospheric Environment*, 44, 2668-2673, <https://doi.org/10.1016/j.atmosenv>, 2010.

2189 Zhu, H., Li, W., Kong, X., and Zhang, X.: Overlooked contribution of salt lake emissions: A case study
2190 of dust deposition from the Qinghai-Xizang Plateau, *Journal of Geophysical Research: Atmospheres*,
2191 130, e2024JD042693, <https://doi.org/10.1029/2024JD042693>, 2025.

2192 Zhu, H. X.: The dust deposition data of the Qaidam Basin [Dataset]. Zenodo.
2193 <https://doi.org/10.5281/zenodo.14382853>, 2024.

2194 Zhu, X., Zhu, K., Xie, M., Huang, A., Ouyang, Y., Chen, F., and Zhao, W.: Analysis of current situation
2195 and future trend of anthropogenic heat emissions in Jiangsu Province, *Climatic and Environmental*

